Post-Punching Shear Response of Two-Way Slabs

By:

Farshad Habibi

April 2012

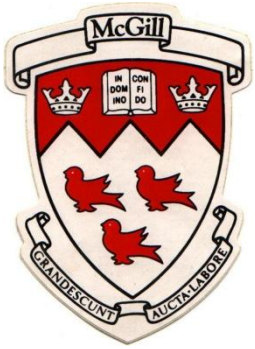

Department of Civil Engineering and Applied Mechanics

McGill University

Montreal, Canada

A thesis submitted to McGill University in partial fulfillment of the requirements of Doctor of Philosophy

To my mother, ***Hoory,*** *for her everlasting love and devotion,*

my father ***Dr. Nader Habibi,*** *for his deep wisdom and never-ending support,*

& my brother, ***Farhad,*** *for being there to encourage me through the hard times*

Abstract

This thesis investigates the post-punching behaviour of reinforced concrete slab-column connections. Seven interior slab-column connections were tested to study the effects of slab thickness, the length of structural integrity reinforcing bars, the distribution of structural integrity reinforcement in slabs with rectangular columns and the placement of structural integrity reinforcement in slabs with drop panels. Results from this test series and from tests by other researchers were compared with predictions using the CSA A23.3-04 design equations for both punching shear and post-punching resistance. The test results demonstrated that the provision of structural integrity reinforcement in accordance with the requirements of CSA A23.3-04 resulted in significant post-punching resistance and the design equations provide a reasonable estimate of this resistance.

In addition, an analytical model for predicting the post-punching shear response of slab-column connections is presented which accounts for the individual contributions of each layer of top reinforcement and each layer of the structural integrity reinforcement. The contribution of each layer of top and integrity reinforcement is governed by three different failure modes, including rupture of the bars, concrete breakout of the bars and pullout of the bars. The predictions are compared with experimental results and the results obtained by the CSA A23.3 Standard design method. There was a good agreement between the predicted results and the experimental results.

Résumé

Cette thèse examine le comportement après poinçonnement des raccords dalle-colonne en béton armé dans le but de fournir le renforcement adéquat pour assurer l'intégrité structurale. Les résultats d'essais sur sept raccords dalle-colonne intérieurs sont présentés. L'étude portait sur les effets de l'épaisseur de la dalle, de la longueur des barres d'armature pour l'intégrité structurale, de la distribution de l'armature d'intégrité structurale dans les dalles avec colonnes rectangulaires et sur le placement de l'armature d'intégrité structurale dans les dalles avec des goussets. Les résultats de cette série d'essai et ceux d'autres chercheurs ont été comparés aux prévisions des équations de calcul de la norme CSA A23.3-04 pour le cisaillement par poinçonnement et la résistance après poinçonnement. Les résultats des essais montrent que la clause d'armature d'intégrité structurale selon les exigences de la norme CSA A23.3-04 produit une résistance importante après poinçonnement; les équations de calcul ont également fourni une estimation raisonnable de cette résistance.

De plus, un modèle analytique permettant de prédire la réponse post-poinçonnement des connexions dalle-poteau est présenté. Ce modèle tient compte de la contribution de chaque lit d'armatures supérieures et chaque lit d'armature d'intégrité structurale. Cette contribution des deux lits d'armature est dictée par trois modes de rupture : rupture des armatures, rupture tronconique du béton et rupture par défaut d'ancrage des armatures. Les prédictions du modèle sont comparées aux résultats expérimentaux et aux résultats obtenus à l'aide de la méthode de dimensionnement de la norme CSA. La corrélation entre les prédictions de la méthode et les résultats expérimentaux est excellente.

Acknowledgments

I owe my deepest gratitude and sincere thanks to my supervisor, Professor Denis Mitchell. This research would not have been possible without his gracious support, continual guidance, and kind patience. It was an honour for me to work under his supervision and I believe that whatever I learnt not only from his extensive knowledge but also from his exemplary personality will inspire me in life. I am also deeply indebted to Dr. William Cook for his invaluable assistance throughout this research program. I could not imagine this research without his generous contribution.

The special thanks go to laboratory technicians Ron Sheppard, Marek Przykorski, John Bartczak and Damon Kiperchuk for their assistance during the experimental part of this research. I would also like to thank my good friend, Hamed Layssi, for great time we had together at McGill and enjoyable company throughout the laboratory work. In addition I would like to thank all my friends in Montreal specially Hooman Keyhan and Iman Shamim for the pleasant moments spent together over recent years. The author would also like to convey thanks to his closest friend Dr. Ali Shirazi for continual support and encouragement throughout his PhD study.

The author acknowledges the financial support provided by the Natural Sciences and Engineering Council of Canada and McGill University for funding this research program.

Above all, the author wishes to express his love and gratitude to his parents and his brother, for their constant support and endless love, through the duration of his studies. Without their support I would probably never have gotten this far.

Table of Contents

List of Figures

List of Tables

Chapter 1: Introduction

1.1 Introduction

Two-way slabs must be designed to have adequate flexural and punching shear resistance. There have been many examples of brittle failures due to punching shear. These failures have occurred during construction, in severe earthquakes, due to corrosion of the top reinforcement and due to design or construction errors. These failures can lead to a catastrophic "progressive collapse", with the initial failure spreading over a large portion of the structure.

If the slab-column connection does not have a secondary defence mechanism, then after punching shear failure, the loads are transferred to adjacent supports. This redistribution of moments and shears may result in punching shear failures at the adjacent slab-column connections, leading to progressive collapse. After the initial punching shear failure, the top flexural reinforcement crossing the punching shear cone and the bottom bars that are adequately anchored in the column, referred to as "structural integrity reinforcement" can provide a link between the slab and the column. These bars can play a significant role in providing a secondary load carrying mechanism after the initial failure and can prevent progressive collapse. Since 1984 the concept of providing structural integrity reinforcement in flat plate structures to prevent progressive collapse appeared in the CSA Standard, "Design of Concrete Structures for Buildings", (CSA 1984).

Previous research on the behaviour of slab-column connections has typically focused on the initial punching shear failure, rather than on the post-punching behaviour. Hence more research is needed to investigate the behaviour of slab-column connections after punching shear failure has occurred. The first part of this research program is aimed at providing experimental

verification of the approach taken in the CSA A23.3 Standard for the design and detailing of structural integrity reinforcement. In the experimental part, the effects of the following parameters on the post-punching behaviour of slab-column connections were investigated:

- **Thickness of slab**

  The prediction of the post-punching shear resistance in accordance with the CSA A23.3-04 standard is independent of slab thickness. The influence of this factor on the post-punching response of slab-column connection was studied.

- **Length of structural integrity bars**

  Based on the CSA A23.3-04 Standard requirement, the structural integrity reinforcement must protrude from the column face a distance equal to twice the development length ($2\ell_d$). The effect of increasing the length of structural integrity bars has been investigated in this study.

- **Column rectangularity and distribution of structural integrity reinforcement**

  The CSA A23.3-04 code assumes that the post-punching shear resistance is a function of the total area of structural integrity reinforcement, without regard to its distribution. Also the CSA approach is independent of column rectangularity. This research examined the appropriateness of these assumptions.

- **Response of slabs with drop panels**

  One of the goals of the experimental part of this research program was to investigate the influence of placing the structural integrity reinforcement near the bottom of the drop panel rather than at a same level as bottom slab reinforcement. In addition the effectiveness of locating the structural integrity reinforcement outside of the column, but within the region of the punching shear cone was investigated.

In addition to the experimental program, an analytical model was developed to predict the complete post-punching response of slab-column connections, considering the contribution of each layer of top reinforcement and each layer of the structural integrity reinforcement. This model is capable of predicting the different possible failure modes in the post-punching response. In addition, predictions using the CSA code design equation and predictions from the analytical model developed in the research program are compared with the experimental results from this study as well as from experiments carried out by other researchers.

1.2 Outline of the Thesis

The thesis has seven chapters:

Chapter 1: "Introduction" presents an introduction to the research program, its objectives and the statement of originality.

Chapter 2: "Literature Review" provides an overview of previous research on the post-punching behaviour of reinforced concrete slab structures and the requirements of current design standards.

Chapter 3: "Experimental Study" describes the details of four full-scale test specimens, the material properties and the test set-up.

Chapter 4: "Responses of Test Specimens" summarizes the results of the experimental study on the post-punching responses of four test specimens.

Chapter 5: "Analytical Model" deals with development of an analytical model capable of predicting the complete post-punching response and different possible failure modes of slab-column connections.

Chapter 6: "Comparison of Test Results and Predictions" presents comparisons of the test results as well as the influence of different parameters on the post-punching response of slab-column connections. Results from this test series and from other researchers are compared with predictions using the CSA code and the analytical model.

Chapter 7: "Conclusions" draws main conclusions from this research program. Some suggestions for further studies are also given in this chapter.

1.3 Statement of Originality

The original contributions of this research program include:

- **Full-scale tests on the slab-column connections**

  Most of the previous experimental studies on the post-punching response of slab-column connections involved testing very small-scale specimens, with very thin slabs, small concrete covers and small bar diameters. In contrast, the experiments in this research program were conducted on full-scale specimens with practical slab thicknesses, concrete covers and bar diameters.

- **Investigation of the influence of key parameters on the post-punching response**

  A unique feature of this experimental study was the investigation of key parameters affecting the post-punching response such as: the effects of slab thickness; the length of the structural integrity reinforcing bars; the distribution of the structural integrity reinforcement in the two principal directions; the influence of column rectangularity; and the location of the structural integrity reinforcement in slabs having drop panels.

- **Development of an analytical model to predict the complete post-punching response**

  An analytical model to predict the complete post-punching response of slab-column connections considering the contribution of each layer of top reinforcement and structural integrity reinforcement is developed and verified. The analytical model is capable of predicting the different possible failure modes during the post-punching response of slab-column connections including: concrete breakout failures of the top and bottom layers of reinforcement; progressive destruction of the concrete above the reinforcement, pullout of the top and bottom reinforcement and possible rupture of the structural integrity bars.

- **Comparing the results of different experimental studies with the predictions**

  The results of different experimental studies from this test series and other researchers on the post-punching response of slab-column connections are compared with the predictions of the CSA Standard and with the analytical model.

It is noted that parts of this thesis have been published before or have been submitted to be published. Parts of Chapters 2, 3 and 6 were published in the technical paper: Habibi, F., Redl, E., Egberts, M., Cook, W.D. and Mitchell, D., "Assessment of CSA A23.3 Structural Integrity Requirements for Two-Way Slabs", Canadian Journal of Civil Engineering, Vol. 39, 2012, pp 351-366. Co-authors Erin Redl and Michael Egberts were Masters students at McGill University, Dr. William D. Cook is a Research Associate and Professor Denis Mitchell is the thesis supervisor.

The paper: Habibi, F., Cook, W.D. and Mitchell, D. "Predicting the Post-Punching Shear Response of Slab-Column Connections", submitted to ACI Journal of Structural Engineering includes some parts of Chapters 5 and 6. This paper co- authored with Dr. William D. Cook and thesis supervisor Professor Denis Mitchell.

Chapter 2: Literature Review

2.1 Introduction

Two-way slabs are very common and provide an economical structural system, but over the past 30 years several failures have occurred that resulted in progressive collapses. Four workers died because of a progressive collapse initiated from a local failure of the roof slab during construction of a 16-storey apartment building at 2000 Commonwealth Avenue in Boston in 1971 (King and Delatte 2004). Similar collapses of slab structure occurred including an apartment structure in Bailey Crossroads in 1973 (Leyendecker and Fattal 1973), a condominium collapse in Cocoa Beach, Florida in 1981 (Lew et al. 1982), several collapses during the Mexico City earthquake of 1985 (Mitchell et al. 1986) (see Fig. 2.1) and an underground parking garage collapse in Switzerland in 2004 (Mirzaei 2010) (see Fig. 2.2).These catastrophic events indicate the need to carefully design and detail reinforced concrete slabs to prevent progressive collapse. Construction errors, design errors, overloading during construction and service, severe seismic loading, corrosion of reinforcement and delamination can lead to punching shear failures in flat plate structures. After a local failure, the load carried by the slab connection redistributes the load to adjacent supports which will likely cause overloading, and hence fail in punching shear. This would result in the collapse of the floor onto the slab below, thereby propagating the collapse both horizontally and vertically throughout the structure and could lead to progressive collapse of the structure. The key to avoiding these failures is to provide a secondary load carrying mechanism after a slab-column connection has failed in punching shear.

Fig 2.1. Progressive collapse of 9-storey flat plate structure in the Mexico City earthquake of 1985 (Mitchell et al. 1986)

Fig 2.2. Parking garage collapse in Switzerland 2004 (Mirzaei 2010)

A number of research programs have been carried out to investigate the post-failure behaviour of slab-column connections. This chapter will provide a brief overview of previous research on the post-punching behaviour of reinforced concrete slab structures. The requirements of current design standards are also presented.

2.2 Literature survey

2.2.1 Park (1964)

Park (1964) reported on tests of uniformly loaded rectangular model slabs (including the slabs tested by Powell (1956)).The slabs were clamped at their edges preventing rotation and in-plane displacement. These experiments demonstrated that reinforced concrete slabs with fully restrained edges can develop “tensile membrane action”, a behaviour which increases the capacity of a slab under gravity loads after initial flexural failure.

Fig 2.3 shows a typical load-deflection response of a slab with edge restraint subjected to uniform load. The slab contained continuous reinforcement which was properly anchored into the supports and with the edges restrained against lateral movement. As the load is increased from *A* to *B*, the slab reaches its enhanced ultimate load at *B*, with the aid of compressive membrane forces. As the slab is loaded, the development of the cracks tends to increase the length of the slab and if the edges are fully restrained against lateral movement then the compressive membrane forces will develop as the edges try to move outward.

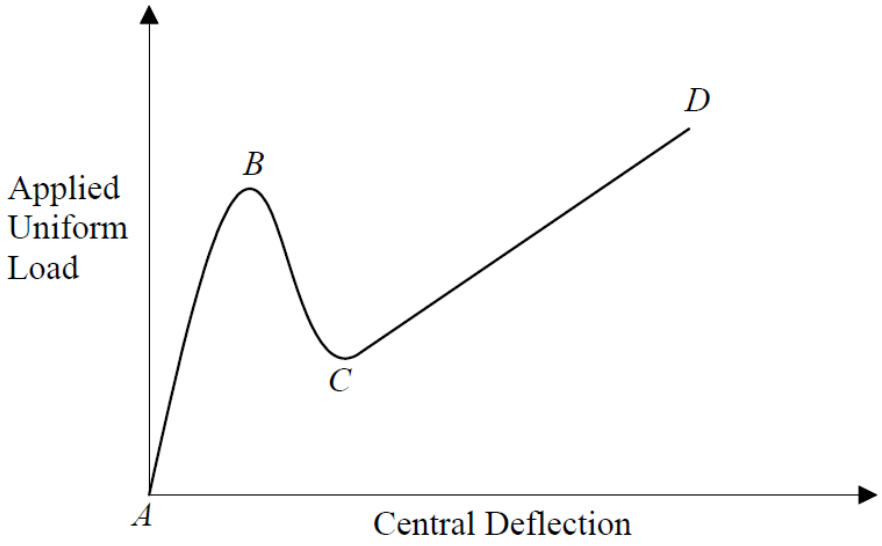

Fig 2.3. Typical load-deflection response of a two-way slab experiencing membrane action (Park 1964)

After the initial flexural failure there is a sudden drop in load with a reduction in the compressive membrane forces. At *C*, the slab edges tend to move inward due to large deflection at central region and because the edges are laterally restrained, tensile membrane forces are developed which enable the slab to carry significant load by catenary action of the reinforcing steel. The slab continues to carry further load with an increase in deflection until the rupture of the reinforcement occurs at D.

Park (1964) proposed the following equation relating the load to the central deflection response of a uniformly loaded rectangular slab, fully restrained at its edges that provides a linear relationship for the slab behaviour between points C and D:

$$\frac{wl_x^{\,2}}{T_x\Delta} = \frac{\pi^3}{4\sum_{n=1,3,\ldots}^{\infty}\frac{1}{n^3}(-1)^{\frac{n-1}{2}}\left\{1-\left[\cosh\left(\frac{n\pi l_y}{2l_x}\sqrt{\frac{T_x}{T_y}}\right)\right]^{-1}\right\}} \tag{2.1}$$

where w is the uniformly distributed load per unit area of the slab; $l_x > l_y$ are the span lengths of the slab, T_x and T_y are the yield forces of the reinforcement per unit width in the x and y direction; and Δ is the maximum value of deflection. This equation assumes that the concrete is cracked through the full depth of the slab and cannot carry any tension. It is also assumed that all of the reinforcement has reached its yield stress, and, has a bilinear, elastic, fully plastic stress-strain relationship.

The dimensionless parameter, $\frac{wl_x^2}{T_x\Delta}$ for an isotropically reinforced square panel becomes 13.56.

Park (1964) stated that the use of this equation with an assumed deflection equal to 0.1 times the shorter clear span would give a conservative estimate of the tensile membrane strength. Black (1975) suggested that assuming this dimensionless parameter equal to 20.0 rather than 13.56 and limiting the deflection equal to 0.15 times the shorter clear span provides a more accurate prediction of strength.

2.2.2 Hawkins and Mitchell (1979)

Hawkins and Mitchell (1979) presented factors influencing the initiation and propagation of progressive collapse in flat plate structures and possible approaches for preventing progressive collapse. Possible defence strategies included the use of higher design loads, provisions for integral beam stirrup reinforcement in the slab around the column, and the provision of bottom reinforcement that is continuous or anchored into the column to enable the development of tensile membrane action. Higher live loads would lead to thicker and therefore an uneconomical structural system that would still not have the ability to arrest progressive collapse. The solution of using integral beam-stirrup reinforcement can prevent shear failure but can often create

placement problems during construction. Hence the provision of continuous bottom reinforcement was recommended as a practical solution.

They suggested that the post-punching shear capacity of a slab could be determined using tensile membrane equations or alternatively the capacity should be taken as not greater than one-half of yielding strength of all the bottom reinforcement passing through the column.

Hawkins and Mitchell (1979) described the difference in the post-punching behaviour of two-way slabs with and without bottom slab reinforcement properly anchored into the column. Fig. 2.4 illustrates the failure of a slab-column connection that contains top reinforcement only. After the punching shear failure the top bars rip out of the top concrete surface, offering little resistance and leading to complete loss of support at the connection.

Fig. 2.5 illustrates the benefit of providing bottom slab reinforcement that is continuous through the column. The specially detailed bottom bars provide the slab an ability to transfer shear to the column and prevent progressive collapse

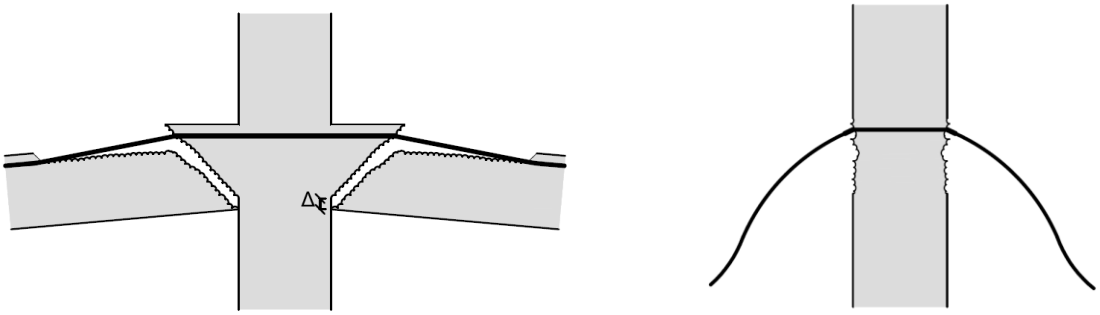

(a) (b)

Fig. 2.4. Slab-column connection with top bars only: (a) Ripping out of top bars after punching shear failure; (b) Loss of support with top bars ineffective.

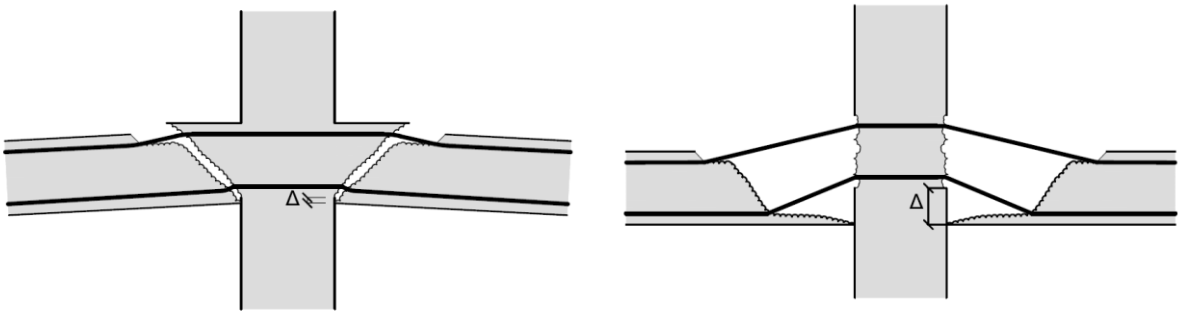

(a) (b)

Fig. 2.5. Slab-column connection containing top bars and continuous bottom reinforcement: (a) Post-punching resistance provided by both top and bottom bars; (b) Post-punching resistance provided by continuous bottom reinforcement.

Additionally, a simplified iterative method was proposed by Hawkins and Mitchell (1979) to predict the tensile membrane response of slabs with uniform load and restrained edges. Assuming that the membrane takes a circular deformed shape and the concrete carries no tension, resulted in the following equation:

$$w = \frac{2T_x \sin\sqrt{6\varepsilon_x}}{l_x} + \frac{2T_y \sin\sqrt{6\varepsilon_y}}{l_y} \tag{2.2}$$

where w is the uniform load; T_x and T_y are the tension per unit length for the x and y directions, respectively; ε_x and $\varepsilon_y = \varepsilon_x l_x^{\,2} / l_y^{\,2}$ are the membrane strains in the *x* and *y* directions, respectively; l_x and l_y are the span lengths of the slab in the short and long directions, respectively.

The relationship between the central deflection, δ, the geometry of the panel and the strain in the reinforcement is:

$$\delta = \frac{3 l_x \varepsilon_x}{2\sin\sqrt{6\varepsilon_x}} \tag{2.3}$$

The complete load deflection response can be predicted by using Eqs. 2.2 and 2.3, together with the stress-strain relationship of the reinforcement.

2.2.3 Regan et al. (1979)

Regan et al. (1979) investigated the role of bottom reinforcement passing through the column on the post-punching response of slab-column connections. They compared the response of a 100 mm thick slab with three 8 mm diameter bottom reinforcing bars in each direction with a similar slab without bottom reinforcement and concluded that the presence of the bottom reinforcement is fundamental to achieve post-punching resistance. They also proposed the following equation to estimate the post punching strength, V_{pp}, based on dowel action of the bars:

$$V_{pp} = 1.3 \sum d_b^{\,2} \sqrt{f_y f_c'} \tag{2.4}$$

where d_b is the bar diameter, f_y is the yield strength of reinforcing bars and f_c' is the concrete compressive strength.

2.2.4 McPeake (1980)

McPeake (1980) carried out an experimental program on thin slabs to study the effect of bottom reinforcement on the post-punching response of slab-column connections. It was observed that the bottom bars had considerable contribution in the form of tensile membrane action rather than dowel action at large deflections.

2.2.5 Mitchell and Cook (1984)

Using a tensile membrane model and the results from one-quarter scale models of two-way slab structures, Mitchell and Cook (1984) recommended a design equation that was adopted in the 1984 CSA Standard for the design of minimum bottom reinforcement. The purpose of these

requirements was to provide a minimum level of structural integrity to the slab system to limit the spread of a local failure to a progressive collapse.

It is assumed the load is carried by a two-way tensile membrane which is supported by one-way catenaries which, in turn, hang from the column (see Fig. 2.6). By assuming that the one-way catenary is subjected to a uniform load equal to $0.5wl_2$ per unit length, from Eq. 2.2 the one-way catenary response can be expressed as:

$$w = \frac{4T_c \sin\sqrt{6\varepsilon}}{l_n l_2} \tag{2.5}$$

where T_c is force in the anchored bottom reinforcement in the one-way catenary; l_n is clear span of one-way catenary; and l_2 is distance measured from the centerline of the panel on one side of the catenary to the centerline of panel on the other side of the catenary.

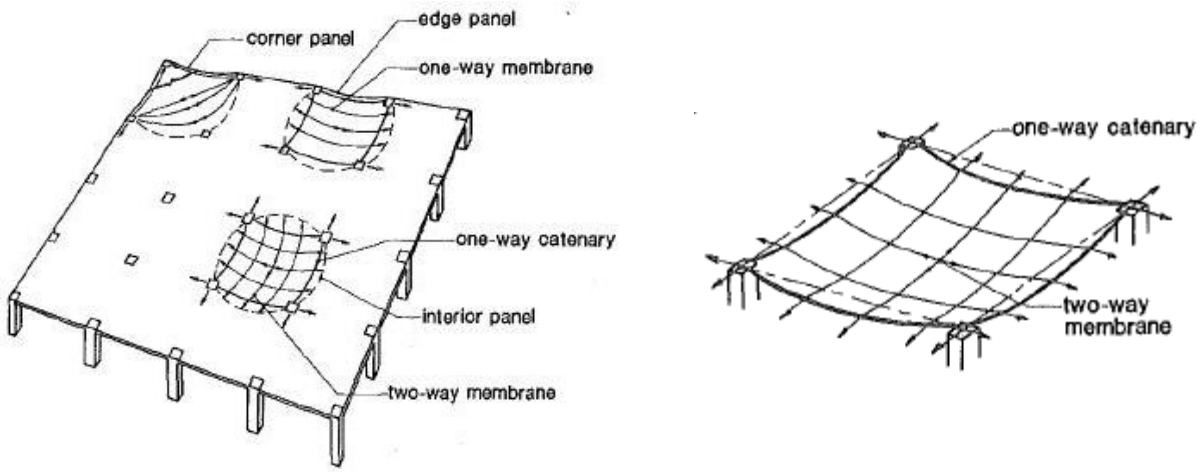

(a) Flat plate structure (b) Interior panel

Fig. 2.6. Development of "Hanging nets" in panels of two-way slab structures (Mitchell and Cook 1984).

Mitchell and Cook (1984) stated that a portion of the bottom flexural reinforcement for structural integrity must extend into the column and be made effectively continuous in each span direction. If a limiting deflection of $0.15l_n$ is used for the one-way catenary, then from Eqs. 2.3 and 2.5 a minimum area of continuous bottom bars in each span direction, A_{sb}, can be written in the form of a design equation as:

$$A_{sb} = \frac{0.5 w_s l_2 l_n}{\phi f_y} \tag{2.6}$$

where w_s is the total specified load per unit area but not less than twice the slab dead load per unit area in kPa, l_n is the clear span in the direction moments are being considered measured face-to-face of supports in mm, l_2 is the span length transverse to l_n measured centre-to-centre of supports in mm, ϕ is the resistance factor for reinforcing bars (0.9 in ACI (ACI Committee 318 1983) and f_y is the specified yield strength of the nonprestressed reinforcement in MPa.

To achieve continuity this reinforcement shall either be lap spliced within the column or reaction area with reinforcement in adjacent spans with a minimum lap splice of ℓ_d, or spliced with bottom bars in the slab outside of the column or reaction area with a minimum lap splice length of $2\ell_d$, or at discontinuous edges these bars must bent, hooked or otherwise anchored into the supports such that the yield stress can be developed at the face of the support.

Mitchell and Cook stated that when the calculated values of A_{sb} differ for adjacent spans due to unequal span lengths or unequal loading then the larger value of A_{sb} must be used in each of these spans to enable the transfer of tension across the supporting member. Since most progressive collapses have occurred during construction, the loading in Eq. 2.6 should not be

taken less than the twice the slab dead load which correspond to typical load levels during construction.

Mitchell and Cook (1984) concluded that the secondary load carrying mechanism which can develop after initial failure is the key in preventing progressive collapse of slab structures.

2.2.6 Mitchell (1993)

Mitchell (1993) proposed a new simplified equation for determining the amount of structural integrity reinforcement. It was assumed that after punching-shear failure the structural integrity reinforcement is capable of yielding and after the slab deflects forms an angle of 30 degrees from the horizontal. This equation gives the summation of the area of bottom reinforcement, $\sum A_{sb}$, connecting the slab to the column or column capital on all faces of the periphery of the column or column capital, as:

$$\sum A_{sb} \geq \frac{2V_{se}}{\phi f_y} \tag{2.7}$$

Where V_{se} is the shear transmitted to the column or column capital due to specified loads but not less than the shear corresponding to twice the self-weight of the slab, ϕ is the capacity reduction factor for tension (0.9), and f_y is the specified yield strength of the bottom bars.

In this equation the likely service load shear, V_{se}, replaced the load $w_s l_n l_2$ in the Eq. 2.6, such that the calculation of the bottom reinforcement no longer required a consideration of each span direction. The resulting equation was adopted by the CSA A23.3 Standard (CSA 1994, 2004) for the design of structural integrity reinforcement with a slight modification of removing the

resistance factor, ϕ, as the failure leading to progressive collapse was deemed a rare loading event, and the variability allowed for by the resistance factor was deemed unnecessary.

2.2.7 Melo and Regan (1998)

Melo and Regan (1998) reported on tests of slabs with a total thickness of 75 mm and having bottom bars passing through the column that were aimed at identifying the type of failure and to calculate the post-punching resistance.

Three different test series were developed to investigate three possible failure modes in the post-punching response. These three failure modes included "destruction of concrete in the zone where they are anchored in the slab", "fracture of the bars", or "destruction of the concrete in the column under the bars". They also stated that dowel action did not play an important role in the post-punching resistance.

Melo and Regan (1998) proposed that the method for breakout resistance described in the ACI code for nuclear safety related structures (ACI Committee 349 1978) could be used to estimate the breakout resistance of the bottom bars embedded in the concrete. Using this method resulted in the following equation for the breakout resistance of an individual bar:

$$V_u = 0.33\sqrt{f_c'}\,\frac{\pi d^2}{2} \tag{2.8}$$

where $0.33\sqrt{f_c'}$ represents the average tensile strength of the concrete, $\frac{\pi d^2}{2}$ is the horizontal projection area of a conical failure surface emanating at an angle of 45 degrees from the centre of the bar, and d is the depth of concrete above the bar. If the bars are spaced closely then the overlap of the conical failures surfaces must be considered.

The development of the forces predicted by Eq. 2.8 requires sufficient length to properly anchor the bottom bars within the intact concrete. Melo and Regan (1998) suggested that the minimum length of the bottom bars be $2d + \ell_d$.

For the post-punching resistance due to rupture of the bars they proposed following equation:

$$V_u = 0.44 \sum A_{sb} f_u \tag{2.9}$$

where f_u is the ultimate strength of the reinforcing steel. They also indicated that if f_u is not known then it can be assumed that $f_u = 1.15 f_y$ resulting in the following equation that is identical to the equation used in the CSA A23.3-04 Standard (CSA 2004) :

$$V_u = 0.50 \sum A_{sb} f_y \tag{2.10}$$

2.2.8 Mirzaei (2010)

Mirzaei (2010) at Ecole Polytechnique Fédérale de Lausanne in Switzerland reported on three series of test programs involving the testing of 125 mm thick slabs supported on eight roller bearings with a vertical load applied to a steel plate on the top of the slab (see Fig. 2.7). He investigated the influence of top and bottom reinforcement, the size of the reinforcing bars, the layout of the reinforcement and the stress-strain characteristics of the reinforcement.

For all of the specimens, 8 mm diameter bars were used as the tensile reinforcement, very strong edge top and bottom reinforcement was provided to avoid unexpected modes of failure. For all of the slabs, the nominal concrete cover was 15 mm.

The first series of tests had no integrity reinforcement and were designed to investigate the effects of various tensile reinforcement ratios on the post-punching behaviour of the slabs. In the second series he considered the effects of additional bottom integrity bars passing through the column with full anchorage and bent-up additional bars acting as shear reinforcement. The

influence of using various types of reinforcing steel and reinforcement steel details were investigated in the third series.

The test results showed that the post-punching strength of slabs without integrity reinforcement was relatively small (about 21% to 37% of the punching strength) due to the fact that the tensile reinforcement ripped out of the concrete surface and became ineffective after the punching shear failure occurred. The specimens that contained structural integrity reinforcement had larger post-punching strengths than that observed in the specimens without integrity reinforcement and reached up to 98% of their punching shear strength.

He considered the breakout resistance of the reinforcing bars and the rupture stress of the bars in determining the post-punching shear strength. Mirzaei (2010) reported that after punching shear failure the only remaining link between the punching cone and the rest of the slab is the top and bottom reinforcing bars. He recommended that the post-punching shear strength of a slab-column connection can be calculated as the sum of the contributions of the top bars crossing the punching shear cone and the integrity reinforcement.

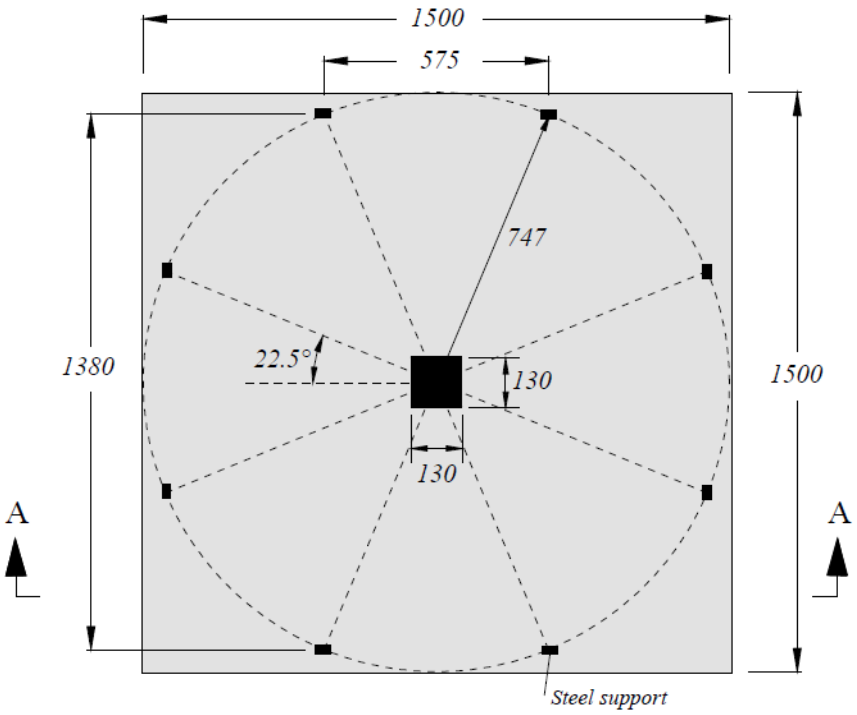

(a) Plan view

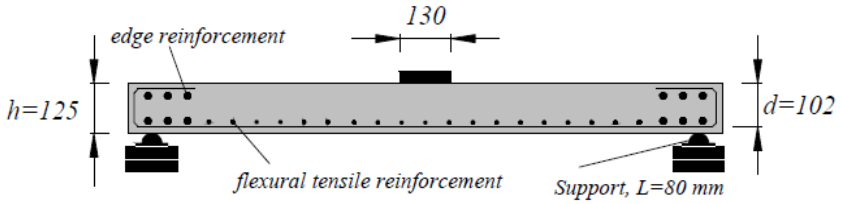

(b) Section view

Fig. 2.7. General dimensions and geometry of the slab tested by Mirzaei (2010)

He used the ACI Code for Nuclear Safety Related Concrete Structures (ACI Committee 349 1978) method for the concrete breakout resistance and accounted for the progressive destruction of the concrete over the reinforcing bars. To develop a mechanical model capable of predicting the post-punching behaviour of slab-column connections he assumed that the top mat of bars in the punching cone region act as a unit pushing outwards on the concrete cover. The total

breakout resistance of the integrity reinforcement was calculated for the bars passing through the column, treating them as having the same depth. The integrity reinforcement contribution was governed either by the maximum breakout strength of the concrete above the bars or by the rupture of the bars.

2.3 Current Design Provisions

2.3.1 CSA A23.3-04

The 1984 CSA Standard used the term "structural integrity reinforcement" and adopted the equation proposed by Mitchell and Cook (1984) to calculate the minimum area of structural integrity reinforcement (Eq. 2.6). Mitchell (1993) proposed a new simplified equation for determining the amount of structural integrity reinforcement. The resulting equation was adopted by the current CSA standard (CSA 2004) to design structural integrity reinforcement. The CSA Standard A23.3-04 stated that a minimum area of bottom reinforcement connecting the slab, drop panel, or slab band to the column or column capital on all faces of periphery of the column or column capital , $\sum A_{sb}$, is given by:

$$\sum A_{sb} = \frac{2V_{se}}{f_y} \tag{2.12}$$

where V_{se} is the shear transmitted to the column or column capital due to specified loads but not less than the shear corresponding to twice the self-weight of the slab and f_y is the specified yield strength of the integrity bars.

The CSA standard requires that the structural integrity reinforcement consist of at least two bars or tendons in each span direction. This reinforcement shall be either lap spliced within the column or reaction area using bottom reinforcement in adjacent spans with a Class A tension lap

splice (Fig. 2.8(a)), spliced outside of the column or reaction area with a minimum lap splice length of $2\ell_d$ (Fig. 2.8(b)), or at discontinuous edges this reinforcement must bent, hooked or otherwise anchored into the supports such that the yield stress can be developed at the face of the support (Fig. 2.8(c)).

2.3.2 ACI 318M-08

The ACI code (ACI 318 Committee 2008) requires that the bottom bars in the column strip be lapped with Class B tension splices and that at least two bottom bars or wires ("integrity steel") in each direction must pass within the region bounded by the longitudinal reinforcement of the column and shall be anchored at exterior supports. The ACI code approach does not specify the minimum area of structural integrity reinforcement required and would typically result in considerably smaller amounts of integrity steel than that required by the CSA Standard approach

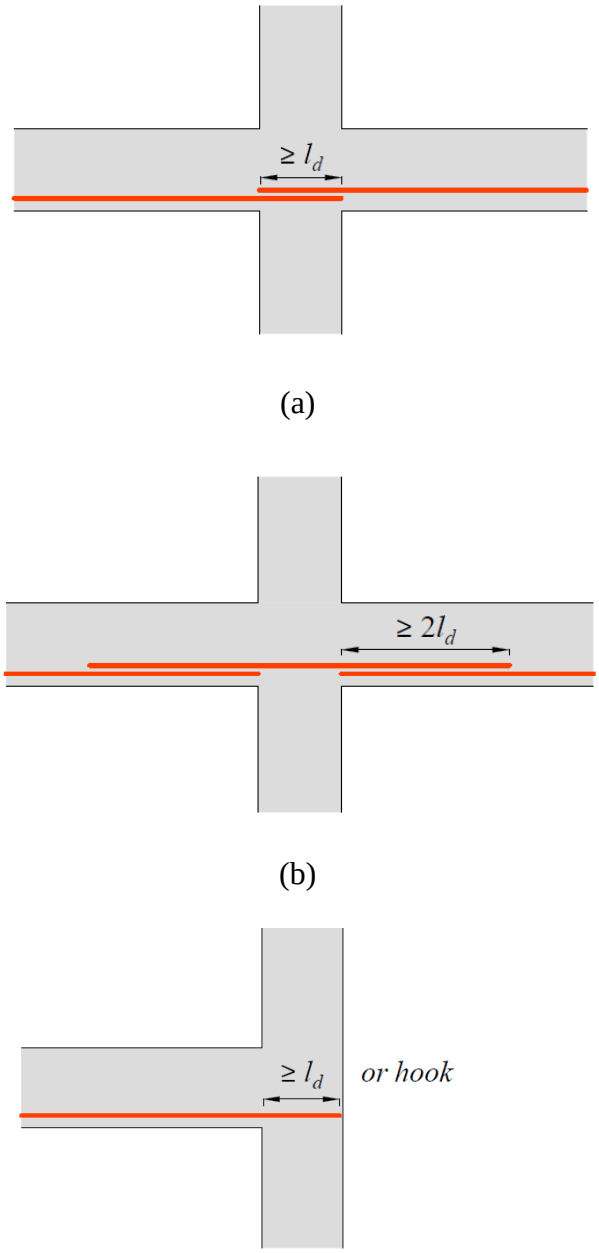

Fig. 2.8. Permissible details to achieve effectively continuous bottom reinforcement: (a) Lap spliced within the column; (b) Spliced outside of the column; (c) Hooked or anchored into an edge or corner column

2.4 Recent Studies at McGill University

As a part of present research program four two-way slab specimens (S1, S2, R1 and R2) were tested by Redl (2009) and Egberts (2009) at McGill University to study the effect of length and arrangement of the structural integrity reinforcement on the post-punching behaviour of slab-column connections.

These specimens were 3.4 m by 3.4 m flat plate slabs with a thickness of 150 mm and with a 250 mm square central column stub in S1 and S2 and a 200 × 300 mm rectangular central column stub in R1 and R2. In all of the specimens, the top and bottom bars were designed based on the requirements of CSA A23.3-04 (CSA 2004). The bottom and top reinforcing steel consisted of 10M bars and 15M bars in each direction, respectively. The top and bottom clear covers were 25 mm for all of the slab specimens. The top and bottom reinforcement for these specimens are shown in Fig. 2.9.

Specimens S1and S2 contained two 15M in each direction for the structural integrity reinforcement. The structural integrity reinforcement consisted of three 15M bars in the direction perpendicular to the long face of the column and two 10M bars in the other direction in specimens R1 and R2. For specimens S1 and R1 the structural integrity reinforcement extended twice the development length of bar ($2l_d$) from the column face in each direction, based on the requirements of CSA A23.3-04 while for specimens S2 and R2 the structural integrity reinforcements extended twice the development length of bar plus twice the effective depth of the slab ($2l_d + 2d$) from column face (see Fig. 2.10).

The results from these experiments are reported in Chapter 6, along with the predictions of the load-displacement responses and the code predicted post-punching resistances.

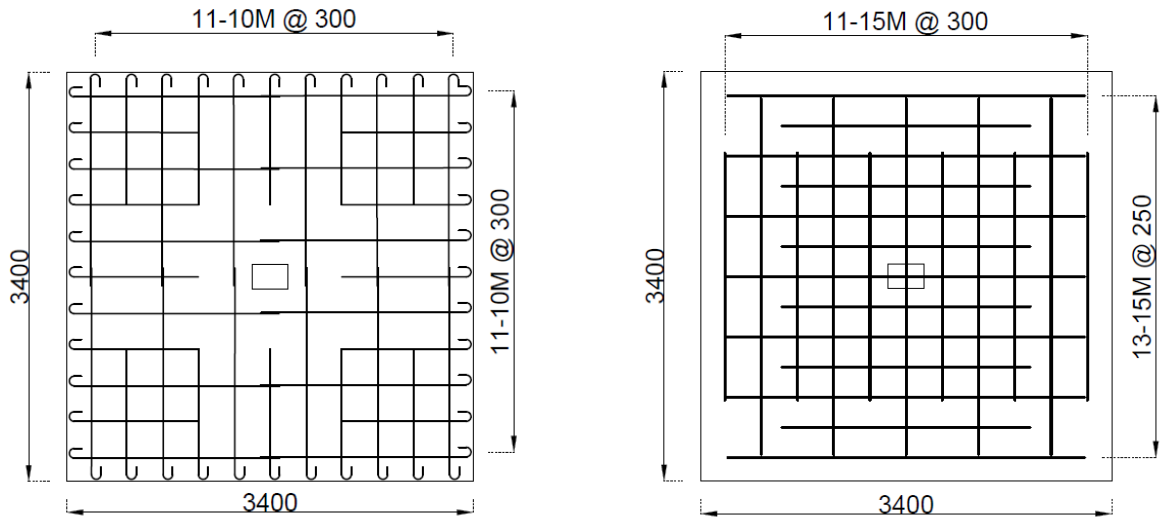

(a) (b)

Fig. 2.9. Details of reinforcement for Specimens S1 and S2 with 250 mm square column and R2 with 200×300 mm column (dimensions in mm): (a) Bottom mat; (b) Top mat. Rectangular column shown in figure (for specimens R1 and R2)

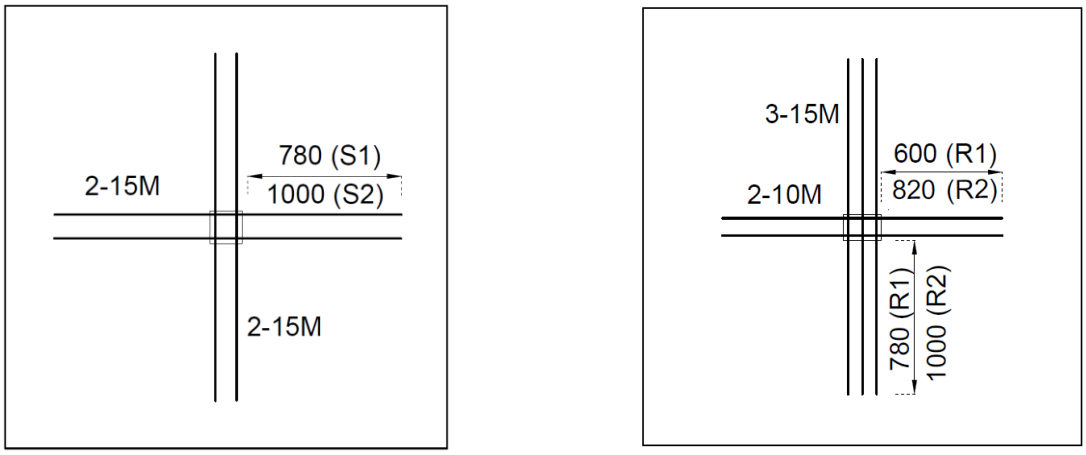

(a) (b)

Fig.2.10. Details of structural integrity reinforcement (dimensions in mm): (a) S1, S2; (b) R1 and R2

Chapter 3: Experimental Study

3.1 Introduction

The first part of the research program is an experimental study on the post-punching behaviour of slab-column connections. Four full-scale interior slab-column connections (SS, RS, D1, D2) were constructed in the Structures Laboratory of the Department of Civil Engineering and Applied Mechanics of McGill University and tested to study the punching failures and post-punching failure behaviour. The purpose of this study is to provide additional experimental verification of the approach taken in the CSA A23.3 Standard (CSA 2004) for the design and detailing of the structural integrity reinforcement. This study also investigates the effects of a number of parameters such as the thickness of the slab, the distribution of the integrity reinforcement and also the influence of column rectangularity on the post-punching behaviour of two-way slabs. In addition, the effects of the presence of a drop panel and the layout of the structural integrity reinforcement in the drop panel region are investigated.

3.2 Prototype Structure

A prototype structure was designed with 6.0 m by 6.0 m bays for loads including a superimposed dead load of 1.0 kPa and a live load of 2.4 kPa for specimens SS and RS and with 5.6 m by 5.6 m bays for loads including a superimposed dead load of 1.0 kPa and a live load of 4.8 kPa for specimens D1 and D2. The load combinations under consideration were: (1) dead load only, with a load factor of 1.4, as well as (2) dead load and live load, with load factors of 1.25 and 1.5, respectively. Design assumptions included a concrete compressive strength of 30 MPa and reinforcing steel yield strength of 400 MPa.

3.3 Details of Test Specimens

The size of the test specimens were chosen to allow the high tensile forces developed in the structural integrity reinforcement and for the transfer of forces from the structural integrity steel to the bottom flexural reinforcement in the slab. Specimens SS and RS were 2300 × 2300 mm flat plates with a thickness of 200 mm. Specimen SS had 225 mm square central column stubs and specimen RS had 180×270 mm rectangular column stubs. Specimens D1 and D2 were 2300 × 2300 × 160 mm thick slabs with a 1825 × 1825 × 90 mm thick drop panel and a 225 mm square column. The column stubs extended 300 mm above and below the slab in all specimens. The top and bottom clear covers were 25 mm for all of the slab specimens. In all specimens the design of the top and bottom reinforcement was based on the requirements of CSA A23.3-04 (CSA 2004).

The bottom reinforcing steel consisted of 10M bars in each direction. Bar lengths and cut-off locations were in accordance with CSA A23.3-04 (CSA 2004) except that for the drop panel specimens, 50% of the bottom bars extended a distance of 75 mm past the centreline of the column in both directions, as required for slabs without drop panels. The bottom reinforcing steel was hooked at the exterior edge of the slab to simulate the continuity of this steel.

The top reinforcement consisted of 15M bars in each direction and the number of bars in the two principal directions was adjusted such that the flexural resistance in both directions were almost equal. Also the amount of flexural reinforcement was chosen such that the slabs would fail in punching shear without failing in flexure. The average effective depth of the top reinforcement mat for specimens SS and RS and for specimens D1 and D2 were 160 mm and 210 mm, respectively. The top and bottom reinforcement for all specimens are shown in Figs. 3.1, 3.2 and 3.3.

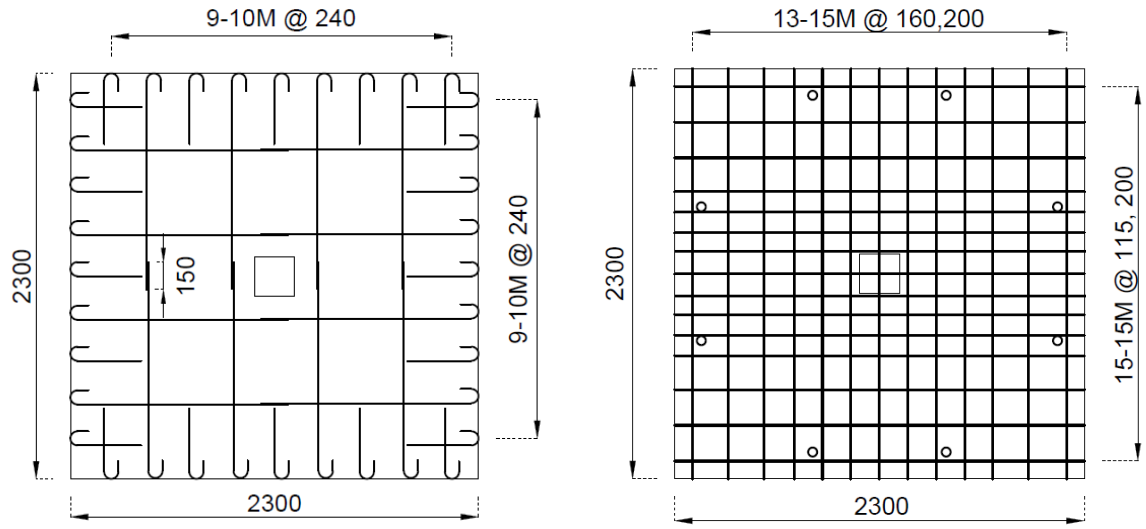

(a) Bottom mat (b) Top mat

Fig. 3.1. Details of reinforcement for specimen SS (dimensions in mm)

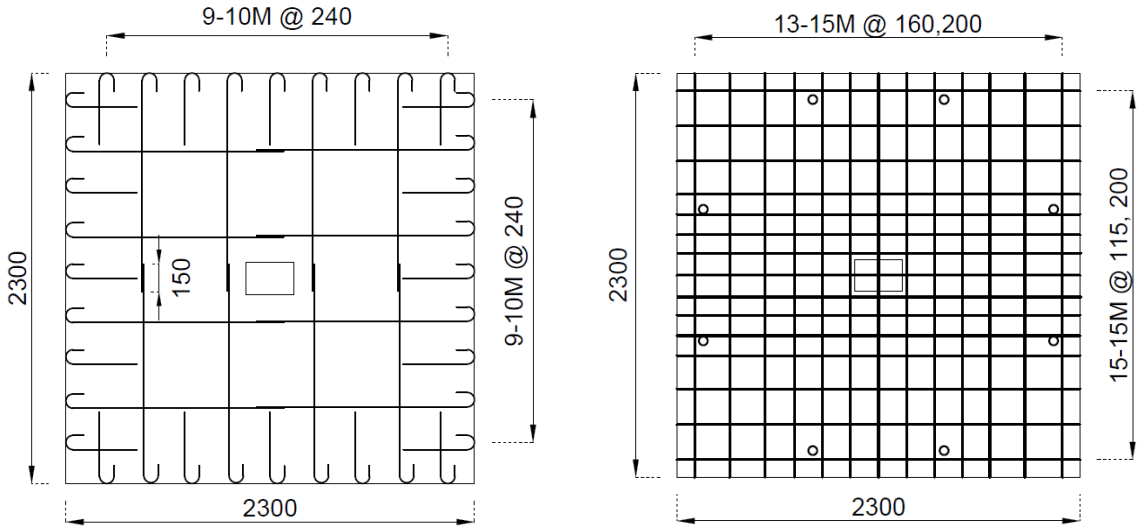

(a) Bottom mat (b) Top mat

Fig. 3.2. Details of reinforcement for specimen RS (dimensions in mm)

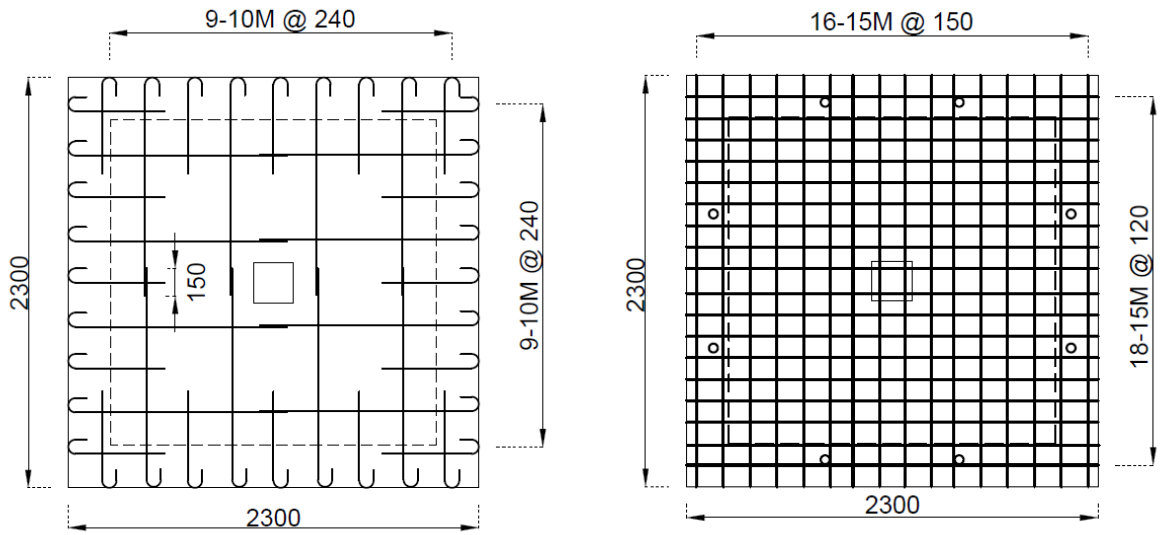

(a) Bottom mat (b) Top mat

Fig. 3.3. Details of reinforcement for specimens D1 and D2 (dimensions in mm)

The structural integrity reinforcement in all specimens had a total area of 1600 mm^2 resulting in a predicted post-punching shear resistance of 320 kN in accordance with the CSA A23.3-04 design expression for the structural integrity reinforcement.

Specimen SS contained two 15M bars passing through the column in each direction for the structural integrity reinforcement. Specimen RS had rectangular columns and the structural integrity reinforcement consisted of three 15M bars in the direction perpendicular to the long face of the column and two 10M bars in the other direction. The purpose of this arrangement of reinforcement was to investigate if a highly irregular layout of structural integrity reinforcement would affect the post-punching resistance. For both specimens the structural integrity reinforcement extended twice the development length of the integrity bars ($2\ell_d$) from the column face in each direction, as required by CSA A23.3-04. The details of the structural integrity reinforcement for specimens SS and RS are shown in Fig. 3.4.

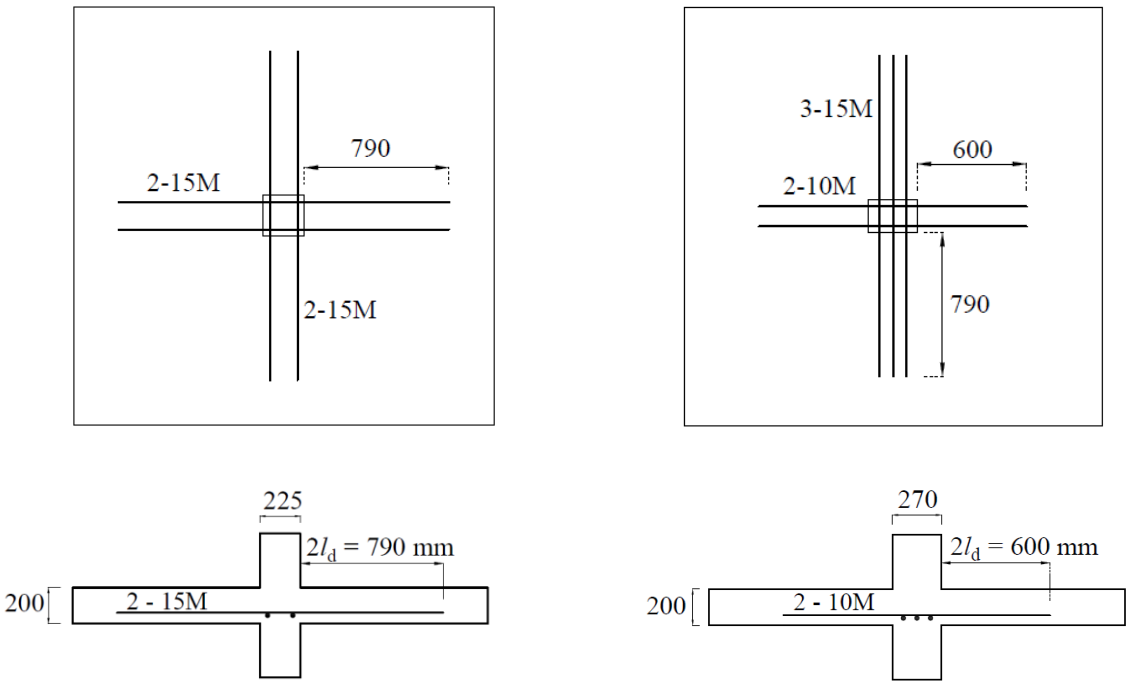

(a) Specimen SS (b) Specimen RS

Fig. 3.4. Details of structural integrity reinforcement in specimens SS and RS (dimensions in mm)

The structural integrity reinforcement in specimen D1 consisted of two 15M bars passing through the column in each direction and was placed in the bottom of the drop panel with a 25 mm clear cover. These bars extended a distance of $2\ell_d$ from the column face (see Fig. 3.5(a)). Specimen D2 contained four 10M structural integrity bars in both directions that were placed at the same level as the bottom mat of reinforcement in the 160 mm thick slab. It is noted that only two bars in each direction passed through the column while the other two bars were placed in the region of the punching shear cone assuming a 45 degree shear failure plane (see Fig. 3.5(b)). These bars extended a distance of $2l_d$ from their intersection with the punching shear failure plane. The purpose of this arrangement of structural integrity reinforcement was to demonstrate

the need for this reinforcement to pass directly through the column in order to be fully effective after punching failure.

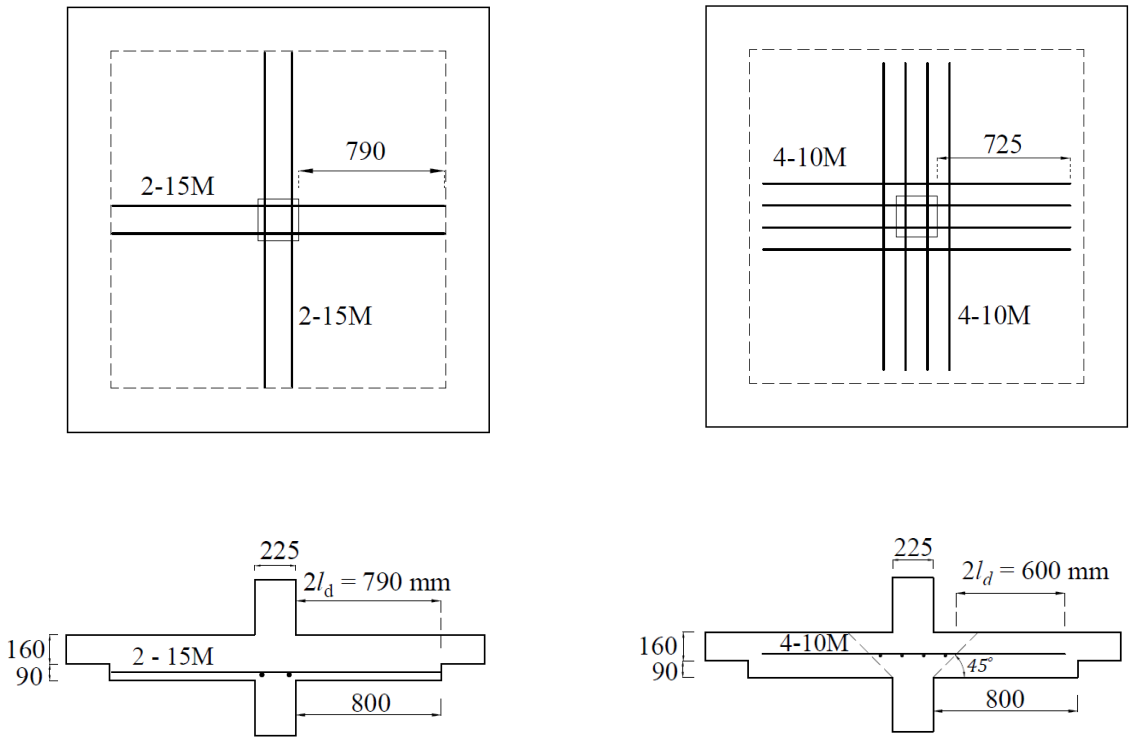

(a) Specimen D1 (b) Specimen D2

Fig. 3.5. Details of structural integrity reinforcement in specimens D1 and D2 (dimensions in mm)

Fig. 3.6 shows the slab reinforcement for specimens SS and RS in the formwork just before casting the concrete. Fig. 3.7 shows the reinforcement layout for specimens D1 and D2 that had drop panels. For all of the slab-column specimens, the column reinforcement consisted of 4 15M vertical bars and 10M ties at a spacing of 100 mm. The clear concrete cover measured to the ties was 25 mm.

(a) Specimen SS

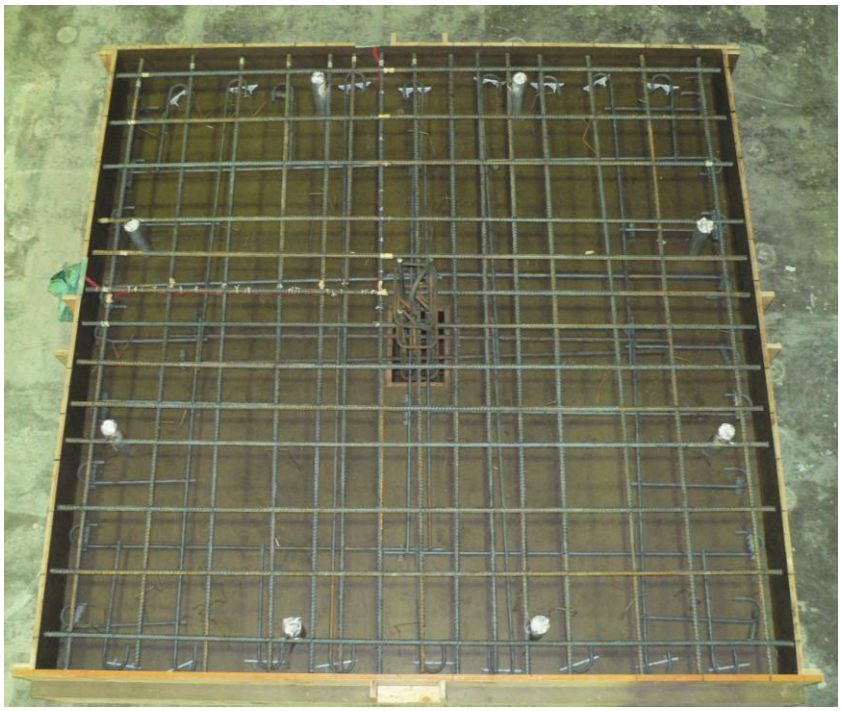

(b) Specimen RS

Fig. 3.6. Photo of reinforcing steel layout in specimens SS and RS

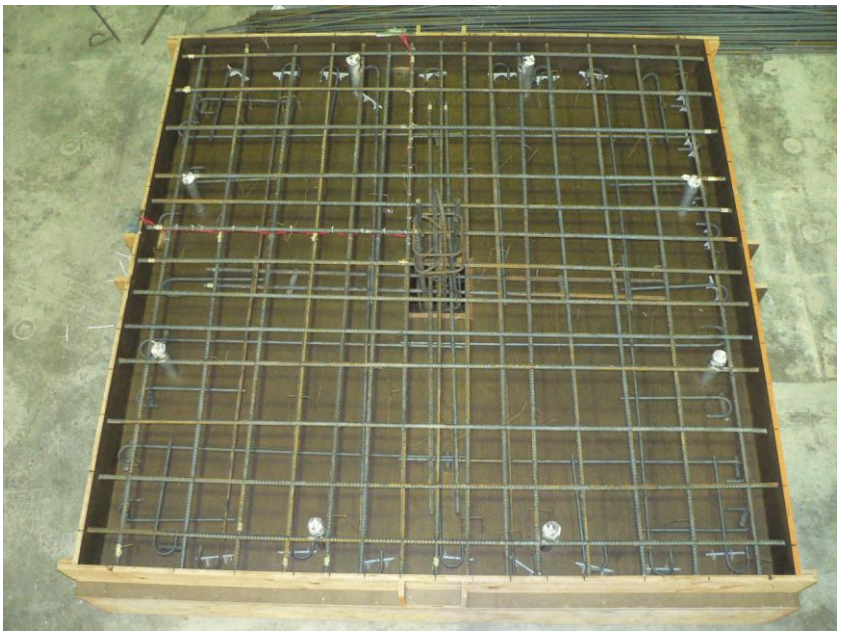

(a) Specimen D1

(b) Specimen D2

Fig. 3.7. Photo of reinforcing steel layout in specimens D1 and D2

3.4 Material Properties

3.4.1 Reinforcing Steel

Grade 400 MPa steel reinforcing bars were used in all of the specimens. Three random tension coupons of each bar size were tested with accordance with ASTM A370-08 (ASTM 2008) to determine values of the yield strength (f_y),yield strain (ε_y), ultimate strength (f_u), ultimate strain (ε_u), , and the strain at strain hardening (ε_{sh}).The average values are reported in Table 3.1. Typical stress-strain responses of the 15M and 10M reinforcing bars are shown in Fig. 3.8.

Table 3.1. Steel reinforcement mechanical properties

Bar Size	Area mm^2	f_y MPa	ε_y %	ε_{sh} %	f_u Mpa	ε_u %
10M	100	460	0.23	0.75	730	13
15M	200	420	0.21	0.50	723	13

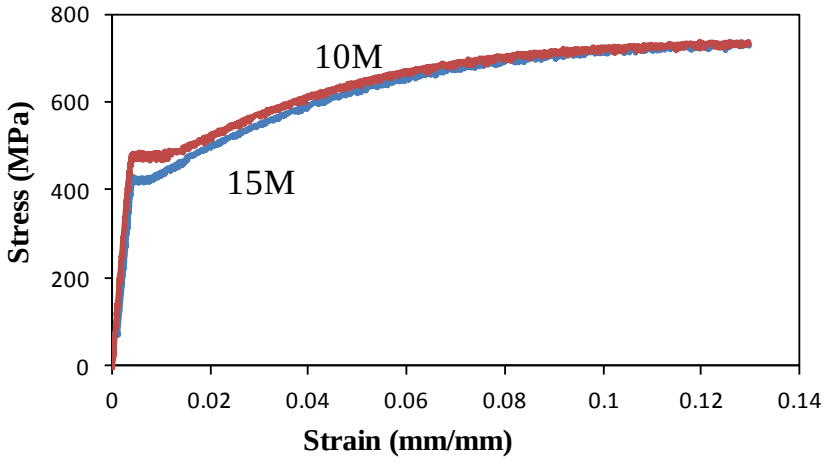

Fig. 3.8. Typical stress-strain curve of reinforcing steel

3.4.2 Concrete

The ready-mix concrete was obtained from a local supplier and the concrete was cast in the Structures Laboratory (see Fig. 3.9). The concrete mix design is summarized in Table 3.2. It is noted that it was desired to have a relatively low compressive strength of about below 30 MPa and hence a relatively high water-to-cementitious material ratio of 0.55 was used by the supplier. Specimens SS and RS were cast together and specimens D1 and D2 were cast using a different batch of concrete with the same mix design.

Three standard 100 × 200 mm cylinders were used to determine the mean value of the concrete compressive strength, f_c', and the splitting tensile strength, f_{sp} . Three flexural beams with dimensions 100 × 100 × 400 mm were used to determine the modulus of rupture, f_r , from four-point loading tests. All cylinders and beam specimens were moist-cured until material testing was performed. Tables 3.3, 3.4, 3.5 and 3.6 provide the material properties based on average values of each test performed on 3 samples for each specimen. Different values of concrete properties are reported because specimen SS was tested at an age of 28 days, while specimen RS was tested at an age of 67 days. Similarly, specimen D1 was tested at an age of 28 days, while specimen D2 was tested at an age of 36 days. The concrete used for specimens D1 and D2 had lower strengths than that used for specimens SS and RS. A typical compressive stress-strain curve of the concrete for specimen SS is shown in Fig. 3.10.

Fig. 3.9. Casting concrete

Table 3.2. Concrete mix design

Components	**Quantity**
Cement, Type GU	223 kg/m^3
SCM, Type F Fly Ash	57 kg/m^3
Sand	901 kg/m^3
Coarse aggregate, 20 mm max.	548 kg/m^3
Coarse aggregate, 14 mm max.	449 kg/m^3
Water	154 L/m^3
Air	60 L/m^3
Air entraining agent	0.09 L/m^3
Retarding agent	0.1 L/m^3
Accelerating agent	-
Water reducing agent	0.53 L/m^3

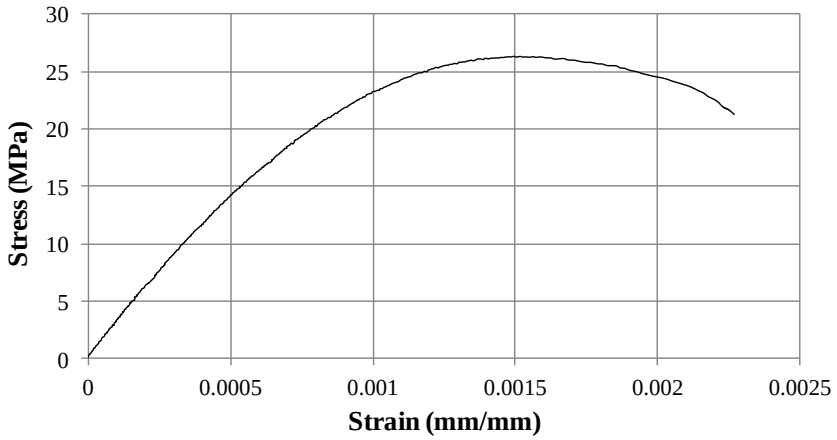

Fig. 3.10. Typical concrete compressive stress-strain (specimen SS)

Table 3.3. Concrete properties for specimen SS

Specimen SS	f_c' MPa	f_{sp} MPa	f_r MPa
#1	27	3.00	2.70
#2	25	3.31	3.87
#3	26	3.74	3.81
Average	26	3.35	3.46

Table 3.4. Concrete properties for specimen RS

Specimen RS	f_c' MPa	f_{sp} MPa	f_r MPa
#1	31	3.26	4.00
#2	30	3.47	3.95
#3	30	2.76	3.71
Average	30	3.16	3.88

Table 3.5. Concrete properties for specimen D1

Specimen D1	f_c' MPa	f_{sp} MPa	f_r MPa
#1	23	2.68	4.45
#2	22	2.49	4.06
#3	22	2.54	3.96
Average	22	2.60	4.16

Table 3.6. Concrete properties for specimen D2

Specimen D2	f_c' MPa	f_{sp} MPa	f_r MPa
#1	22	2.97	4.33
#2	21	2.84	4.12
#3	22	2.73	4.26
Average	22	2.90	4.23

3.5 Test Set-Up

The loading apparatus and test setup are shown in Figs.3.11 and 3.12. The lower column stub of the specimen rested on a steel pedestal. A uniformly distributed load on the test specimen was simulated by eight loading points on slab surface near the points of contraflexure in the two-way prototype structure. The loading points on either side of the slab are 2000 mm apart. The locations of the loading points are shown in Figs. 3.11, 3.12 and 3.13. For each pair of loading points, steel distribution beams that spanned 750 mm between adjacent loading points were used below the slab. Each beam distributed the load to the top surface of the slab using two 19 mm diameter high-strength threaded steel rods. Eight 100 × 100 ×19 mm steel plates were used to provide a bearing area on the slab surface at the loading points. Four hydraulic jacks were

connected to a single hydraulic pump to load the slab. Four load cells were placed under the hydraulic jacks to measure the load applied by each jack. Each jack was connected to a steel distribution beam using a 25.4 mm high-strength steel threaded rod located a distance of 1000 from the centre of the column (see Fig. 3.11).

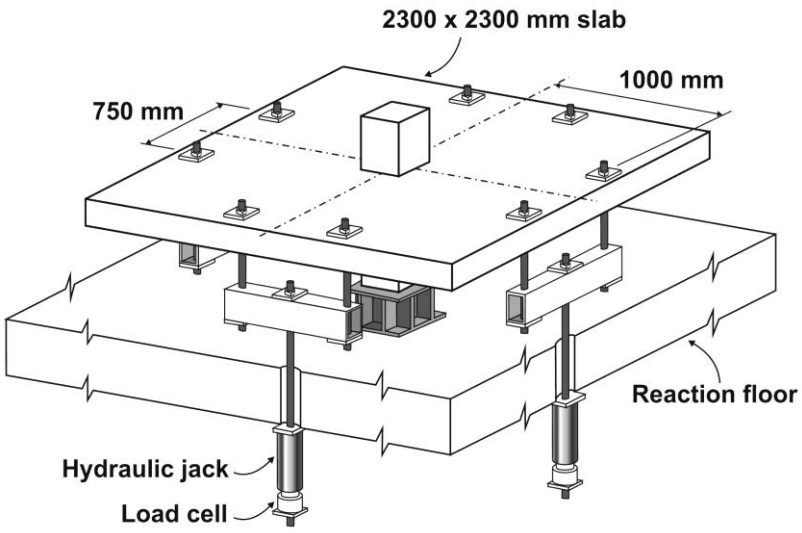

Fig. 3.11. Test specimen and loading apparatus

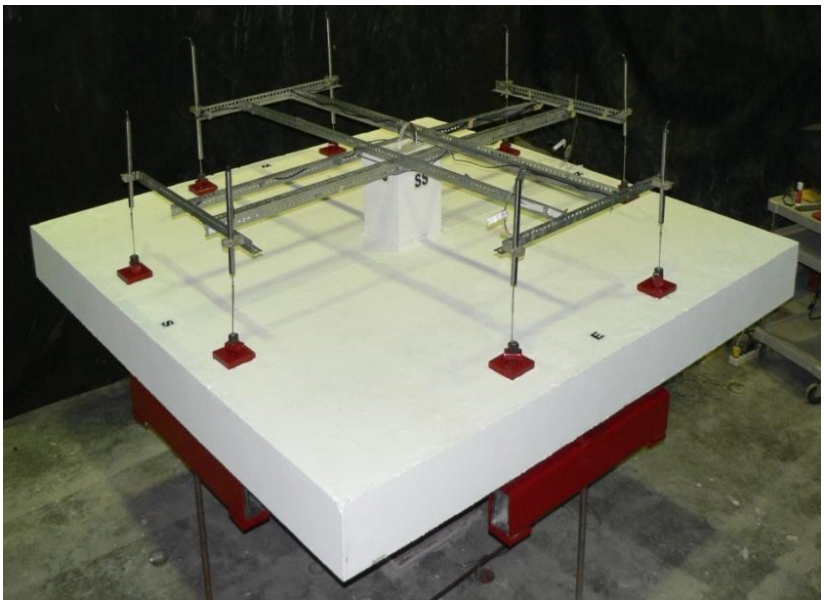

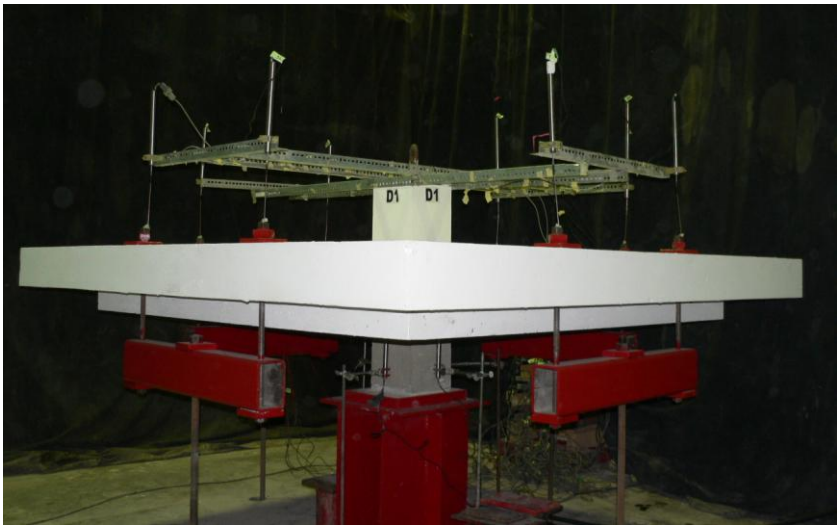

Fig. 3.12. Photo of LVDT locations and test Set-Up

3.6 Instrumentation

Electrical resistance strain gauges on one-half of the top bars in the two principal directions measured strains at the locations in line with the faces of the column. The gauges had an

electrical resistance of 120 ohms and had a 5 mm long gauge length. The strain gauge locations for all specimens are shown in Fig. 3.13. The deflections of the slab were measured by using linear voltage differential transformers (LVDTs) at each loading point. Strain gauges and LVDTs were connected to the computer system which automatically recorded strain and deflection for the entire testing duration.

3.7 Test procedure

Load was applied in small increments of approximately 40 kN with "load control" until punching failure occurred and then "deflection control" was used for the remainder of the test. In each increment, the loads, deflections and strains were recorded. The crack widths on the top surface of the slab were measured and the crack pattern was recorded at each load stage up until punching shear failure occurred. Testing was continued well after the punching shear failure occurred as the structural integrity reinforcement resisted the applied loads. Testing continued until a displacement of about equal to the slab thickness was attained.

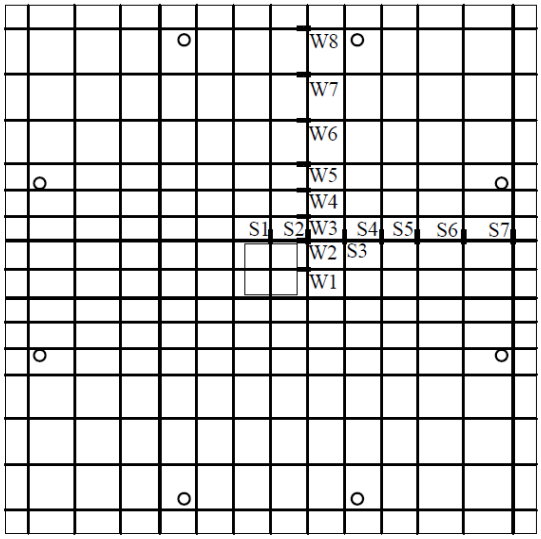

(a) Specimen SS

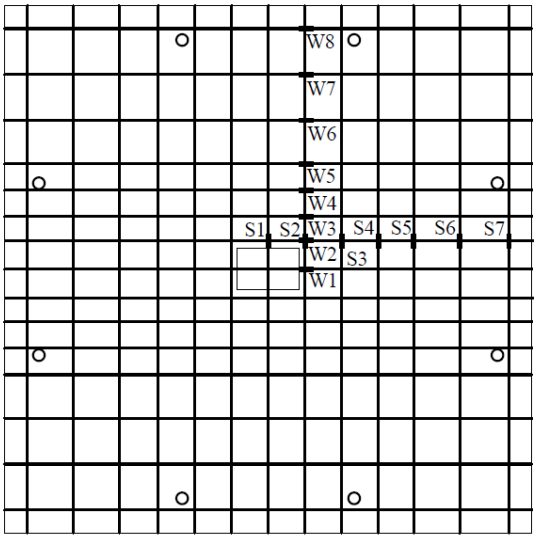

(b) Specimen RS

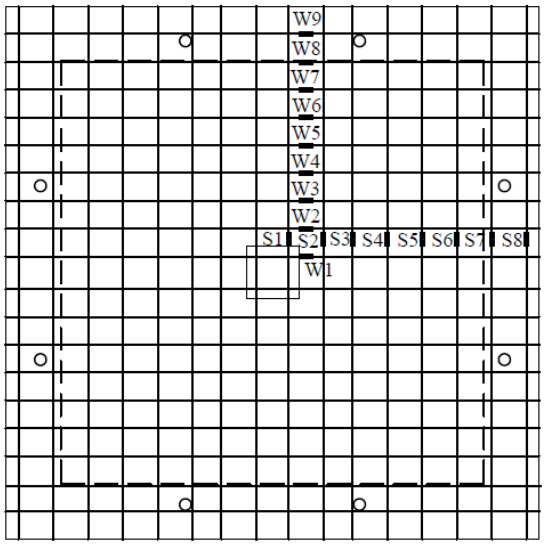

(c) Specimen D1

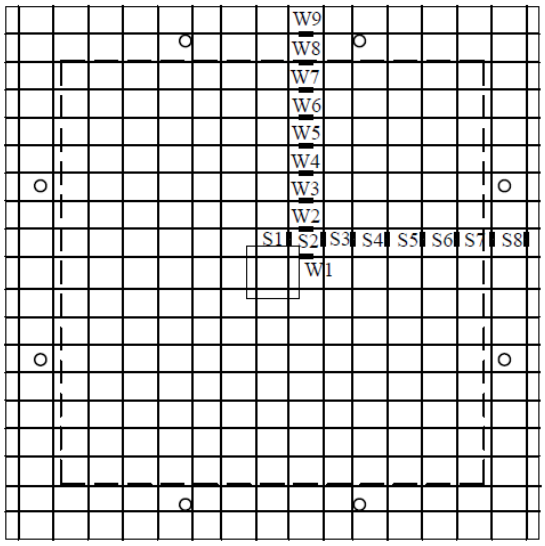

(d) Specimen D2

Fig. 3.13. Locations of strain gauges and loading points

Chapter 4: Responses of Test Specimens

4.1 Introduction

The results of four full-scale test specimens (SS, RS, D1 and D2) are reported. The measured total loads and average deflections at key stages in the loading of each specimen are presented in separate tables. The key stages in the loading included first cracking loads, loads at yielding of the reinforcing steel, shears causing punching shear failures, maximum post-punching loads and the ultimate deflections taken as the average deflection when the post-punching load drops below 80% of the maximum post-punching load.

The total load calculated was determined from the sum of the eight applied loads plus the self-weight of the test specimen and the weight of loading apparatus. The average deflection is the average of the measured deflections at the eight loading points.

4.2 Specimen SS

4.2.1 Test Description

Fig. 4.1 shows the total load versus average deflection response for specimen SS and Table. 4.1 summarizes the total loads and corresponding average deflections at key stages in the loading of specimen SS. Specimen SS was a 2300 × 2300 mm flat plate with a thickness of 200 mm and 225 mm square column. The specimen had two 15M bars passing through the column in each direction as structural integrity reinforcement.

First flexural cracking was observed near the corners of the column at load stage 4 with a corresponding shear load of 146 kN and resulted in change of stiffness in the load-displacement response. As the load increased, the cracks grew both in length and width and extended the full

width of the specimen. Fig. 4.2 shows that at service load level (267 kN) the cracks extended across the full width of the slab (stage 7).

First yielding of the top reinforcement occurred in a bar in the upper layer of the top mat, with the bar passing through the column (strain gauge S1) at a total load of 347 kN with a corresponding average deflection of 6 mm. At this stage, extensive cracking occurred in the slab before punching shear failure occurred (see Fig. 4.3).

The punching-shear failure occurred at a total applied shear of 527 kN and a corresponding average displacement of 12 mm. After punching shear failure the slab exhibited a considerable drop in load to 213 kN with a corresponding deflection of 18 mm. The top surface of the slab soon after punching shear failure is shown in Fig. 4.4.

Loading continued after punching shear failure with a significant loss in stiffness. As the slab displaced downwards, relative to the column, the top bars experienced tension and tended to rip out of the top surface of the slab due to the small cover (see Figs. 4.5 and 4.6). For typical slabs, designed in accordance with CSA A23.3-04 (CSA 2004), the top mat of bars rips out at an early stage in the post-punching response and offers little resistance, whereas only the structural integrity reinforcement is capable of providing significant post-punching resistance at very large displacements. The maximum post-punching shear load was 397 kN at a deflection of 61 mm. After this stage the test specimen was able to sustain large deflections while maintaining a load near its maximum post-punching resistance. There was a sudden drop in the load at load stage 38 at a shear of 318 kN and a corresponding deflection of 188 mm. This drop in load carrying capacity was due to the pullout of the upper layer of structural integrity reinforcement in N-S direction. Testing was stopped when the load dropped significantly and spalling of the concrete cover in the column was observed.

After testing was completed, the loose concrete was removed from top surface of the slab and the angle of inclination of the integrity reinforcement near the column face was measured. Table 4.2 presents the angles of the integrity bars measured from the horizontal in each direction. The average measured angle was 29 degrees which is close to the assumed value of 30 degrees for the design of the structural integrity reinforcement by the CSA A23.3-04 (CSA 2004) standard. Figs. 4.7 and 4.8 show the condition of the slab-column connection after testing and after cutting the reinforcement and removing the slab. The cover spalling immediately under the 15M bars (Fig. 4.8) illustrates the fact that significant forces are being transferred by the integrity bars to the column. Hence it is prudent to pass the integrity bars through the column core, rather than relying on the cover concrete in the column to provide support for these bars.

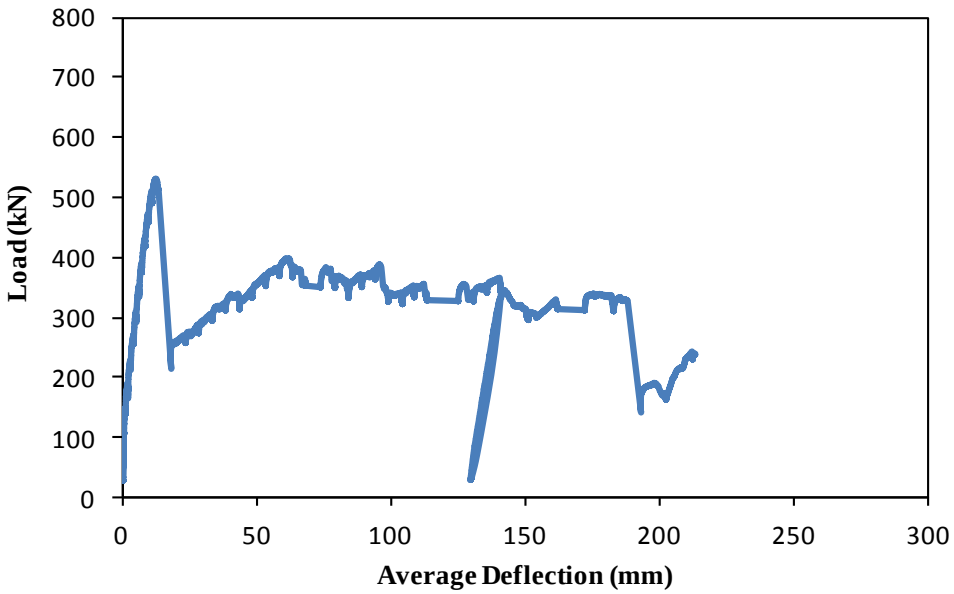

Fig 4.1. the total load versus average deflection response for specimen SS

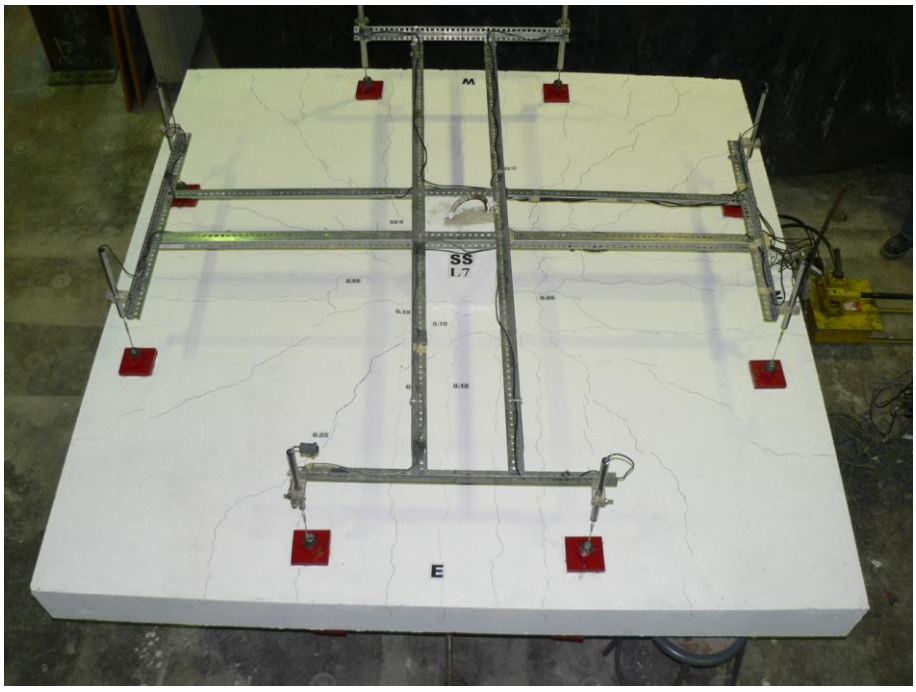

Fig. 4.2. Crack pattern in specimen SS at service load level

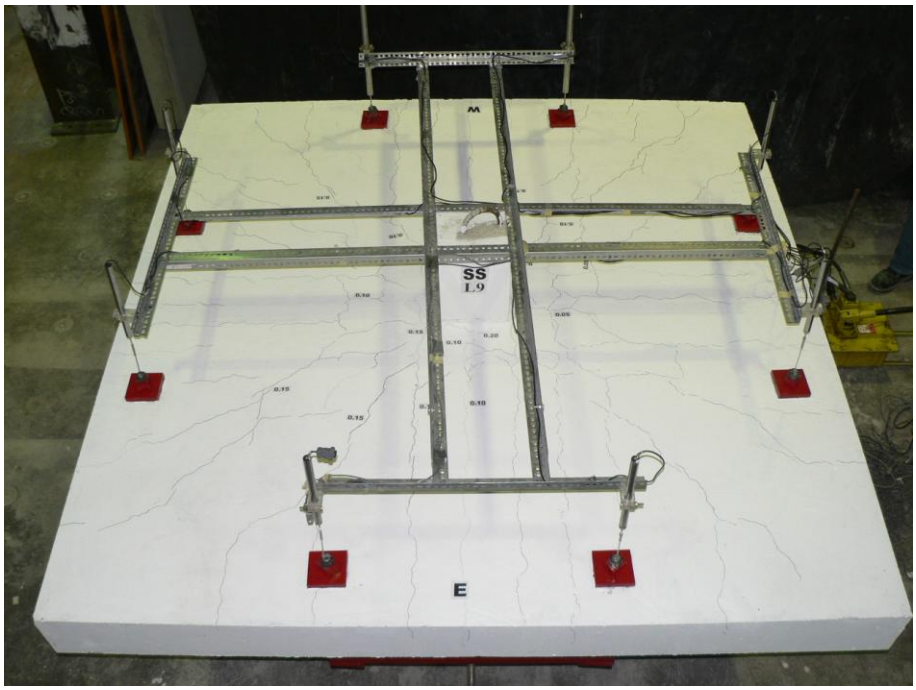

Fig. 4.3. First yielding of top reinforcement and extensive cracking of the slab before punching failure (specimen SS)

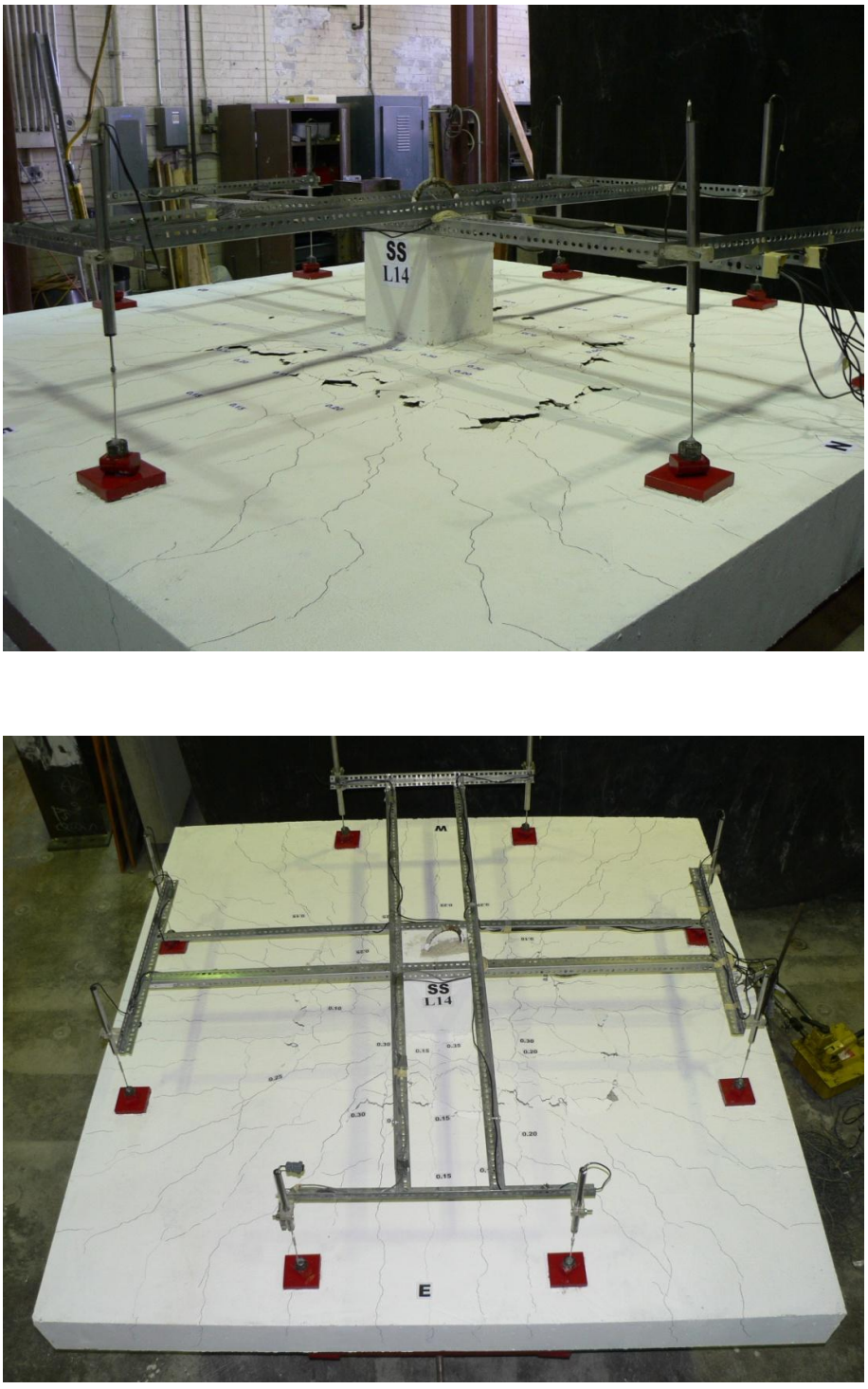

Fig. 4.4. Top surface of slab just after punching shear failure occurred (specimen SS)

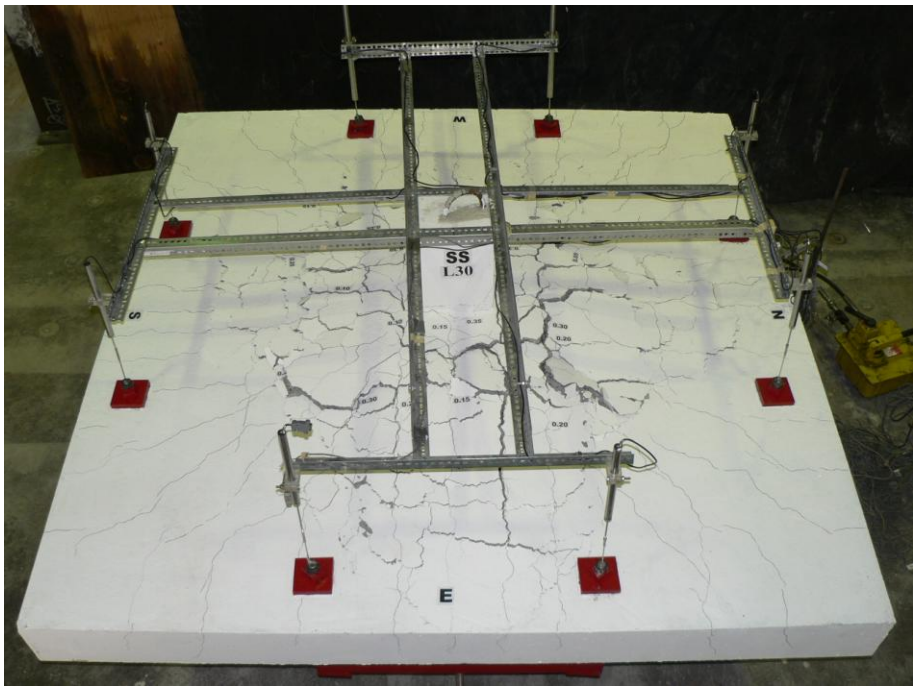

Fig. 4.5. Ripping out of top mat of reinforcement at a displacement of 98 mm (specimen SS)

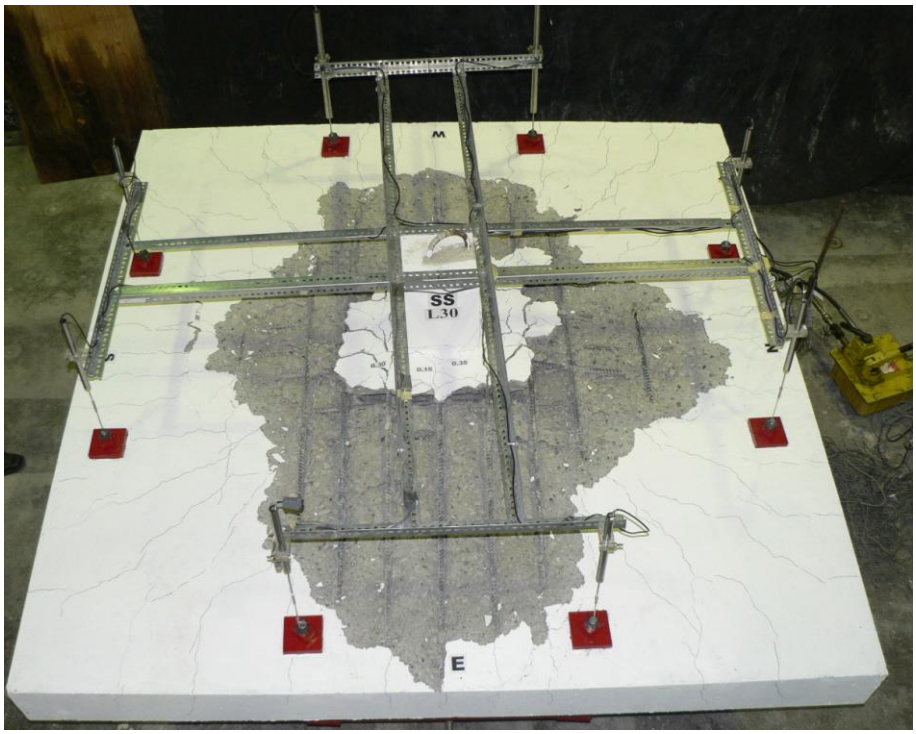

Fig. 4.6. Progressive ripping out of top steel after damaged concrete was removed at a displacement of 98 mm (specimen SS)

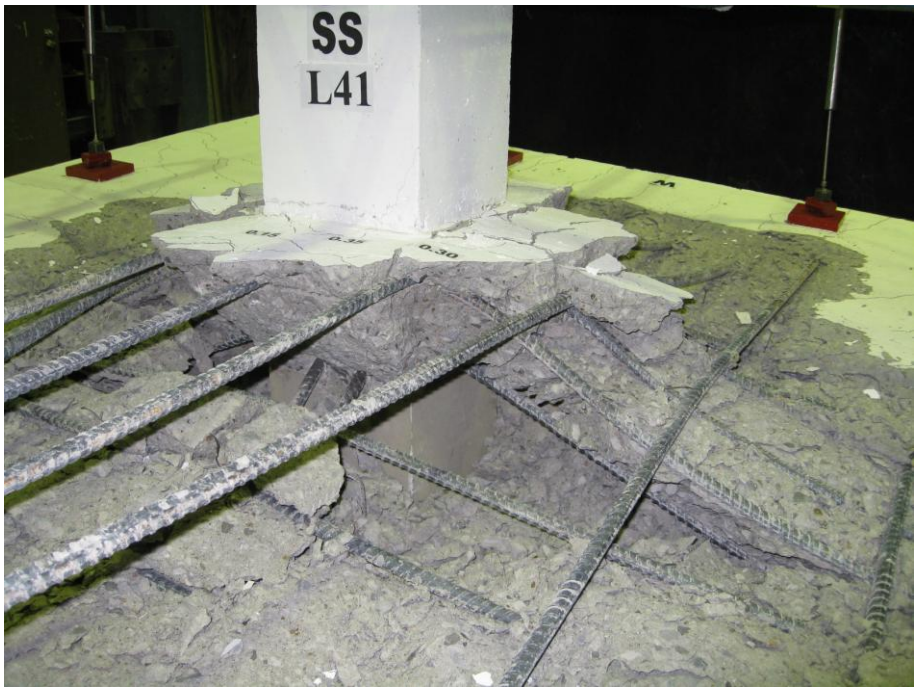

Fig. 4.7. Integrity reinforcing bars after testing completed (specimen SS)

Fig. 4.8. Integrity reinforcing bars after slab removal (specimen SS)

Table 4.1. Summary of key load stages in the testing of specimen SS

Stage	Load, kN	Deflection, mm
First Cracking	146	0.9
First Yield (Top Bars)	347	6
Punching Shear Failure	527	12
Maximum Post-punching Load	397	61
Ultimate Deflection	318	188

Table 4.2. Angle of structural integrity reinforcement of specimen SS

Direction	Angle of structural integrity reinforcement, degrees
North face	25
South face	27
East face	34
West face	30
Average	29

4.2.2 Top Reinforcement Strains

The top reinforcement in specimen SS, consisted of 15M bars in each direction with $f_y = 420\,\text{kN}$ and $\varepsilon_y = 0.21\%$. Locations of strain gauges in specimen SS are shown in Fig. 3.13 (a). The data collected from the strain gauges installed on both directions is presented in Figs. 4.9 and 4.10.At an applied shear of 347 kN the strain gauge readings indicated that the upper layer of the top

reinforcing steel was yielding. It is noted that due to the significant damage close to the column, some gauges near the column ceased working after punching shear failure occurred. Gauge S5 in the upper layer of the top mat was damaged during casting and hence no data is presented for this gauge. Figs. 4.9 and 4.10 show that the bars near the column experienced greater strain than the bars further from the column during the loading. The strains of top bars dropped off after punching shear failure. Fig. 4.11 shows the strain distributions in both layers of top reinforcement at the approximate service load level and at the punching shear failure level. The service load is assumed to be 267 kN, which is approximately 60% of the nominal predicted punching shear strength using the ACI Code (ACI Committee 318 2011) and the specified concrete compressive strength of 30 MPa. At the service load level, the maximum steel strain reached 0.0015 which is nearly 70% of the yield strain of the steel. The maximum steel strain at the punching shear failure level was 0.0045, that is about twice the yield strain. During the post-punching response the measured values from gauges S1 through S4 and W1 through W4 show these bars experienced considerably higher strains than the bars further from the column, indicating that the top bars closer to the column initially participate in the post-punching response.

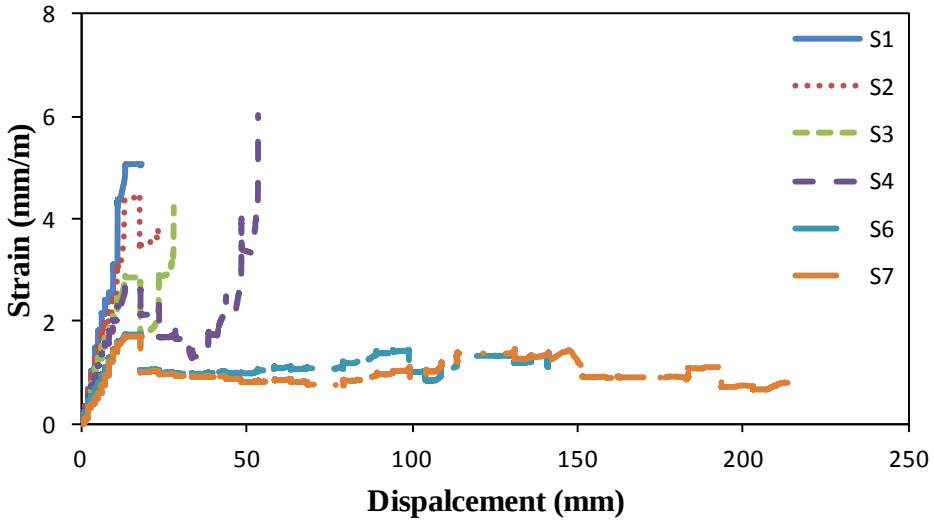

Fig. 4.9. Strain-displacement behaviour of upper layer of top mat (specimen SS)

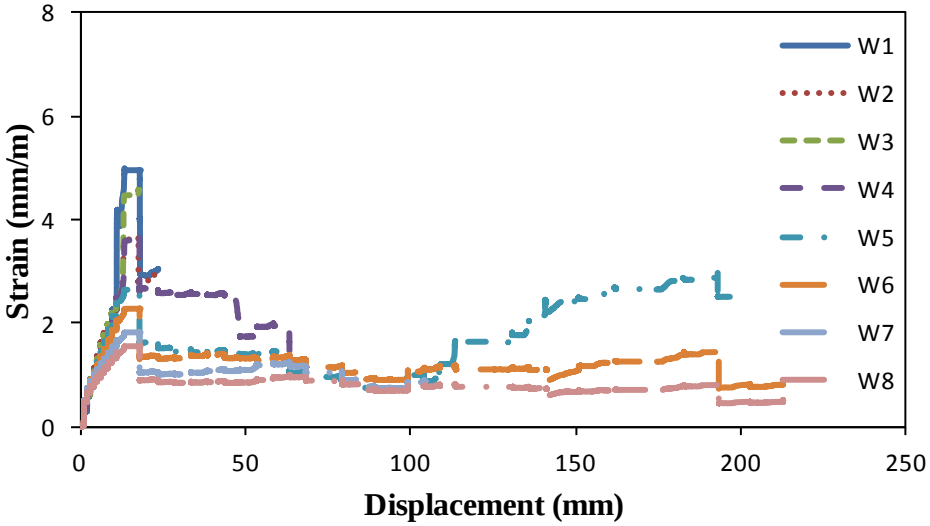

Fig. 4.10. Strain-displacement behaviour of lower layer of top mat (specimen SS)

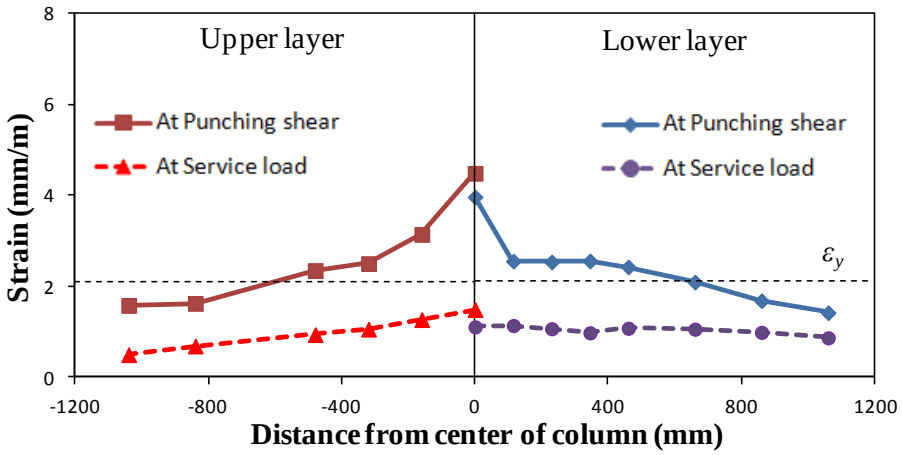

Fig. 4.11. Strain distribution of top mat at punching shear failure (specimen SS)

4.2.3 Concrete Cracking

The total load versus maximum crack width in the region within a distance of 1.5*d* from the column face ("interior cracks") and outside of this region ("exterior cracks") for Specimen SS is shown in Fig. 4.12. The crack widths on the top surface of the slab were measured at each load stage up until punching shear failure occurred. As can be seen from Fig. 4.12 the crack widths near outer edges of the specimen were initially larger than crack width near the column due to more concentrated distribution of top bars near the column. The maximum crack width was 0.35 mm when punching shear failure occurred. During the post punching shear response the cracks in the concrete near the edges of the slab specimen closed up which suggested that concrete near the outer edges of the slab were experiencing compression due to the fact that the bottom reinforcing bars in the slab, acting in tension, were anchored in this region.

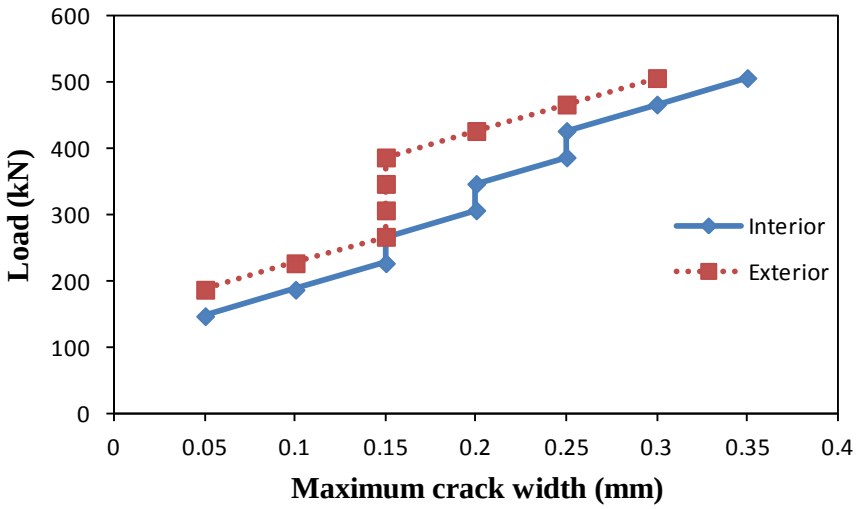

Fig. 4.12. Load versus maximum crack width for specimen SS

4.3 Specimen RS

4.3.1 Test Description

The total load versus deflection response of specimen RS is shown in Fig. 4.13 and a summary of the key load stages is presented in Table. 4.3. Specimen RS was a 2300 × 2300 mm flat plate with a thickness of 200 mm and with 180×270 mm rectangular column stubs. The structural integrity reinforcement consisted of three 15M bars in the direction perpendicular to the long face of the column and two 10M bars in the other direction.

The load-deflection curve exhibits a change in stiffness at load stage 4 when first cracking occurred at a load of 148 kN. Fig. 4.14 shows the crack pattern at service load level (267 kN) for specimen RS.

At load stage 10 with a total load of 355kN and corresponding average deflection of 6 mm, data from strain gauges showed that the top reinforcement was yielding near the column (strain gauge

S3). At this stage cracking around the column was extensive, forming a ring that is characteristic of impending punching shear failure (see Fig. 4.15).

At a shear of 527 kN and a corresponding average displacement of 12 mm abrupt punching shear failure occurred with a sudden drop in load. Fig. 4.16 shows the punching shear failure stage. The failure followed by an increase in resistance as the deflection increased due to the presence of the structural integrity reinforcement and the contribution of top reinforcement in the post-punching response.

After punching shear failure, as further load was applied, the progressive destruction of the concrete occurred and the top bars started to rip out of the top concrete surface. The top surface of the slab, after a number of top bars crossing the punching shear cone had ripped, out is shown in Figs. 4.17 and 4.18. At load stage 34, the maximum post-punching shear of 360 kN was reached at a corresponding average displacement of 51 mm. After this stage the specimen offered resistance over large displacements until a sudden drop occurred in the load at a deflection of 122 mm due to pullout of the structural integrity reinforcement. Testing was stopped when the structural integrity reinforcing steel was observed to pull out and the load dropped significantly. Loose concrete was removed from top surface of the slab and the angles of inclination of the structural integrity reinforcing bars from the horizontal plane were measured. Table 4.4 provides the measured angles of the integrity bars in each direction. The average measured angle was 29.5 degrees which is almost equal to the assumed value of 30 degrees by CSA code (CSA 2004). Fig 4.19 shows the inclination of the structural integrity reinforcement at large slab displacements after testing was stopped. For further inspection the structural integrity reinforcement was cut off near the column face. Fig. 4.20 shows the condition of the slab-column connection after cutting the reinforcement and slab removal.

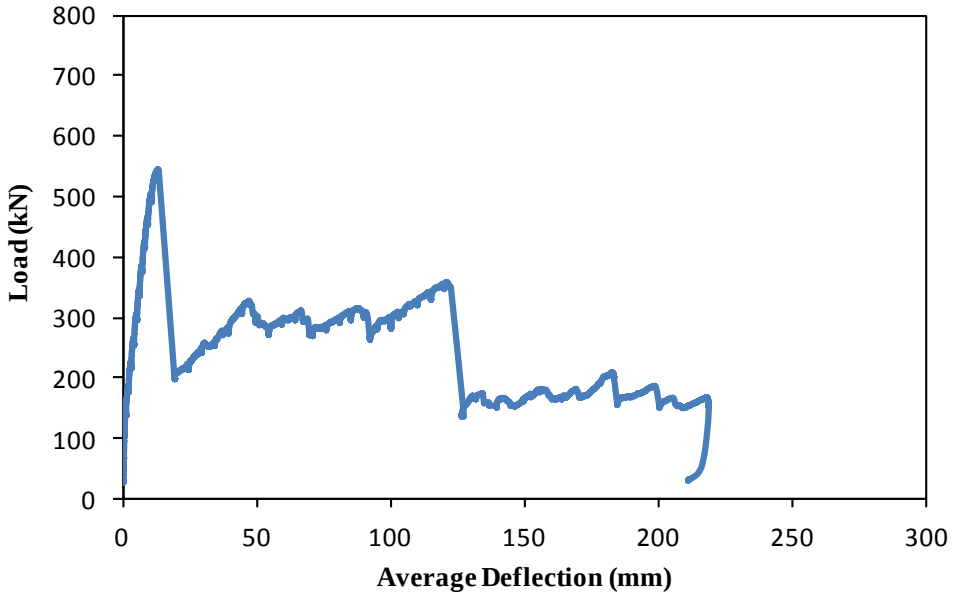

Fig 4.13. Total load versus average deflection response for specimen RS

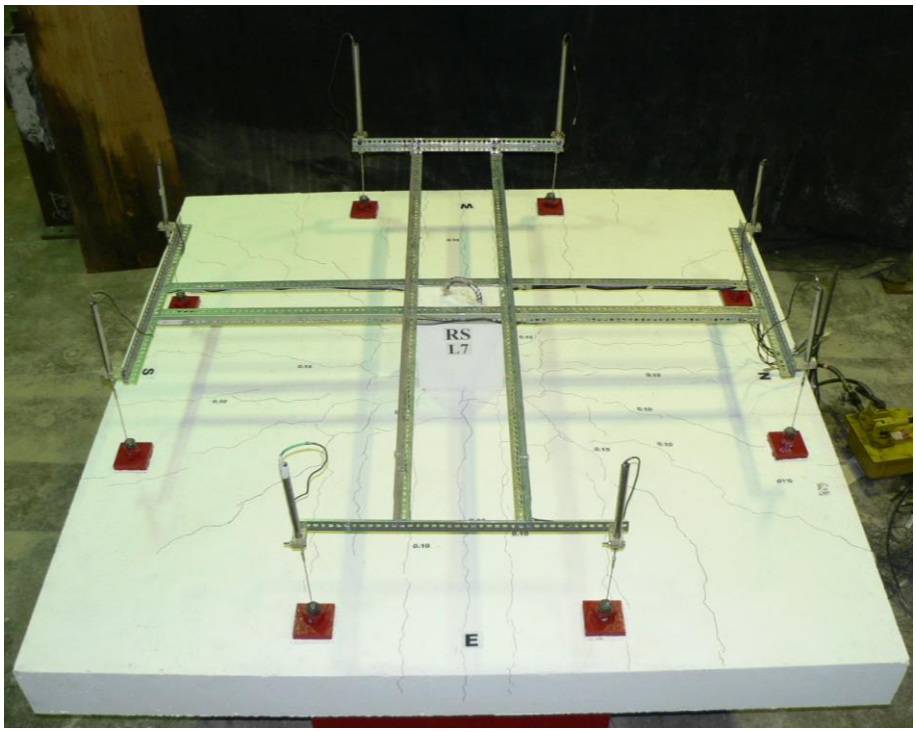

Fig. 4.14. Crack pattern in specimen RS at service load level

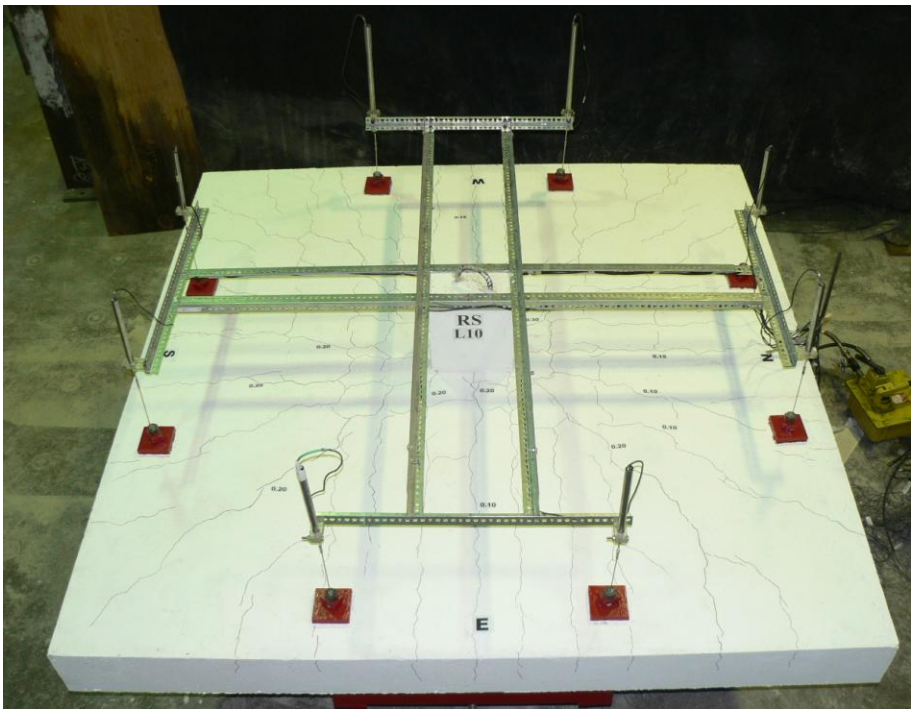

Fig. 4.15. First yielding of top reinforcement and extensive cracks around column before punching failure (specimen RS)

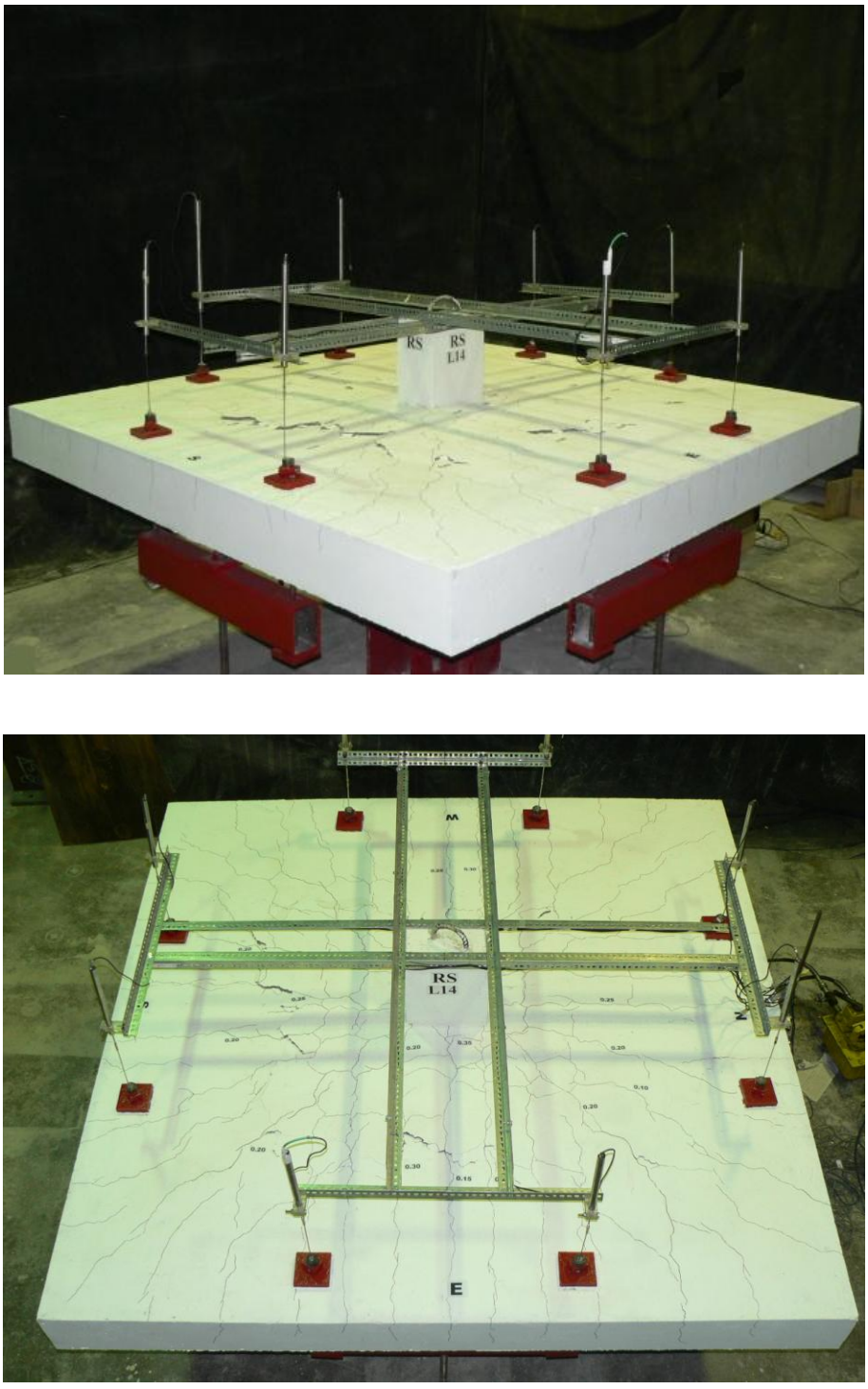

Fig. 4.16. Top surface of slab just after punching shear failure (specimen RS)

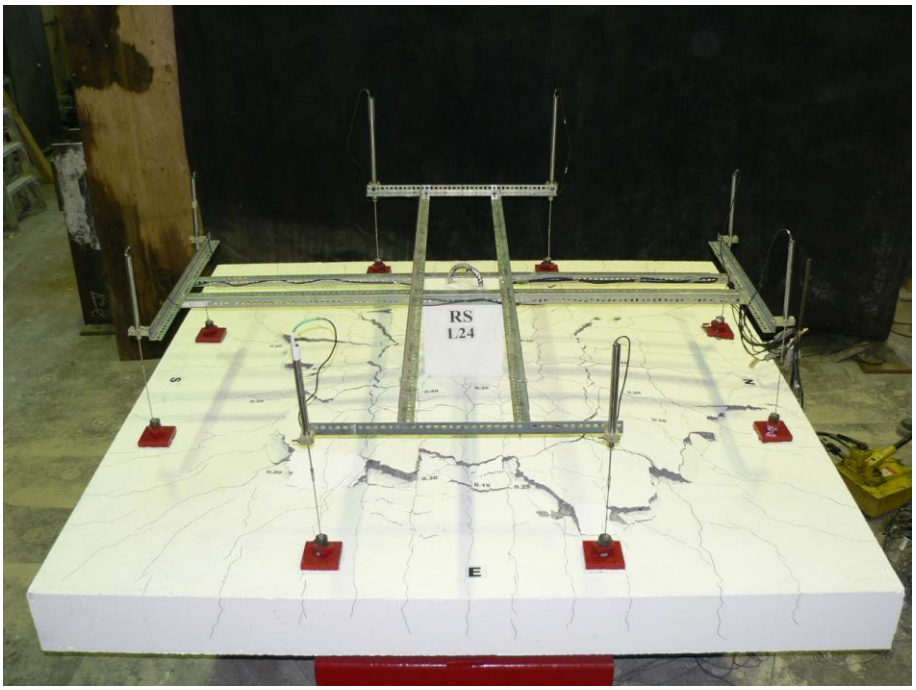

Fig. 4.17. Progressive destruction of concrete and ripping out of top mat of reinforcement at a displacement of 70 mm (specimen RS)

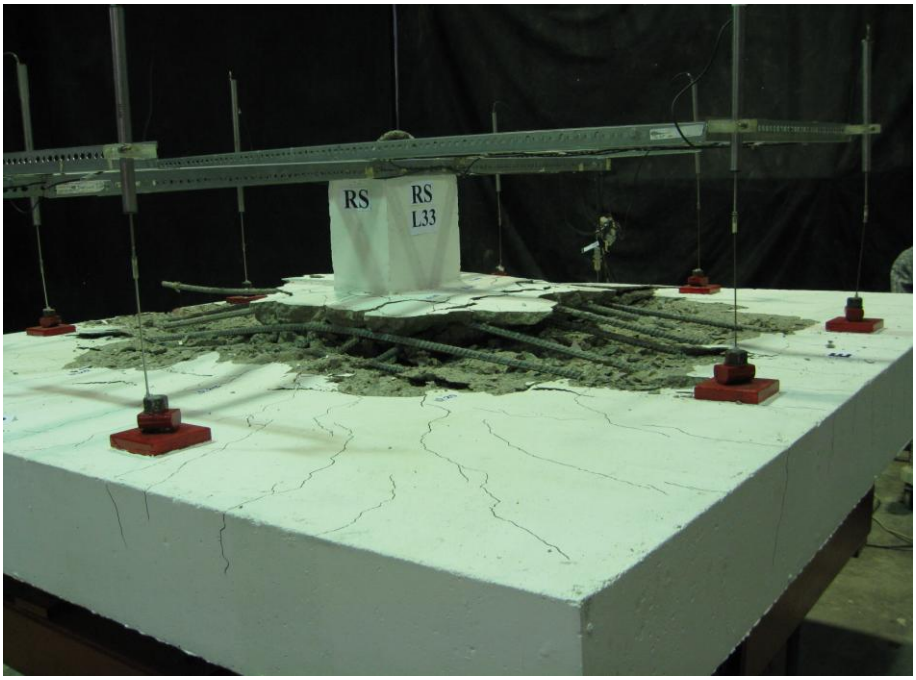

Fig. 4.18. Progressive ripping out of top steel after damaged concrete was removed at a displacement of 114 mm (specimen RS)

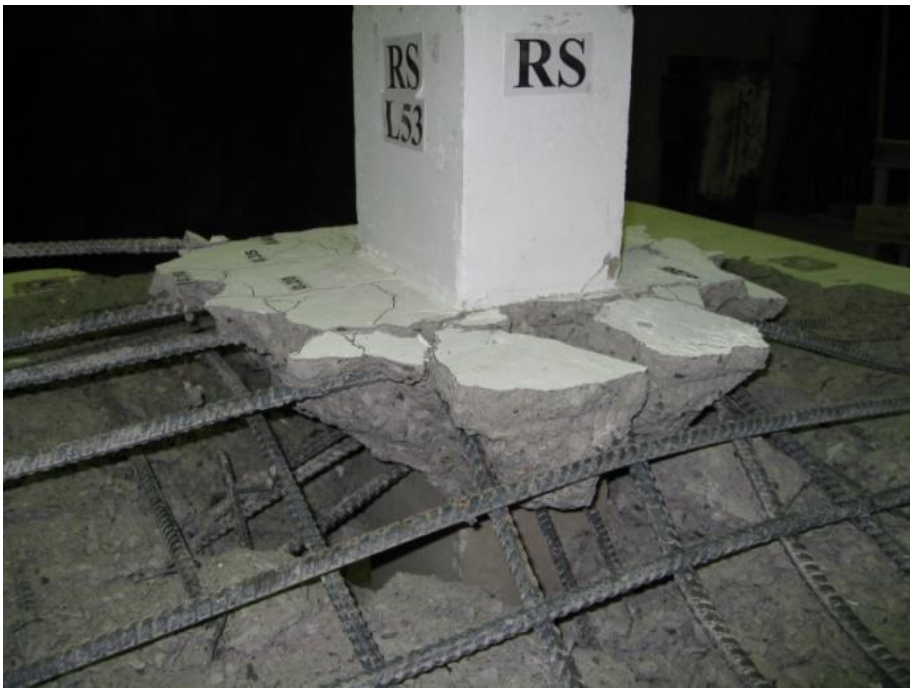

Fig. 4.19. Inclination of structural integrity reinforcement in specimen RS after testing completed

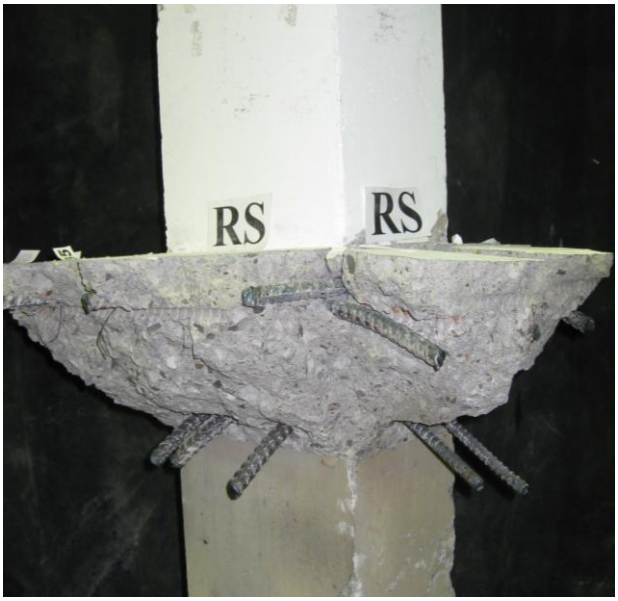

Fig. 4.20. Integrity reinforcing bars after slab removal (specimen RS)

Table 4.3. Summary of key load stages in test of specimen RS

Stage	Load, kN	Deflection, mm
First Cracking	148	0.8
First Yield (Top Bars)	355	6
Punching Shear Failure	547	13
Maximum Post-punching Load	360	51
Ultimate Deflection	288	122

Table 4.4. Measured angles of structural integrity bars for specimen RS

Direction	Angle of structural integrity reinforcement, degrees
North	25
South	32
East	29
West	32
Average	29.5

4.3.2 Top Reinforcements Strains

The top reinforcement in specimen RS, consisted of 15M bars in each direction with $f_y = 420\,\text{kN}$ and $\varepsilon_y = 0.21\%$. Locations of the strain gauges in the specimen are shown in Fig. 3.13 (b). Figs. 4.21 and 4.22 present the measured values of the strains in the upper layer and lower layer of top

reinforcement. Gauge W7 in the lower layer of the top mat was damaged during casting and hence no data was presented for this gauge. It is noted that due to the significant damage close to the column, some gauges near the column ceased working after punching shear failure occurred. The first yield was recorded in gauge S3 near the column in the upper layer of the top mat at a corresponding shear of 355 kN. As can be seen from Figs. 4.21 and 4.22 the measured values from the gauges near the column were higher than those further from the column. The strain distributions in both layers of top reinforcement at the approximate service load level and at the punching shear failure level are shown in Fig. 4.23. The service load is assumed to be 267 kN, which is approximately 60% of the nominal predicted punching shear strength using the ACI Code (ACI Committee 318 2011) and the specified concrete compressive strength of 30 MPa. The maximum steel strains were 0.0014 and 0.0064 at the service load level and the punching shear failure level, respectively. As shown in Figs. 4.21 and 4.22 the bars closer to the column experienced greater strains than other bars during the post-punching response indicating that these bars participate in the initial post-punching response.

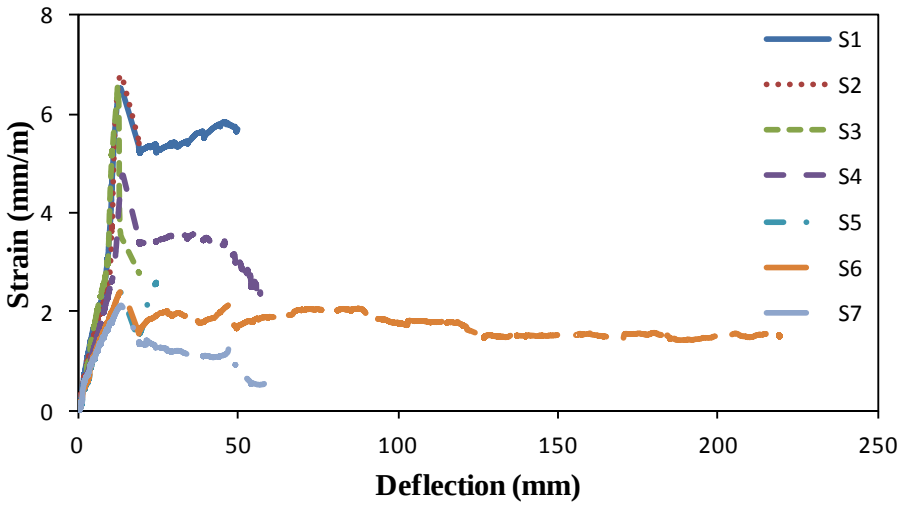

Fig. 4.21. Strain-displacement behaviour of upper layer of top mat (specimen RS)

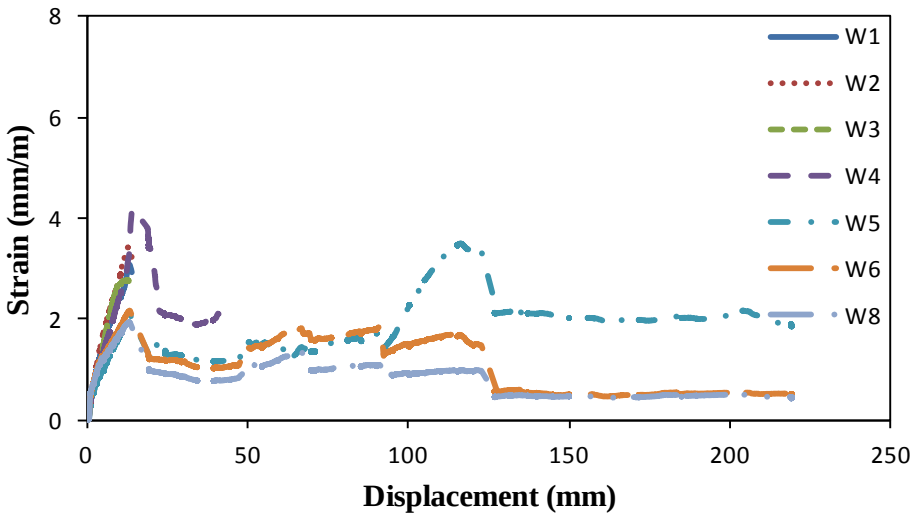

Fig. 4.22. Strain-displacement behaviour of lower layer of top mat (specimen RS)

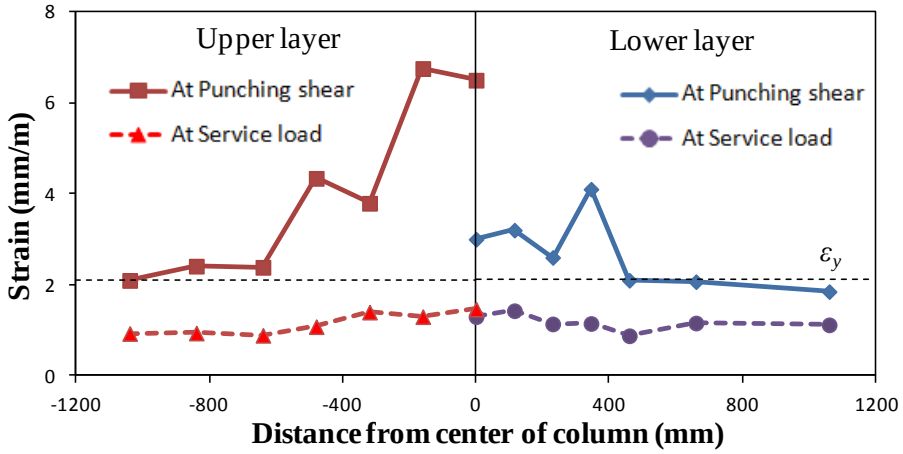

Fig. 4.23. Strain distribution of top mat at punching shear failure (specimen RS)

4.3.3 Concrete Cracking

Fig. 4.24 illustrates the total load versus maximum crack width in the region within a distance of 1.5*d* from the column face ("interior cracks") and outside of this region ("exterior cracks") for Specimen RS until punching shear failure occurred. The maximum crack width was 0.40 mm at

punching shear failure, occurring in the interior region near the column. After punching shear failure the exterior cracks near the edges of the specimen closed up indicating that this region goes into compression during the post-punching response.

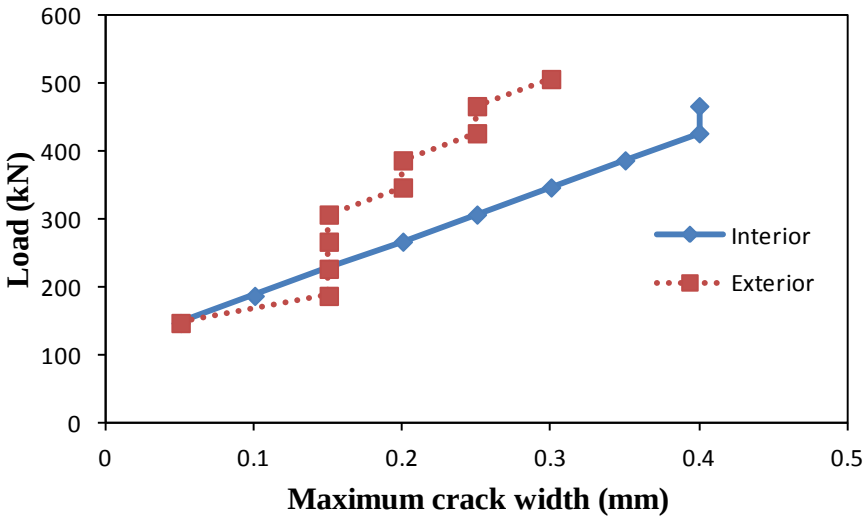

Fig. 4.24. Load versus maximum crack width for specimen RS

4.4 Specimen D1

4.4.1 Test Description

Specimens D1 had a 2300 × 2300 × 160 mm thick slab with a 1825 × 1825 × 90 mm thick drop panel and 225 mm square column stubs. The structural integrity reinforcement in specimen D1 consisted of two 15M bars passing through the column in each direction and was placed in the bottom of the drop panel. Fig. 4.25 shows the total load versus average deflection response for specimen D1.

The load-deflection response was stiffer up to first cracking at a load of 179 kN. The first cracks occurred in the North-South direction, perpendicular to the lower layer of top reinforcement. As

the load increased the cracks propagated toward the edges of the slab. Fig 4.26 shows the crack pattern at service load level (396 kN). First yielding occurred in the third bar from the centre of the specimen in the lower layer of the top mat (gauge W3) at a total load of 554 kN and a corresponding average deflection of 5.0 mm. Fig. 4. 27 shows the top surface of the slab after first yielding of the top reinforcement. At this stage the extensive cracks before punching failure are evident.

Before abruptly failing in punching shear, the specimen reached an ultimate load of 728 kN and a corresponding deflection of 7 mm. After punching-shear failure, the slab-column connection experienced a sudden drop in load to 204 kN and an increase in deflection to 14 mm. Fig. 4.28 shows the punching shear failure stage for specimen D1. After failure, a different resisting mechanism was set up to offer resistance involving both the top bars that cross the punching shear cone and the bottom structural integrity reinforcement. Hence the slab was still able to carry further load after punching shear failure. The upper layer of top bars ripped out first from the top surface of the slab in the East direction at a total load of 430 kN with a corresponding average deflection of 46 mm. The ripping out of the top mat of reinforcement continued relatively equally in the N-S and E-W directions as the slab displaced downward. Figs. 4.29 and 4.30 show the progressive ripping out of top bars from the top surface of the slab in specimen D1. The slab offered resistance over large displacements until the maximum post-punching shear load, 519 kN, was reached with a corresponding average deflection of 155 mm. Testing was stopped when the load dropped significantly and local crushing and splitting of the column cover immediately below the structural integrity bars was observed. Figs. 4.31and 4.32 show the inclination of the structural integrity reinforcement and the condition of the slab-column connection at large slab displacements after the testing was completed. Table. 4.5 summarizes

the total load and corresponding average deflection at key stages for specimen D1. After concrete was removed from around the column, the angles of inclination of the structural integrity reinforcement were measured and the results are presented in Table. 4.6.

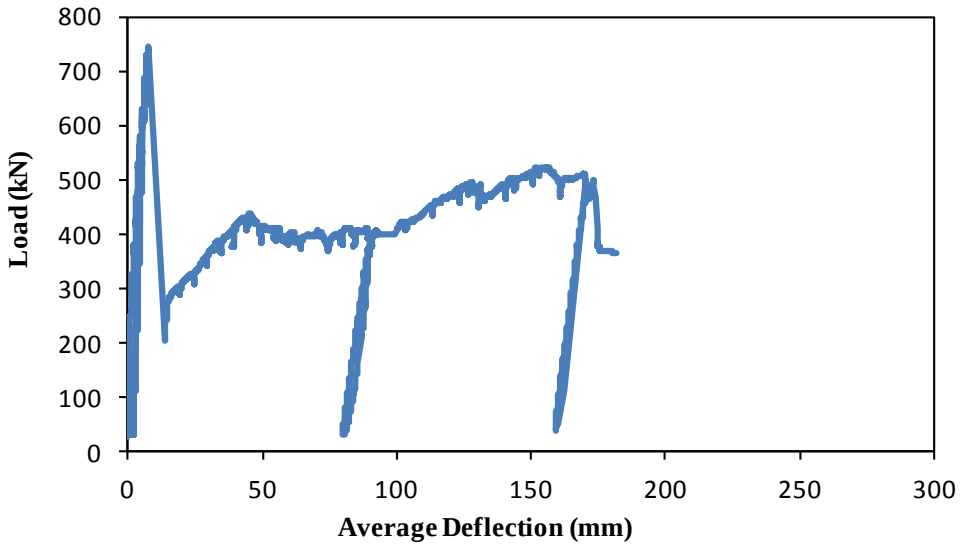

Fig 4.25. Total load versus average deflection response for specimen D1

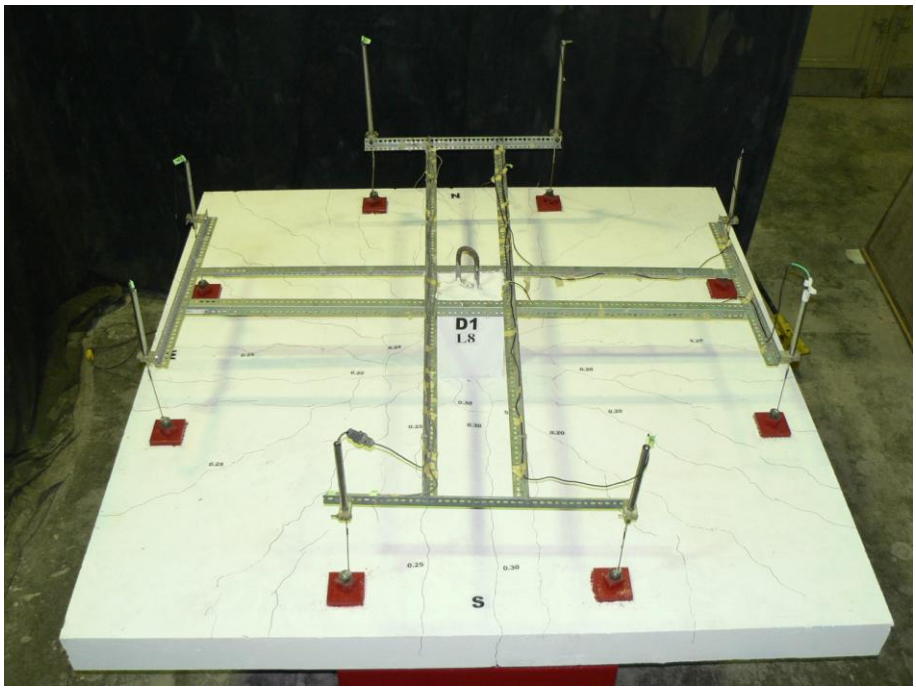

Fig. 4.26. Crack pattern in specimen D1 at service load level

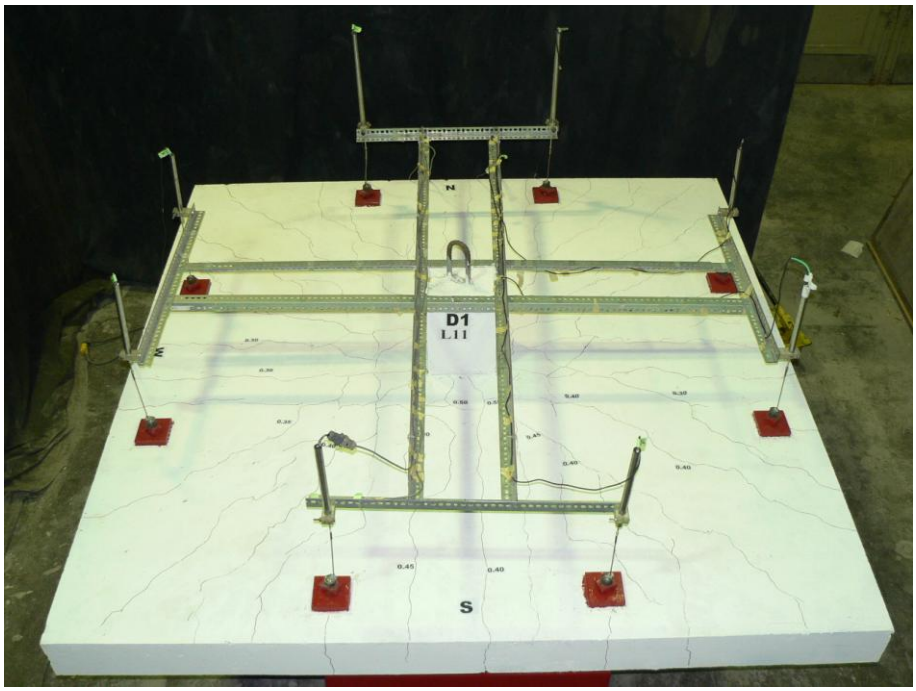

Fig. 4.27. First yielding of top reinforcement and extensive cracks of the slab before punching failure (specimen D1)

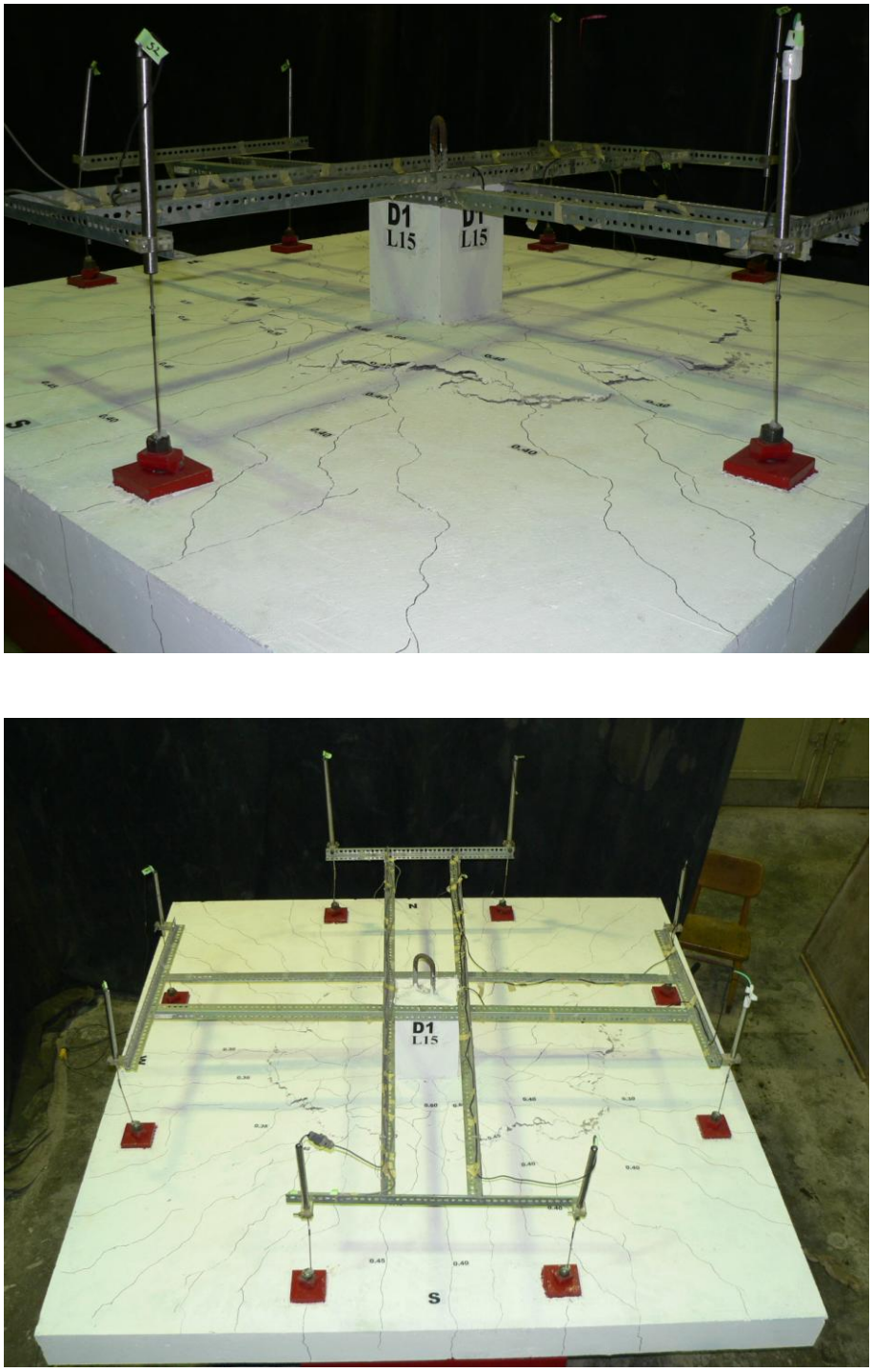

Fig. 4.28. Top surface of slab just after punching shear failure (specimen D1)

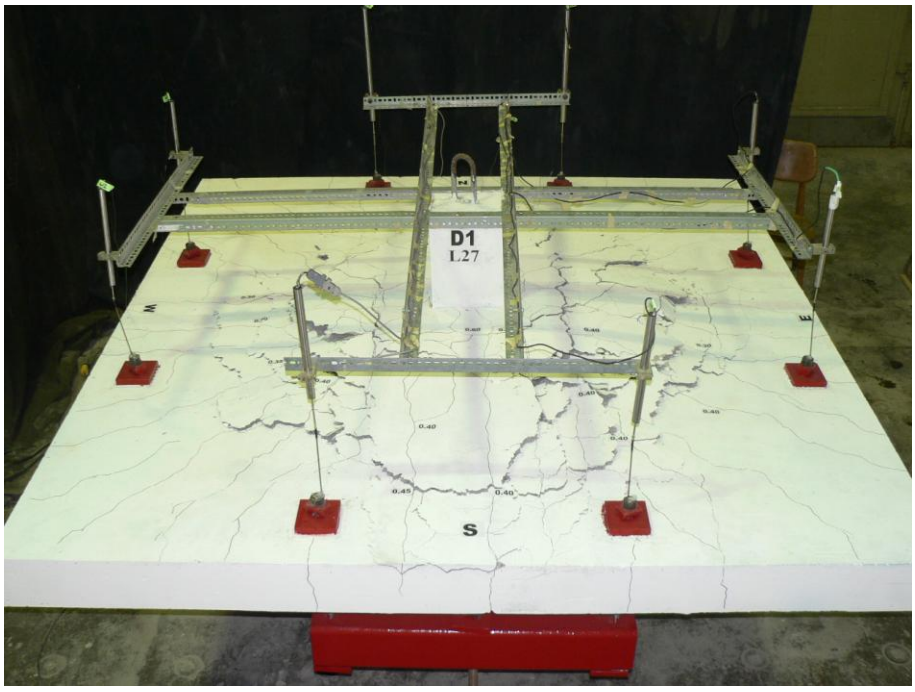

Fig. 4.29 Ripping out of top mat of reinforcement at a displacement of 75mm (specimen D1)

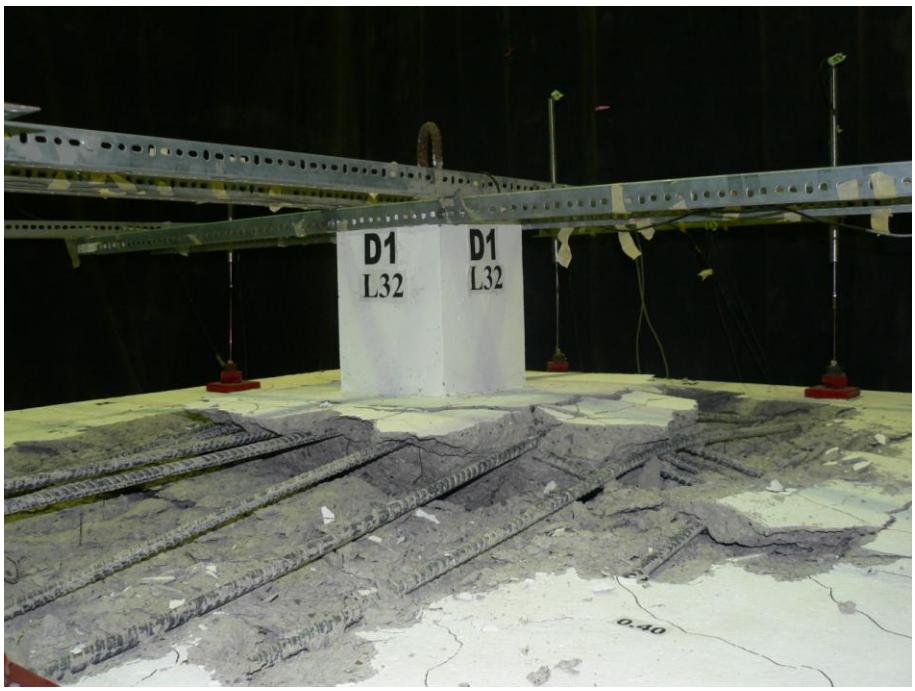

Fig. 4.30. Progressive ripping out of top steel after damaged concrete was removed at a displacement of 100 mm (specimen D1)

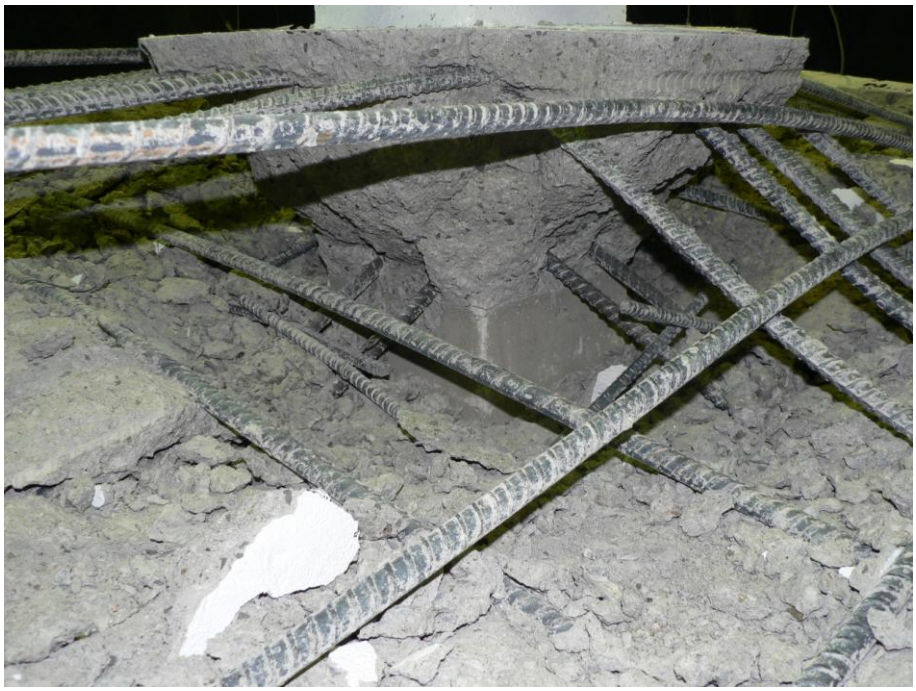

Fig. 4.31. Inclination of structural integrity reinforcement after testing completed (specimen D1)

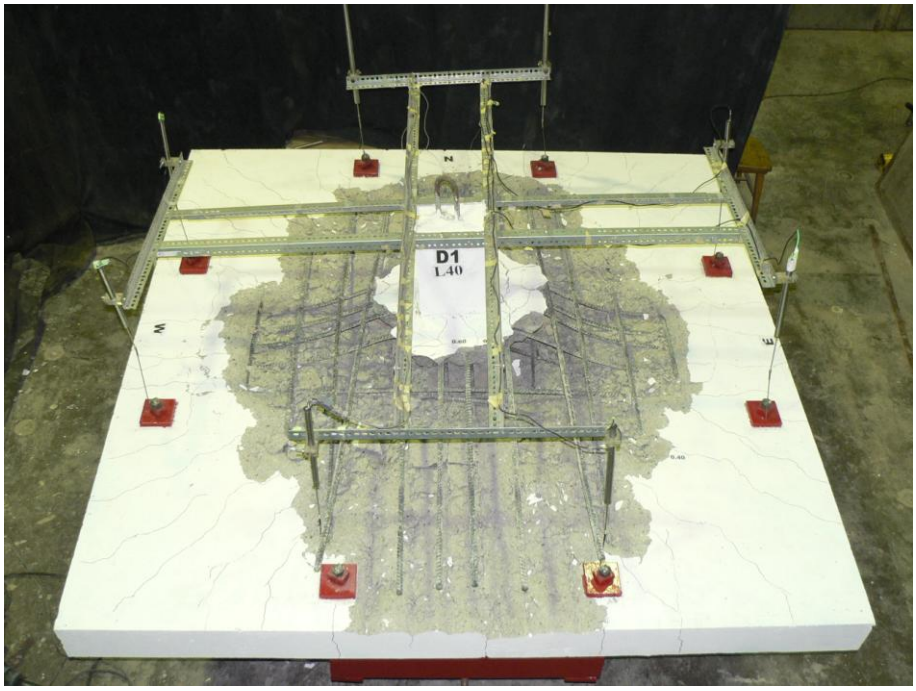

Fig. 4.32. Completion of test (specimen D1)

Table 4.5. Summary of key load stages in test of specimen D1

Stage	Load, kN	Deflection, mm
First Cracking	179	0.6
First Yield (Top Bars)	554	5
Punching Shear Failure	728	7
Maximum Post-punching Load	519	155
Ultimate Deflection	415	174

Table 4.6. Measured angles of structural integrity bars of specimen D1

Direction	Angle of structural integrity reinforcement, degrees
North	22
South	27
East	25
West	27
Average	25

4.4.2 Top Reinforcement Strains

Figs. 4.33 and 4.34 present the data collected from the strain gauges placed on the top reinforcement of specimen D1. The top reinforcement consisted of 15M bars in each direction with $f_y = 420\,\text{kN}$ and $\varepsilon_y = 0.21\%$. Locations of the strain gauges in specimen D1 are shown in Fig. 3.13 (c). Where no data is presented, the strain gauge was damaged either during casting of the concrete or during testing. First yielding was recorded at the third bar from the column

centreline in the lower layer of top bars. The strain-displacement curves for the top reinforcement closely resemble the shape of the shear-displacement curve (Fig. 4.25). The strains increased until punching shear failure occurred and then dropped off. The bars closer to the column experienced higher strains compared to the bars further from the column. Fig. 4.35 shows the strain distributions in both layers of top reinforcement at the approximate service load level and the punching shear failure level. The service load was assumed to be 396 kN, which is approximately 60% of the nominal predicted punching shear strength using the ACI Code (ACI Committee 318 2011) and the specified concrete compressive strength of 30 MPa. At the service load level the maximum strain in the steel was 0.0015 which is about 70% of the yield strain. At the punching shear failure level the maximum strain in the top reinforcement was 0.0028 which is greater than the yield strain.

After the punching shear failure the bars closer to the column started to gain strain with increasing slab deflection during the post-punching response whereas the strain in bars further from the column tended to remain fairly constant and considerably less than the yield strain of the reinforcing steel.

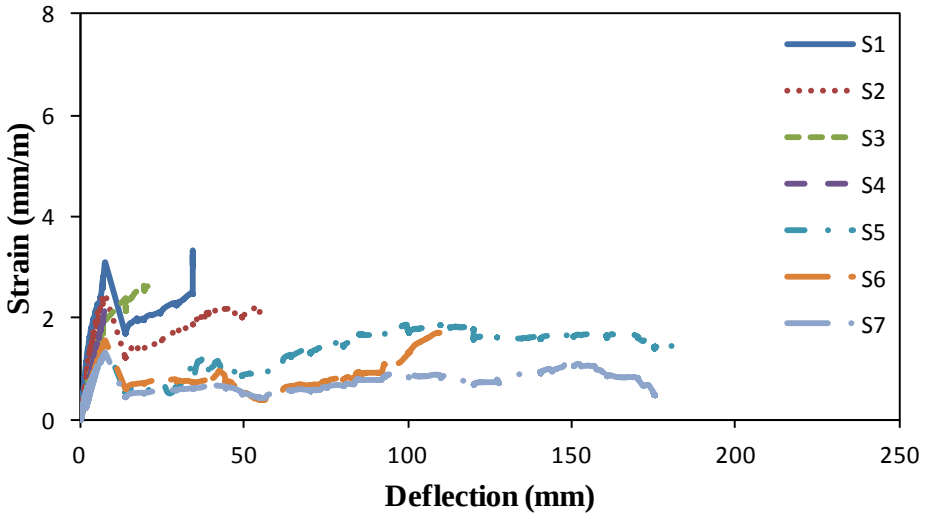

Fig. 4.33. Strain-displacement behaviour of upper layer of top mat (specimen D1)

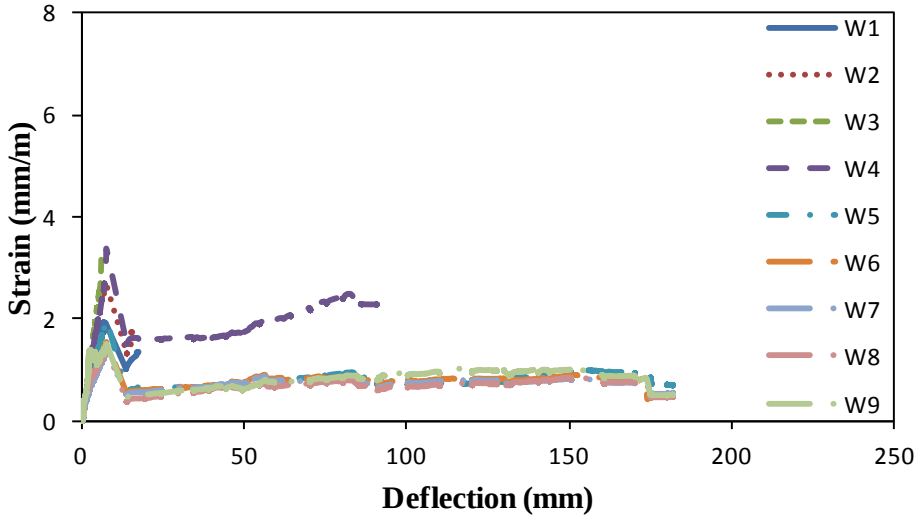

Fig. 4.34. Strain-displacement behaviour of lower layer of top mat (specimen D1)

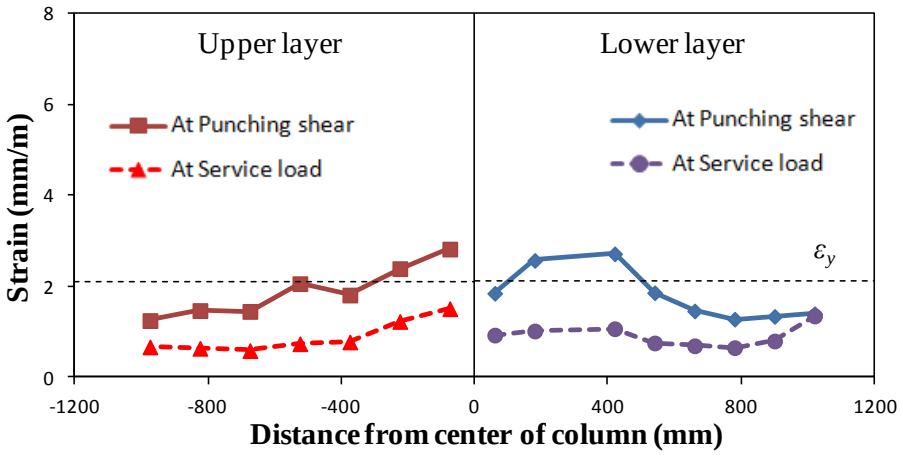

Fig. 4.35. Strain distribution of top mat at punching shear failure (specimen D1)

4.4.3 Concrete Cracking

Fig. 4.36 shows the total load versus maximum crack width in the region within a distance of 1.5*d* from the column face ("interior cracks") and outside of this region ("exterior cracks") for Specimen D1. The interior cracks were widest (0.6 mm) just before punching shear failure. After punching shear failure the exterior cracks closed up as the slab displacement increased. The closure of these cracks throughout the post-punching response indicated that the concrete near the outer edges of the slab were experiencing compression.

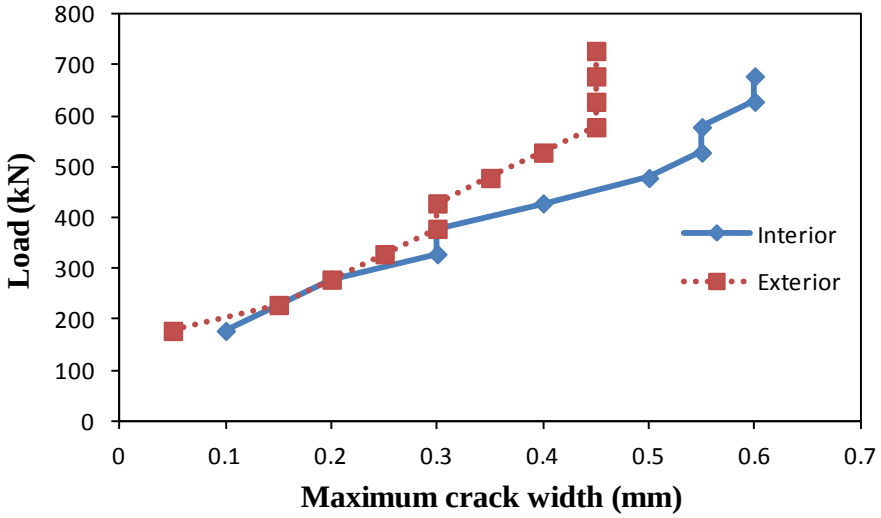

Fig. 4.36. Load versus maximum crack width for specimen D1

4.5 Specimen D2

4.5.1 Test Description

Specimens D2 had the same dimensions as specimen D1. Specimen D2 contained four 10M structural integrity bars in both directions that were placed at the same level as the bottom mat of reinforcement in the 160 mm thick slab rather than at the bottom of the drop panel. In this specimen, two of the structural integrity bars in each direction passed through the column cage while the remainder was placed outside of the column in the punching shear cone region to demonstrate whether or not the bars outside of the column would be effective.

Fig. 4.37 shows the total load versus average deflection response of the specimen D2 and a summary of key load stages during the test is presented in Table 4.7.The drop in stiffness upon first cracking is apparent at load stage 4 with a corresponding shear load of 228 kN (see Fig. 4.37). The first crack occurred in the East-West direction, perpendicular to the upper layer of top reinforcement. Cracks along the centerline of the specimen extended the full width of the

specimen in all four directions in subsequent load stages. Fig. 4.38 shows that at service load level (396 kN) the cracks extended across the full width of the slab (stage 8).

First yielding in the top mat of steel occurred at a total load of 607 kN with a corresponding average deflection of 6 mm. The first reinforcing bar to yield was the first bar from the centre of the column in the lower layer of top reinforcement. At this stage extensive cracking formed around the column as shown in Fig. 4.39. The specimen withstood a peak shear of 704 kN and a corresponding deflection of 8 mm. The punching shear failure occurred with a sudden drop in the total load from 704 kN to 170 kN. Fig. 4.40 shows the slab at the punching shear failure stage.

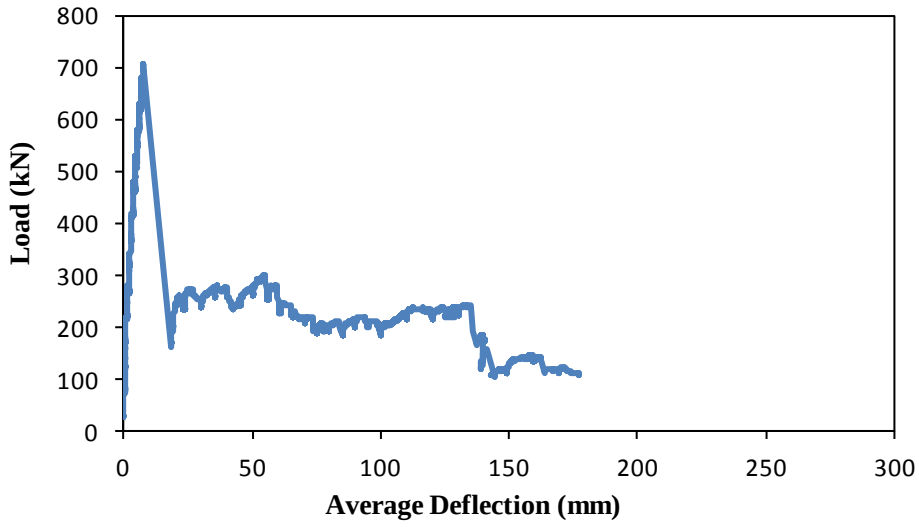

Fig 4.37. Total load versus average deflection response for specimen D2

Loading continued after punching shear failure with significant loss in stiffness compared to the initial loading response. As the deflection of the specimen increased progressive destruction of concrete above the reinforcement was evident and the top bars started to rip out from top surface

of the slab. Figs. 4.41 and 4.42 show the progressive destruction of the concrete and the ripping out of the top bars from the top surface of the slab in specimen D2.

As the post-punching displacements increased the 10M bars outside of the column lost their effectiveness due to the fact that these bars suffered breakout failures from the inclined bottom surface of the punching cone (see Fig. 4.43). This breakout failure resulted in a drop of load to 294 kN. Testing was stopped when the load dropped significantly at a displacement of 175 mm. Fig. 4.44 shows the condition of the slab-column connection after completion of the test. Table 4.8 presents the angles of inclination of structural integrity bars that passed through the column cage after the loose concrete was removed from the top surface of the slab.

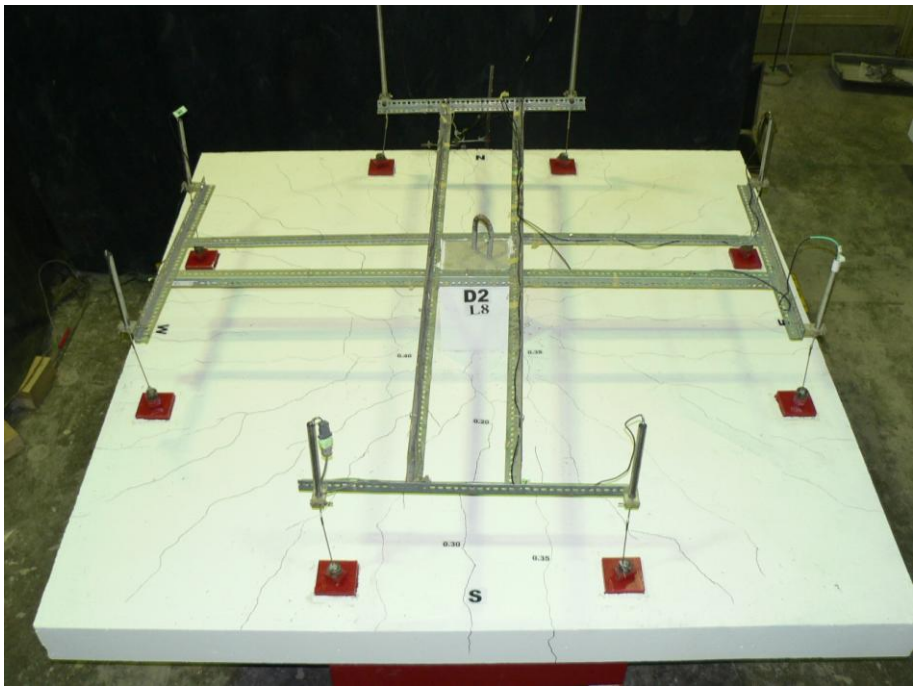

Fig. 4.38. Crack pattern in specimen D2 at service load level

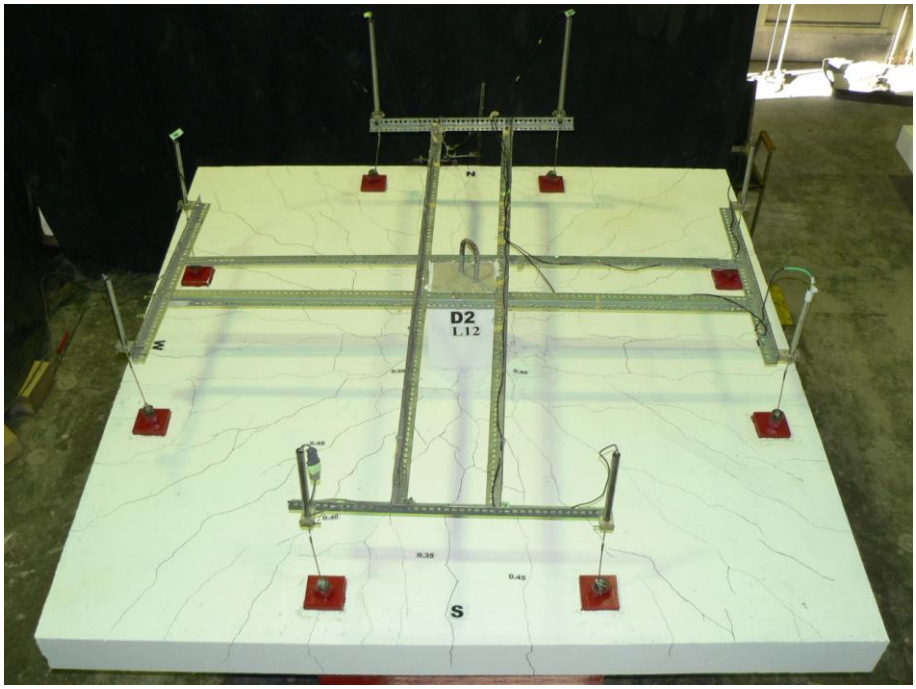

Fig. 4.39. First yielding of top reinforcement and extensive cracks of the slab before punching failure (specimen D2)

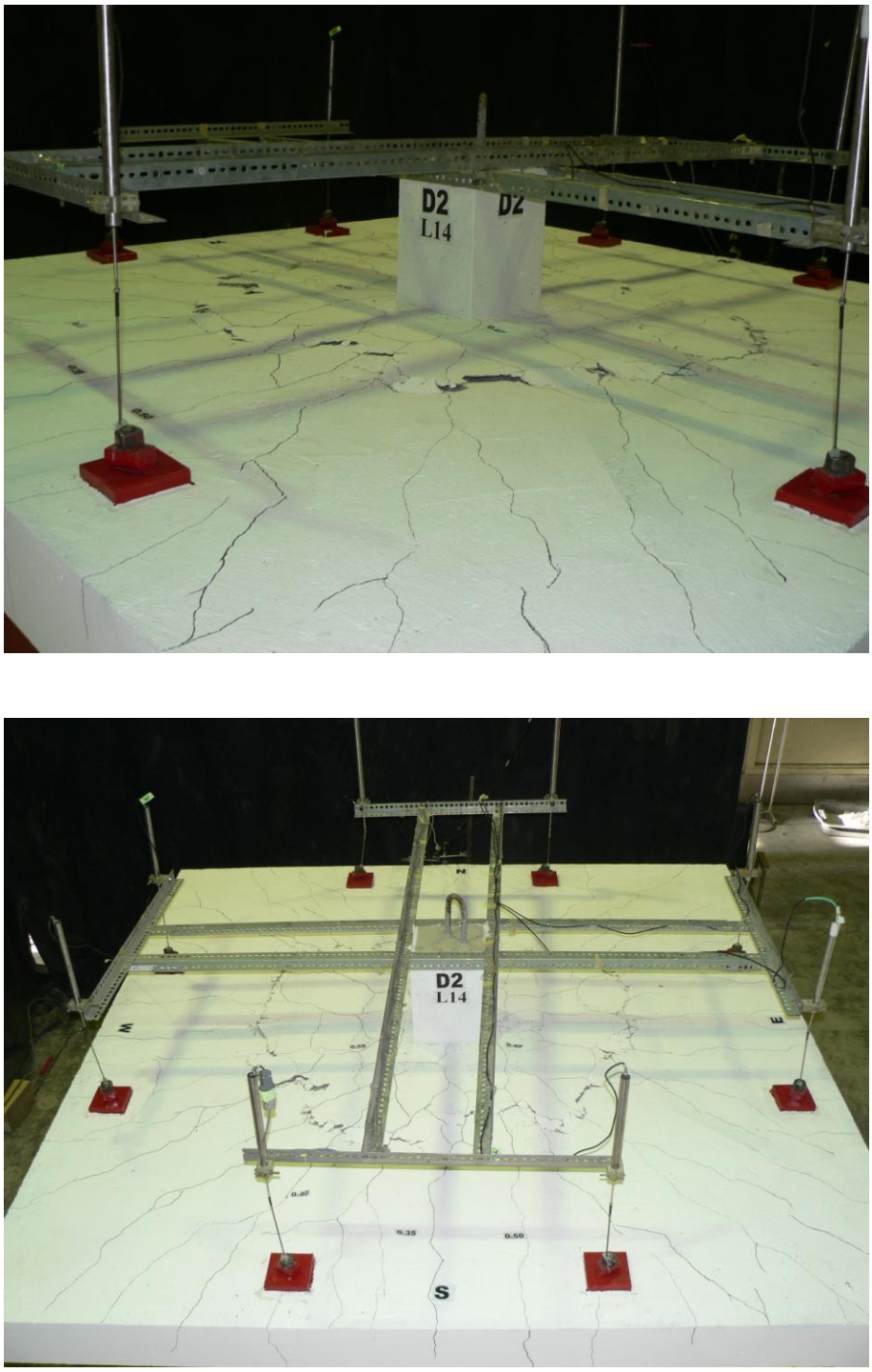

Fig. 4.40. Top surface of slab just after punching shear failure (specimen D2)

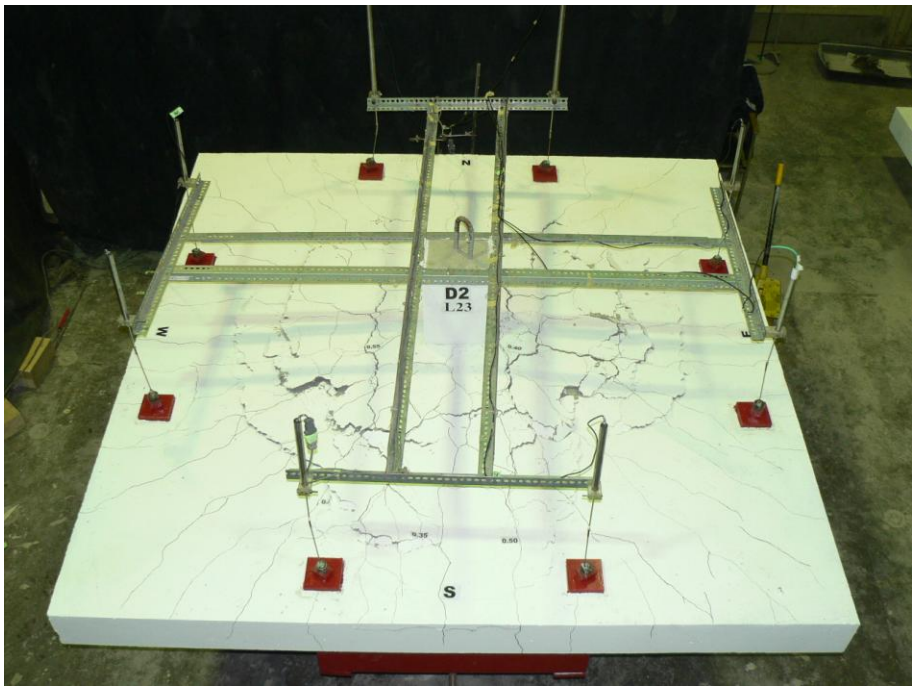

Fig. 4.41. Ripping out of top mat of reinforcement at a displacement of 55 mm (specimen D2)

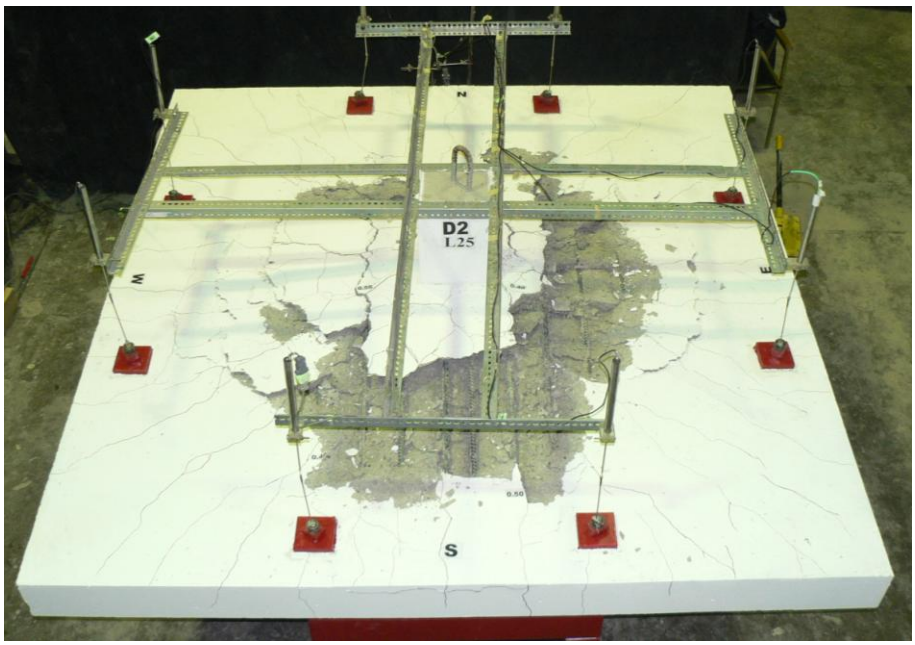

Fig. 4.42. Progressive ripping out of top steel after damaged concrete was removed at a displacement of 65 mm (specimen D2)

Fig. 4.43. Inclination of structural integrity reinforcement at end of testing with 10M bars breaking out of the bottom surface of the punching cone (specimen D2)

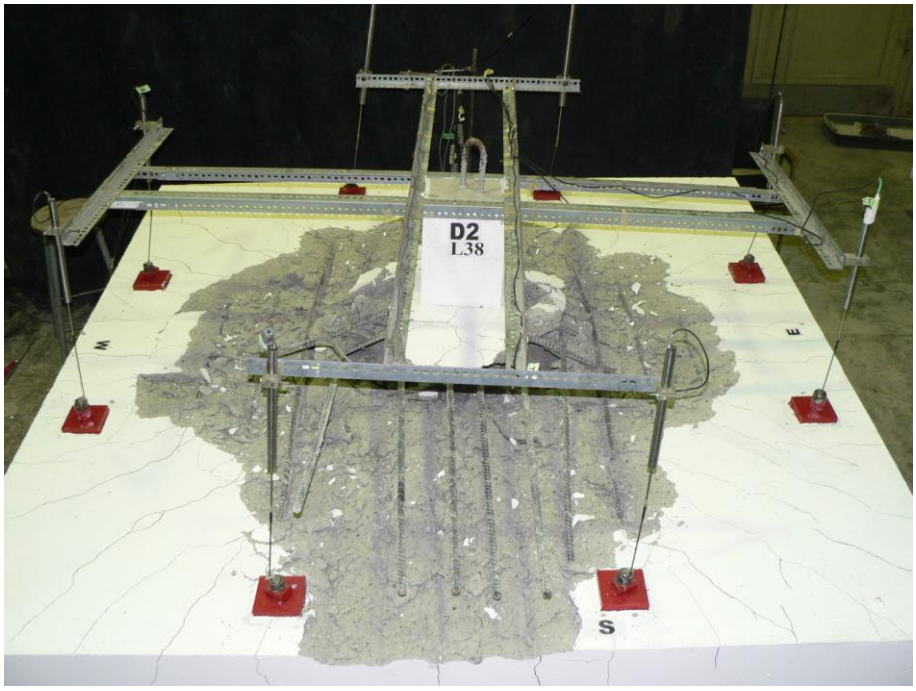

Fig. 4.44. Completion of test (specimen D2)

Table 4.7. Summary of key load stages in testing of specimen D2

Stage	Load, kN	Deflection, mm
First Cracking	228	1
First Yield (Top Bars)	607	6
Punching Shear Failure	704	8
Maximum Post-punching Load	294	54
Ultimate Deflection	235	136

Table 4.8. Angle of structural integrity reinforcement of specimen D2

Direction	Angle of structural integrity reinforcement, degrees
North	26
South	24
East	29
West	28
Average	27

4.5.2 Top Reinforcements Strains

Strain-displacement curves for the upper layer and lower layer of the top mat in specimen D2 are shown in Figs. 4.45 and 4.46. The top reinforcement consisted of 15M bars in each direction with $f_y = 420\,\text{kN}$ and $\varepsilon_y = 0.21\%$. Locations of strain gauges in specimen D2 are shown in Fig. 3.13 (d). The highest strains were recorded in the first bar from the centre of the slab in both

directions. During the post-punching response the gauges near the column measured higher values than gauges located further from the column. Fig. 4.47 shows the strain distributions in both layers of top reinforcement at an approximate service load level and the punching shear failure level for specimen D2. The service load was assumed to be 396 kN (at 60% of the nominal predicted punching shear strength calculated with 30 MPa concrete). The maximum steel strains were 0.0012 and 0.0024 at the service load level and at the punching shear failure level, respectively.

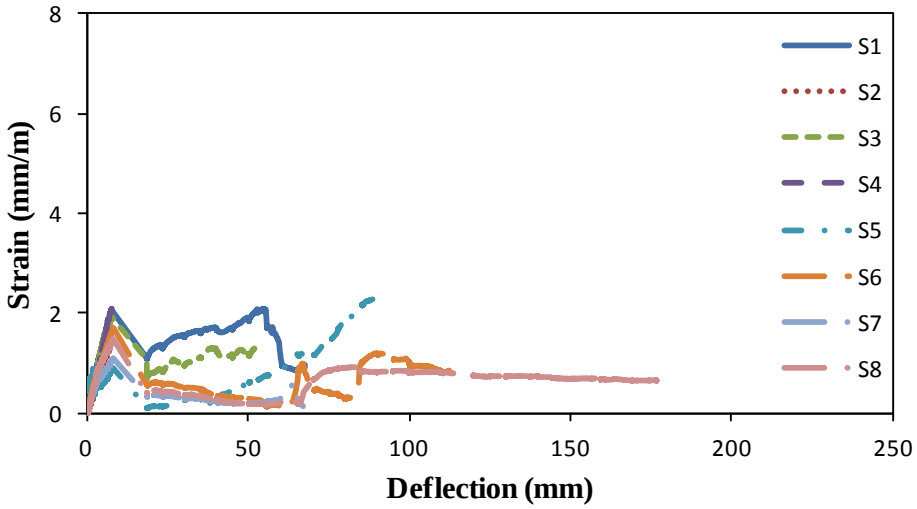

Fig. 4.45. Strain-displacement behaviour of upper layer of top mat (specimen D2)

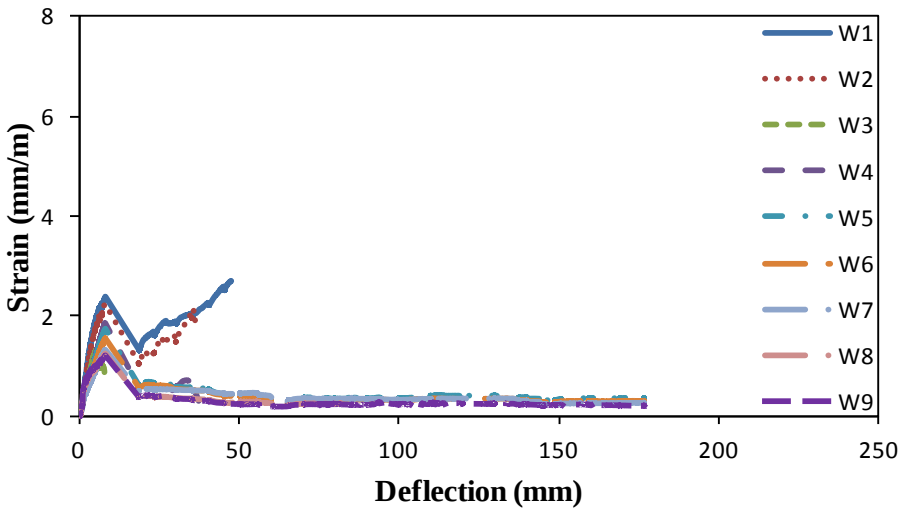

Fig. 4.46. Strain-displacement behaviour of lower layer of top mat (specimen D2)

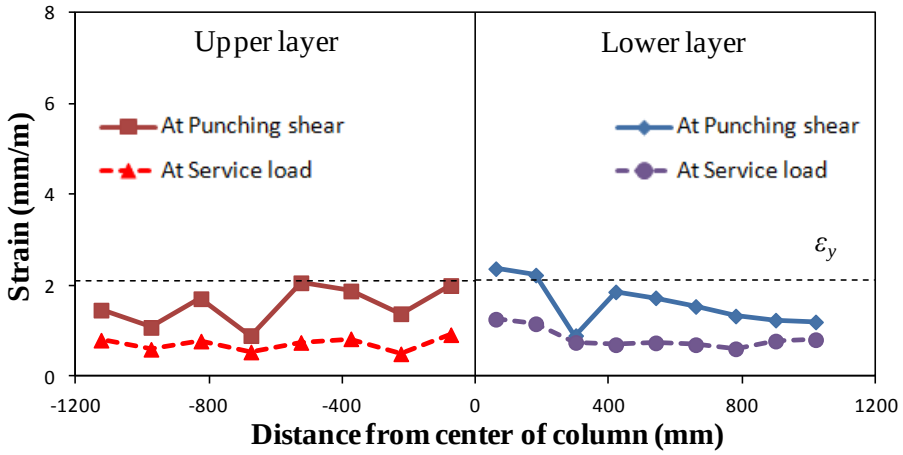

Fig. 4.47. Strain distribution of top mat at punching shear failure (specimen D2)

4.5.3 Concrete Cracking

The total load versus maximum crack width for specimen D2 is shown in Fig. 4.48. From this figure it can be seen that the values for the maximum crack near the column within a distance of 1.5*d* from the column face ("interior cracks") were close to those measured outside of this region

(exterior cracks). The maximum crack width at punching shear failure was 0.55 mm near the column and 0.50 mm near the slab edges.

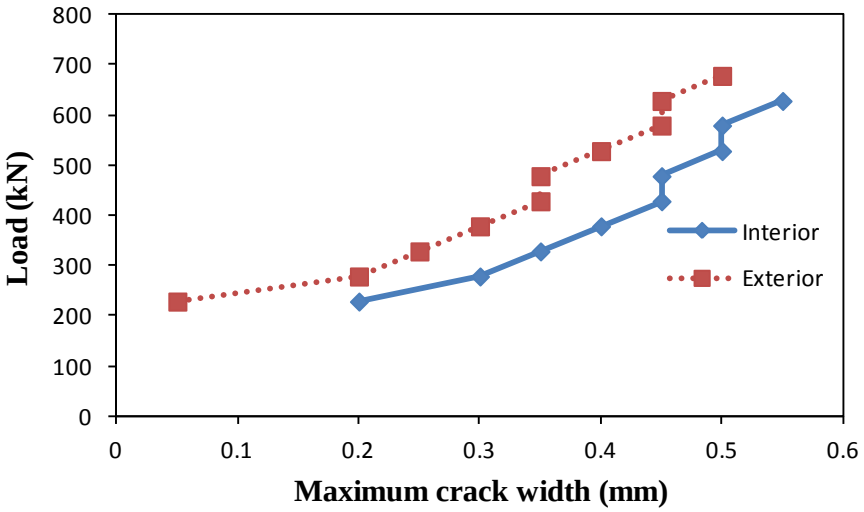

Fig. 4.48. Load versus maximum crack width for specimen D2

Chapter 5: Analytical Model

5.1 Introduction

After the initial punching shear failure, the top flexural reinforcement crossing the punching shear cone and the bottom structural integrity bars that are adequately anchored and pass through the column can provide post-punching resistance. This reinforcement can play a significant role in providing a secondary load carrying mechanism after initial failure and can prevent progressive collapse. The post-punching shear strength of a slab-column connection can be calculated as the sum of the contributions of the top bars crossing the punching shear cone and the structural integrity reinforcement.

This chapter presents an analytical method that has been developed to predict the post-punching response of slab-column connections, taking into account the individual layers of both the top reinforcement and the structural integrity reinforcement. The method is capable of predicting the different possible failure modes in the post-punching response, including rupture (thicker slab), breakout, or bond (pullout) failures (thinner slab or short embedment length of bars) of the reinforcement.

5.2 Post-Punching Behaviour of Slab-Column Connections

Immediately after an initial punching shear failure there is a sudden drop in load and a different resisting mechanism is set up involving both the top bars that cross the punching shear cone region together with the bottom structural integrity reinforcement. Fig. 5.1 shows three stages in the response of specimen SS with a 200 mm thick slab containing top reinforcement and structural integrity reinforcement. Fig. 5.1(a) shows the top surface of the slab soon after punching shear failure occurred, while Fig. 5.1(b) shows the slab-column connection after a

number of top bars crossing the punching shear cone have ripped out of the top surface. This ripping out of the top mat of reinforcement continues as the slab displaces downward until only the development length of the top bars remains in the concrete at which point the top bars lose their anchorage and become ineffective.

Immediately after punching shear failure the structural integrity reinforcing bars initially exhibit dowel action and as the displacement increases they start to rip out of the concrete damaged by the punching shear failure. Large tensile strains develop in the structural integrity bars and the inclination of the exposed integrity bars increases with increasing displacement. At large displacements the post-punching shear resistance depends only on the bottom structural integrity reinforcement. The resistance from the structural integrity reinforcement is due to the vertical component of the bars which develop large tensile stresses and become inclined as the slab deflects (see Fig. 5.1 (c)). The integrity bars continue to offer resistance over large displacements until they either rupture or pullout of the concrete.

Different codes assume different angles for the punching shear cone as shown in Fig. 5.2. The ACI Code (2011) and the CSA Standard (2004) assume a constant angle of 45º (Fig. 5.2(a)) resulting in the cone reaching a distance of d from the column face. The EC2 Code (2004) assumes that the punching shear cone extends to $1.5d$ (34º angle) and the CEB-FIP Code (1993) assumes this distance to be $2d$ (26.6º angle) measured from the column face (see Figs. 5.2(b) and (c)). It has been observed in experiments that the failure surface is about 45º near the column, but becomes flatter near the top surface of the slab, surfacing about $2d$ from the column face. In this study, the failure surface shown in Fig. 5.2(d) was assumed to determine the effective number of top bars that pass through the punching shear failure cone and hence participate in the post-punching response.

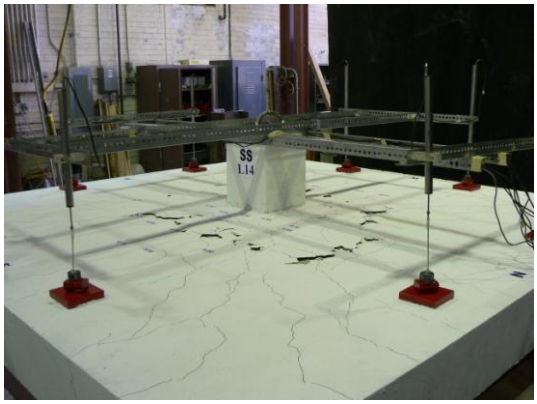

(a)

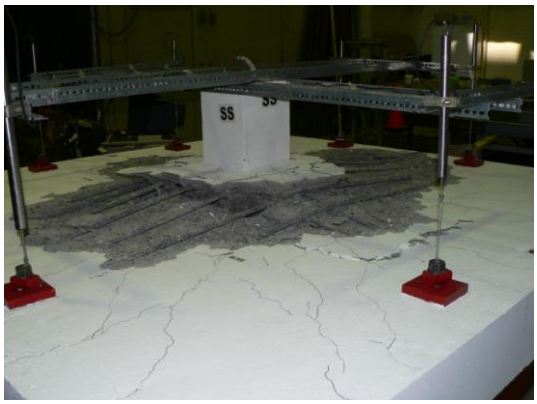

(b)

(c)

Fig. 5.1. Stages in the post-punching response of a slab-column connection containing structural integrity reinforcement: (a) top surface soon after punching shear; (b) ripping out of top mat of reinforcement; and (c) inclination of structural integrity reinforcement at large slab displacements.

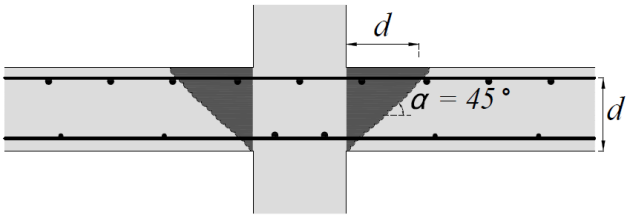

(a)

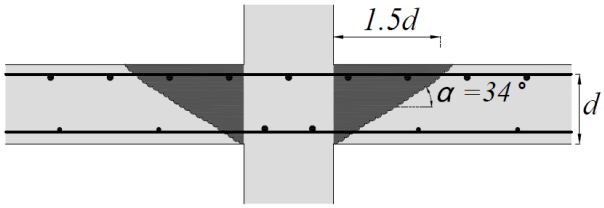

(b)

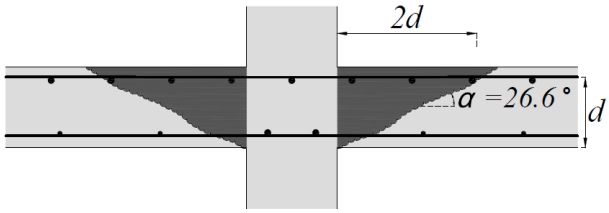

(c)

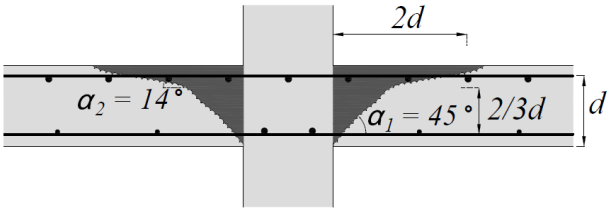

(d)

Fig. 5.2. Different assumed angles of the punching shear cone: (a) 45º (ACI Code (2001) and CSA Standard (2004)); (b) 34º (EC2 (2004)); (c) 26.6º (CEB-FIP(1993)); and (d) assumed failure plane after punching.

5.3 Mechanism of Shear Transfer after Punching Shear Failure

After a punching shear failure, both the effective top bars and the structural integrity reinforcement undergo tension as the slab deflects. Fig. 5.3 shows the mechanism of shear transfer after punching shear failure. It is the vertical component of the force in these bars that provides the post-punching shear resistance. The vertical component is limited by either: the breakout resistance of the concrete above the bar; pullout of the reinforcement when the remaining embedded portion of the bar equals the development length; or rupture of the bars in tension.

The post-punching shear strength of a slab-column connection, V_{pp}, can be calculated as the sum of the contributions of the top bars crossing the punching shear cone, $\sum V_t$, and the integrity reinforcement, $\sum V_i$.

$$V_{pp} = \sum V_t + \sum V_i \tag{5.1}$$

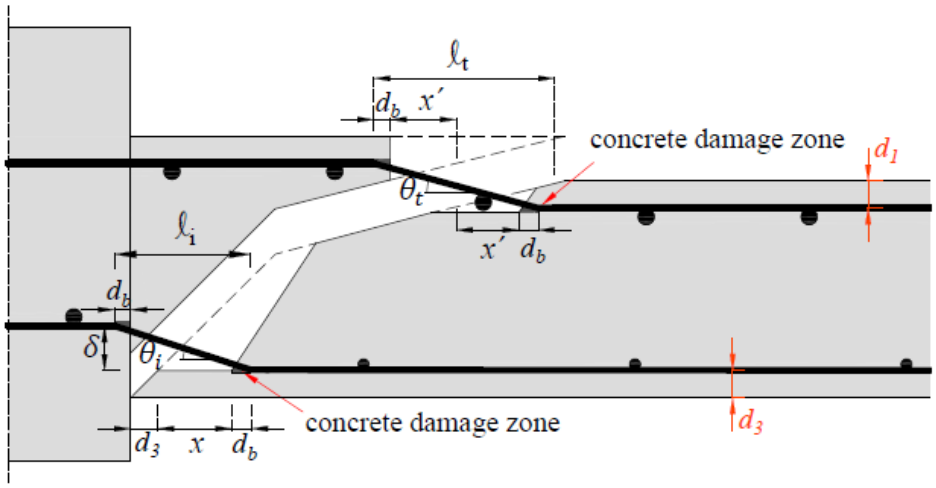

Fig. 5.3. Mechanism of shear resistance after punching shear failure.

It is assumed that after the punching shear failure, the dowel action and bending of the bars is negligible, with tensile stresses in the bars providing the shear resistance. The exposed length of the bars in the model includes a concrete damage zone at the locations where the bar enters the concrete of a length equal to the bar diameter, d_b (see Fig. 5.3).

Based on the equilibrium conditions, the vertical component of the force developed in a reinforcing bar, V, is related to the tensile stress developed in the bar, f_s, and the angle of inclination of the reinforcement, θ, by the following equation:

$$V = A_s f_s \sin\theta \tag{5.2}$$

where A_s is the effective area of the reinforcing bar. From the geometry of inclined reinforcement the strain in the bar can be calculated by:

$$\varepsilon_s = \frac{1}{\cos\theta} - 1 \tag{5.3}$$

Applying compatibility of deformations and using Eq. 5.3, the deflection of slab can be expressed as:

$$\delta = \ell \tan\theta = \ell \tan\left[\cos^{-1}\left(\frac{1}{1+\varepsilon_s}\right)\right] \tag{5.4}$$

where ℓ is the horizontal length of the exposed reinforcing bar. As shown in Fig. 5.3 the horizontal exposed length, ℓ_i, of the structural integrity reinforcement is given by:

$$\ell_i = d_3 + x + 2d_b \tag{5.5}$$

and the horizontal exposed length, ℓ_t, of the top bars is given by:

$$\ell_t = 2x' + 2d_b \tag{5.6}$$

To determine the relationship between the tensile stress and strain of the reinforcement, an idealized stress-strain curve of reinforcing steel has been used (Fig. 5.4).

The curve has an elastic region, a yield plateau and a strain hardening region based on equation proposed by Kunnath et al.(2009). The relationship is given by:

$$f_s = \begin{cases} E_s \varepsilon_s & \text{if} \quad \varepsilon_s \le \varepsilon_y \\ f_y & \text{if} \quad \varepsilon_y < \varepsilon_s \le \varepsilon_{sh} \\ f_u + \left(f_y - f_u\right)\left(\dfrac{\varepsilon_u - \varepsilon_s}{\varepsilon_u - \varepsilon_{sh}}\right)^p & \text{if} \quad \varepsilon_{sh} < \varepsilon_s \le \varepsilon_u \end{cases} \tag{5.7}$$

where the initial slope of the strain hardening region is E_{sh} and $p = E_{sh}\dfrac{\varepsilon_u - \varepsilon_{sh}}{f_u - f_y}$

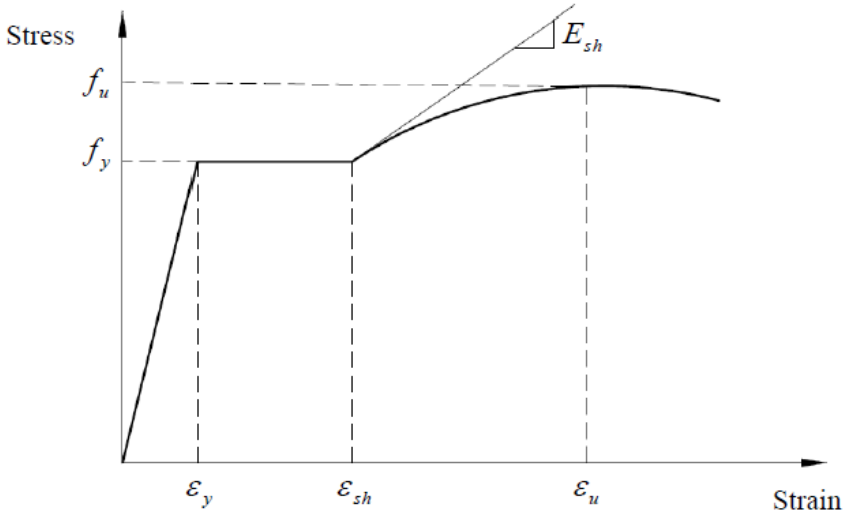

Fig. 5.4. Idealized stress-strain curve of reinforcing steel

5.4 Concrete Breakout Strength

The ACI Code for Nuclear Safety Related Concrete Structures (ACI Committee 349 1978) provides a method for calculating the concrete breakout strength of an embedded reinforcing bar in concrete when the bar is loaded in the direction of a free edge. The breakout strength is taken as the vertical component of the tensile strength of the concrete acting on the surface of the concrete breakout cone and is given by:

$$V_n = A_{ch} f_{ct,eff} = \frac{\pi}{2} d^2 f_{ct,eff} \tag{5.8}$$

where V_n is the nominal concrete breakout strength, A_{ch} is the horizontal projection of the conical failure surface, $f_{ct,eff}$ is the effective tensile strength of the concrete above the reinforcing bar and d is the depth of concrete over the reinforcing bar measured to the center of the bar. It is assumed that the failure surface is radiating out at 45º from the location where the bar enters into the concrete (see Fig. 5.5).

For multiple bars with a centre-to-centre spacing, *s*, greater than or equal to *2d*, the total breakout resistance is equal to the number of effective bars, *n*, times the breakout resistance of a single bar (Eq. 5.8). For *n* bars having a center-to-center spacing of less than *2d* the conical failure surface is reduced due to the overlapping of the failure cones as shown in Fig. 5.6. The total horizontal projected area of the conical failure surface for *n* reinforcing bars with $s < 2d$ is given by:

$$A_{ch} = n\frac{\pi}{2} d^2 - 2(n-1)\left(\frac{\gamma}{2} d^2 - \frac{s}{4} d \sin\gamma\right) \tag{5.9}$$

where $\gamma = \cos^{-1}(s/2d)$ is in radians.

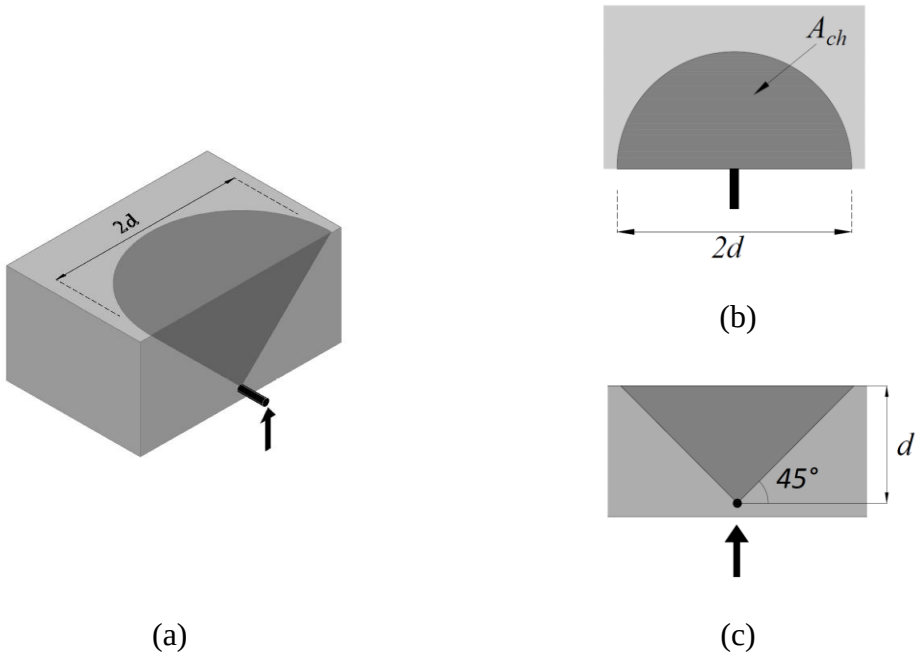

Fig. 5.5. ACI Code for Nuclear Safety Related Concrete Structures (1978) model for concrete breakout strength above a single bar assuming a 45º failure plane: (a) isometric view; (b) plan view; and (c) elevation view.

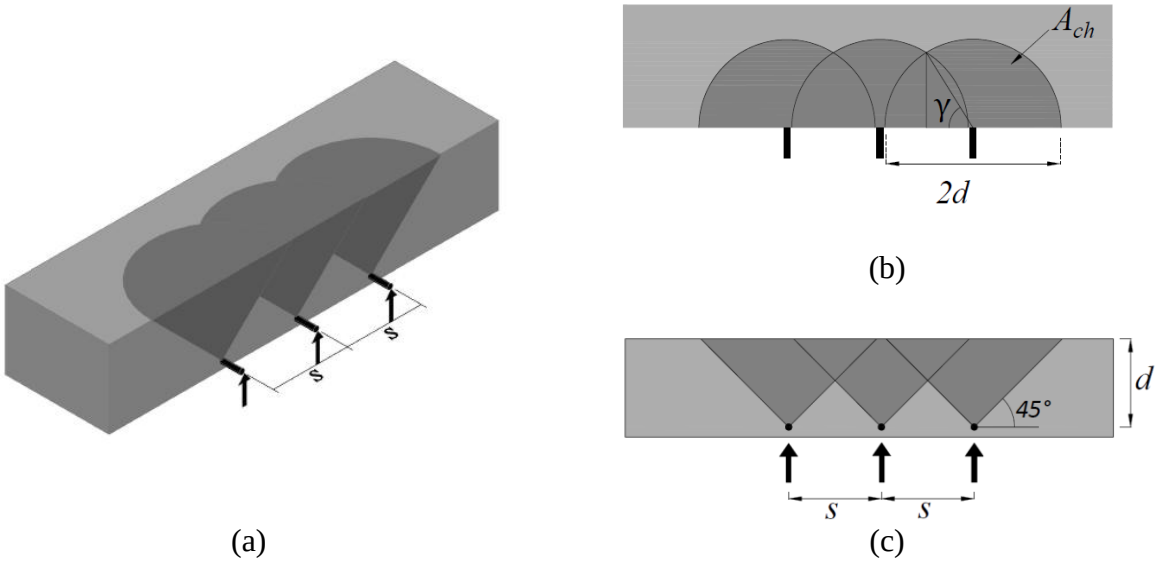

Fig. 5.6. Concrete breakout failure surface for three reinforcing bars: (a) isometric view; (b) plan view; and (c) elevation view.

In order to predict the breakout resistance of each layer of the structural integrity reinforcement it is necessary to account for the changing depth of concrete above the bars due to the influence of the shape of the punching shear failure plane (see Fig. 5.2) and for the loss of concrete above the integrity bars due to the progressive destruction of the concrete as the top bars rip out (see Fig. 5.7). Fig. 5.7(a) shows a section along a single bar with the breakout progressing a distance of $d_3 + x$ from the column face, with the breakout cone intersecting the punching shear failure plane (i.e., $x \le 2d/3$).

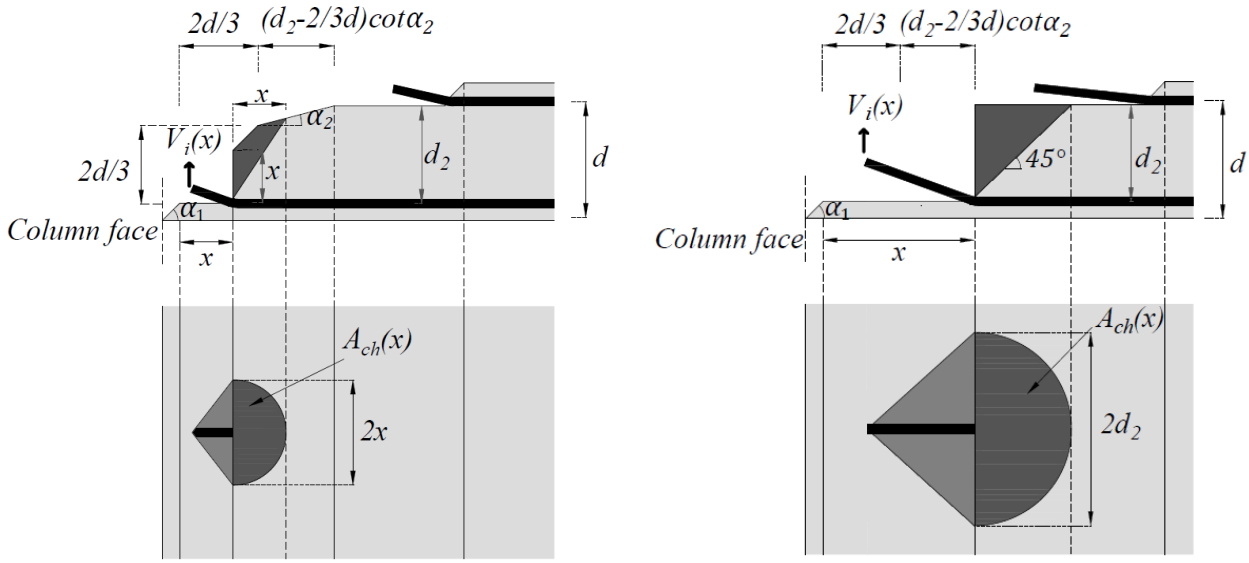

(a) $x \le \frac{2d}{3}$, ($\alpha_1 = 45°$, $\alpha_2 = 14°$) (b) maximum breakout resistance

Fig. 5.7. Model to estimate progressive destruction of concrete over structural integrity reinforcing bar.

As shown in Fig. 5.7(a), the thickness of the concrete directly above the bar is x and it is assumed that in calculating the breakout resistance the diameter of horizontal projection of the conical failure surface is $2x$.

The concrete breakout resistance can be expressed as the vertical component of the horizontal projected area, which is a function of *x*, multiplied by the effective tensile strength of the concrete as:

$$V_i(x) = A_{ch}(x) f_{ct,eff} \tag{5.10}$$

To calculate the horizontal projection of the conical failure surface, $A_{ch}(x)$, for more than one structural integrity bar, the interaction between the failure surfaces of the breakout cones must be considered. For *n* structural integrity bars, the horizontal projection of the conical failure surface is given by:

$$A_{ch}(x) = \begin{Bmatrix} n\frac{\pi}{2}x_1^{\,2} - \mathrm{A}_1(\mathrm{x}_1) & \text{if} & \mathrm{x} \le \frac{2\mathrm{d}}{3} \\ n\frac{\pi}{2}x_2^{\,2} - A_1(x_2) & \text{if} & \frac{2\mathrm{d}}{3} < x < \frac{2d}{3} + \left(d_2 - \frac{2d}{3}\right)\cot\alpha_2 \\ n\frac{\pi}{2}d_2^{\,2} - A_1(d_2) & \text{if} & \mathrm{x} \ge \frac{2d}{3} + \left(d_2 - \frac{2d}{3}\right)\cot\alpha_2 \end{Bmatrix} \tag{5.11}$$

where $\alpha_1 = 45°$; $\alpha_2 = \arctan(0.25) = 14°$; $x_1 = x$; $x_2 = \left(x - \frac{2d}{3}\right)\tan\alpha_2 + \frac{2d}{3}$ and the term $A_1(x)$ provides a correction for the interaction of the overlapping failure cones when the spacing of the bars, *s*, is less than $2x$ and is given by:

$$A_1(x) = 2(n-1)\left[\frac{\gamma(x)}{2}x^2 - \frac{s}{4}x\sin\gamma(x)\right] \text{ where } \gamma(x) = \begin{Bmatrix} \cos^{-1}\left(\frac{s}{2x}\right) & \text{if} & \frac{\mathrm{s}}{2\mathrm{x}} \le 1 \\ 0 & \text{if} & \frac{\mathrm{s}}{2\mathrm{x}} > 1 \end{Bmatrix}$$

From correlations with the test results, where the splitting tensile strength, f_{sp}, is known, the effective tensile strength of the concrete for determining breakout of the structural integrity bars can be taken as:

$$f_{ct,eff} = 0.85 f_{sp} \tag{5.12}$$

If f_{sp} is not known, then the effective tensile strength of concrete can be estimated by:

$$f_{ct,eff} = 0.50\sqrt{f_c'} \tag{5.13}$$

Fig. 5.7(b) shows the situation when the concrete breakout strength above the structural integrity bars reaches a maximum. Beyond this stage, the concrete breakout strength remains constant due to the constant concrete thickness above the bars and hence the contribution of these bars to the shear resistance is also constant.

The same approach used for the structural integrity reinforcement can be used in determining the progressive breakout of the top bars. The breakout strength of the concrete cover over a single top bar, with the breakout progressing to a distance of x' from the crack face (see Fig. 5.3) is equal to:

$$V_t(x')_{total} = A_{ch}(x') f'_{ct,eff} \tag{5.14}$$

where A_{ch} is the horizontal projection of the conical failure surface and $f'_{ct,eff}$ is the effective tensile strength of concrete in determining the breakout resistance for the top bars which can be taken as:

$$f'_{ct,eff} = 0.55 f_{sp} \tag{5.15}$$

where f_{sp} is the splitting tensile strength of concrete. If the test results for the splitting tensile strength of concrete, f_{sp}, is not available then the effective tensile strength of the concrete can be estimated by:

$$f'_{ct,eff} = 0.33\sqrt{f'_c} \tag{5.16}$$

The reduced values of tensile strength for determining the breakout resistance of the top bars is due to the fact that the top concrete cover is in the cracked tension zone of the slab and is typically subjected to larger shrinkage strains.

For typical top bar spacings and slab concrete covers, the interaction between the breakout cones need not be considered. Hence the projected area of the breakout cone, $A_{ch}(x')$, can be calculated by:

$$A_{ch}(x') = \begin{cases} \frac{\pi}{2}(x' \tan\alpha_2)^2 & \text{if} \quad x' < d_1 \cot\alpha_2 \\ \frac{\pi}{2} d_1^{\,2} & \text{if} \quad x' \geq d_1 \cot\alpha_2 \end{cases} \tag{5.17}$$

where d_1 is the depth of concrete over the top bar measured to the centre of the bar.

5.5 Pullout or Rupture of Reinforcing Bars

After punching shear failure occurs, large tensile strains develop in the reinforcement and the inclinations of the exposed bars increase with increasing displacement (see Fig. 5.3). The reinforcement offers resistance over large displacements until it either ruptures or suffers pullout from the concrete.

At each increment of deflection the strain in a reinforcing bar can be determined by the compatibility expression, Eq. (5.4). The computed strain in the reinforcing steel is used to check if rupture of the steel occurs. If rupture occurs then the contribution of the steel to the post-

punching resistance becomes zero. If rupture does not occur, then the pullout resistance of the remaining embedded portion of the bar is checked. The bar can continue to provide shear resistance until the remaining embedded length is reduced to the development length of the bar, ℓ_d, at which point the bar loses its anchorage and pullout occurs. Fig. 5.8 illustrates when pullout is predicted for the top bars and the structural integrity bars (see Figs. 5.8(a) and 5.8(b)).

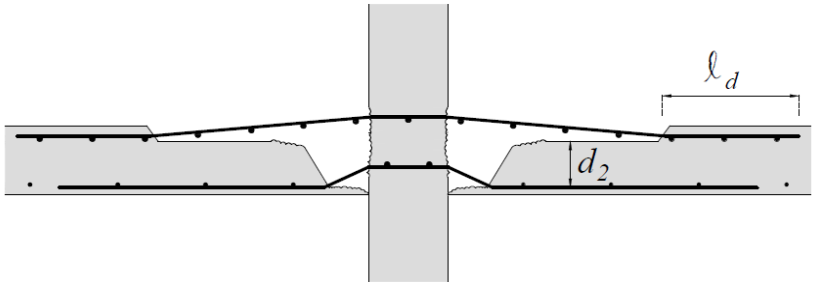

(a) end of the contribution of top bars

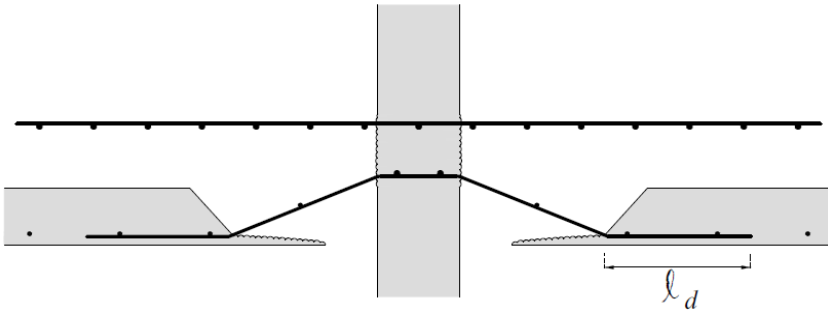

(b) end of the contribution of structural integrity bars

Fig. 5.8. Pullout of the reinforcement.

The ACI code (ACI Committee 318 2011) proposed the following equation to calculate the development length of deformed bars or deformed wires in tension:

$$\ell_d = \left(\frac{f_y}{1.1\lambda\sqrt{f_c'}} \frac{\psi_t \psi_e \psi_s}{\left(\frac{c_b + K_{tr}}{d_b} \right)} \right) d_b \qquad (5.18)$$

In which the confinement term $\left(\frac{c_b + K_{tr}}{d_b} \right)$ shall not be taken greater than 2.5 , c_b is smallest amount of the side cover, the cover over the bar (in both cases measured to the centre of the bar) and the centre-to-centre spacing of the bars, K_{tr} is a factor that represents the contribution of confinement reinforcement across potential splitting planes. The term ψ_t is the traditional reinforcement location factor, ψ_e is a coating factor, ψ_s is the reinforcement size factor and the factor λ is used for lightweight concrete.

In determining the development length, the ACI Code (ACI Committee 318 2011) design expression for development length (Eq. 5.18) was used, assuming that the stress in the embedded reinforcement corresponds to the horizontal component of the force in the exposed inclined reinforcement. The 2011 ACI Code design expression (Eq. 5.18) is based on the research by Orangun et al. (1977) and includes an implicit strength reduction factor of 0.8. In checking for pullout the development length was taken as 0.8 times the development length determined using Eq. 5.18.

Chapter 6: Comparison of Test Results and Predictions

6.1 Introduction

This chapter presents the comparison of the test results of seven interior slab-column connections (S1, S2, R2, SS, RS, D1 and D2). It is noted that the specimen R1 experienced significant tilting during loading and hence the result of this specimen has been excluded. A study was made of the effects of slab thickness, length of structural integrity reinforcing bars, distribution of structural integrity reinforcement in slabs with rectangular columns and the placement of structural integrity reinforcement in slabs with drop panels. Results from this test series and other researchers were compared with predictions using the CSA A23.3-04 design equations for both punching shear and post-punching resistance. Also the analytical model, developed in Chapter 5, was used to predict the complete post-punching responses of the test specimens.

6.2 Comparison of Test Results and Influence of Different Parameters

6.2.1 Influence of Slab Thickness

Three specimens (S1, SS and D1) are compared to investigate the effect of the slab thickness on the post-punching response of the slab-column connections (see Fig. 6.1). All three slabs had the same area of structural integrity reinforcement. Fig. 6.2 shows the effect of slab thickness on the post-punching response of the slab-column connections. Slab S1, had a total slab thickness of 150 mm, an average effective depth, d_{tav} , for the top mat of reinforcement of 110 mm and an average effective depth, d_{iav} of 100 mm measured from the top surface of the slab to the level of the structural integrity reinforcement. This slab exhibited a maximum post-punching resistance, V_{se}, of 314 kN while slab SS (h of 200 mm and d_{iav} of 160 mm) and slab D1 (h of 250 mm and

d_{iav} of 210 mm) had post-punching resistances of 397 kN and 519 kN, respectively. Increasing the depth of the concrete above the structural integrity bars increases the concrete breakout resistance, resulting in higher loads to cause ripping out of these bars. This increased breakout resistance of the concrete has resulted in the ability of the structural integrity bars to develop strains well into the strain hardening range for specimen D1. Fig. 6.3 shows the final condition of the three specimens with different slab thicknesses.

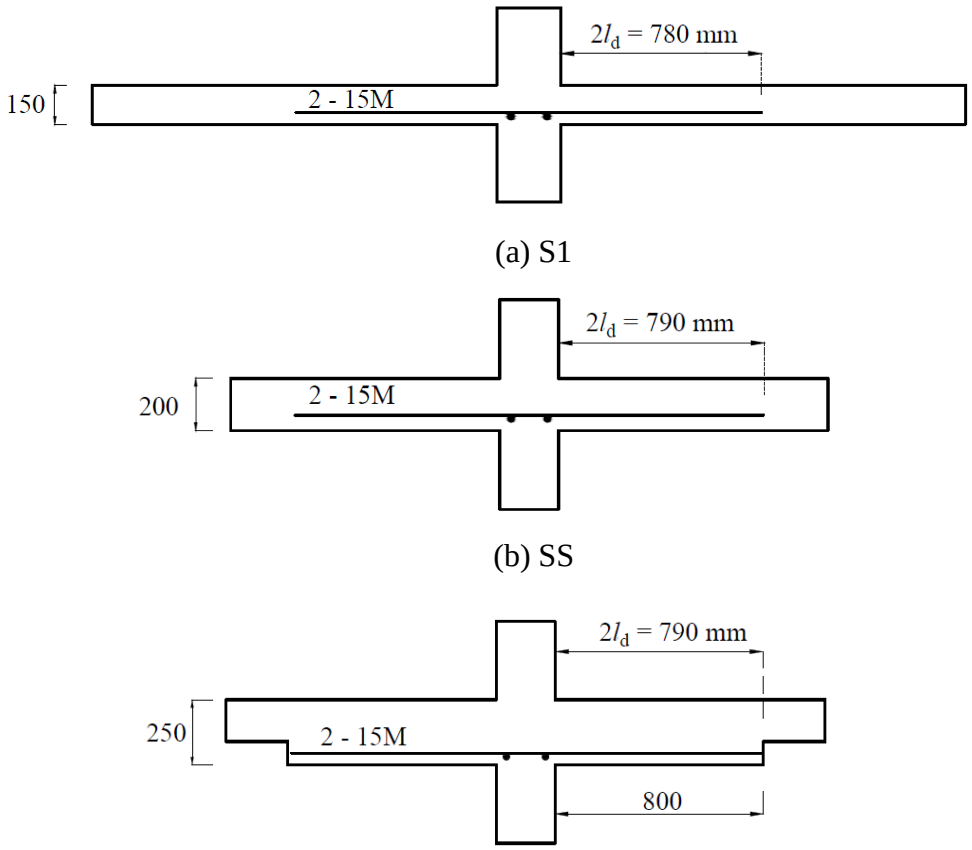

Fig. 6.1. Details of test specimens: influence of slab thickness (top and bottom flexural reinforcement not shown)

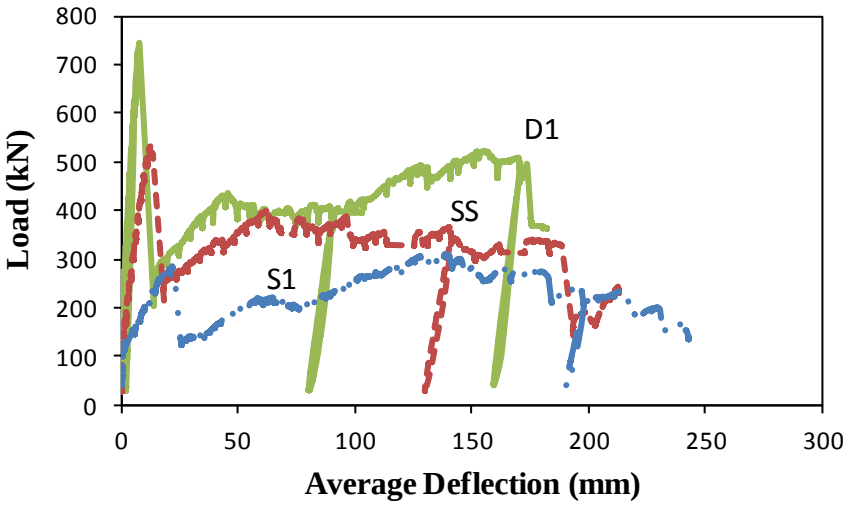

Fig. 6.2. Load versus average deflection responses: Influence of slab thickness

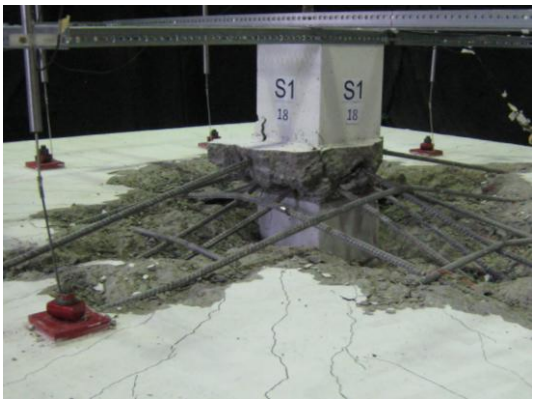

(a) S1(Redl 2009) (*h*=150 mm)

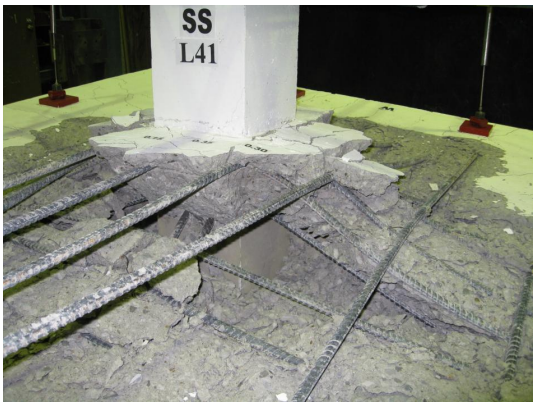

(b) SS (*h*=200 mm)

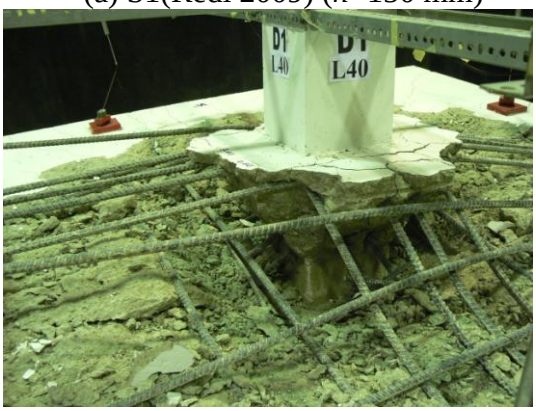

(c) D1 (*h*=250 mm)

Fig. 6.3. Test specimens after testing completed: influence of slab thickness

6.2.2 Influence of Length of Structural Integrity Bars

Slabs S1 and S2 were compared to study the influence of increasing the length of the structural integrity reinforcement on the post-punching response of slab-column connections. Fig. 6.4 shows the details of the two specimens and Fig. 6.5 presents the load-versus average deflection responses of the specimens. Slab S1 was designed and detailed in accordance with the CSA A23.3-04 requirements with two 15M integrity bars extending a distance of $2\ell_d$ into the slab from the column faces, while slab S2 had the same amount of integrity reinforcement but the bars extended $2\ell_d + 2d$ into the slab. The peak post-punching resistances, V_{se}, of slabs S1 and S2 were 314 and 333 kN and the ultimate displacements, Δ_u (taken as the average deflection when the post-punching load drops below 80% of V_{se}) were 183 and 234 mm, respectively. The increase in the length of the structural integrity reinforcement, resulted in a small increase in the post-punching resistance, however, the ultimate deformability increased by 28%. The test specimens after testing was completed are shown in Fig. 6.6.

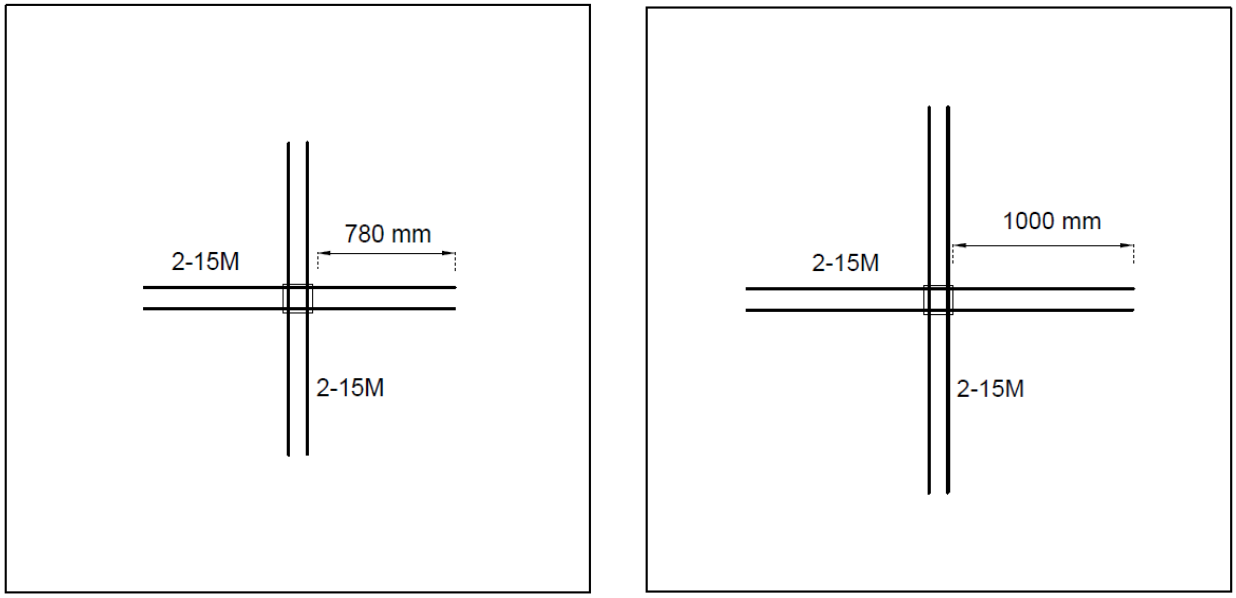

(a) S1 (b) S2

Fig. 6.4. Details of length of structural integrity reinforcement in specimens S1 and S2 (top and bottom flexural reinforcement not shown)

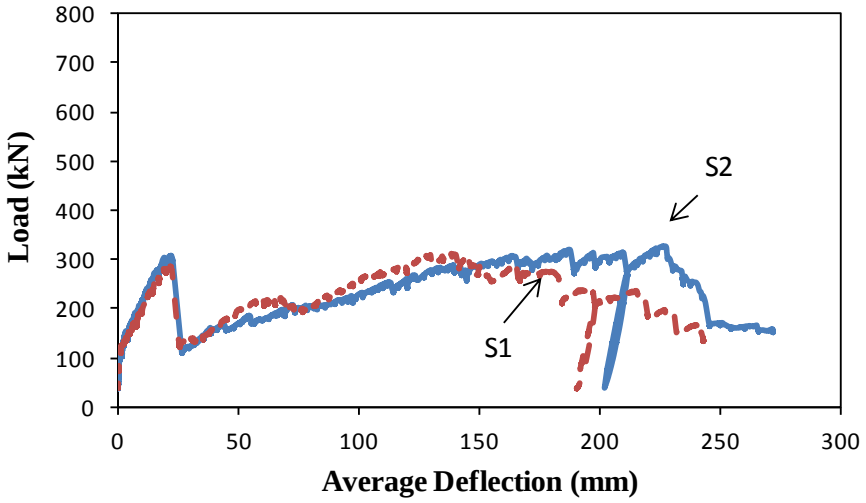

Fig. 6.5. Load versus average deflection responses: Influence of length of integrity reinforcement

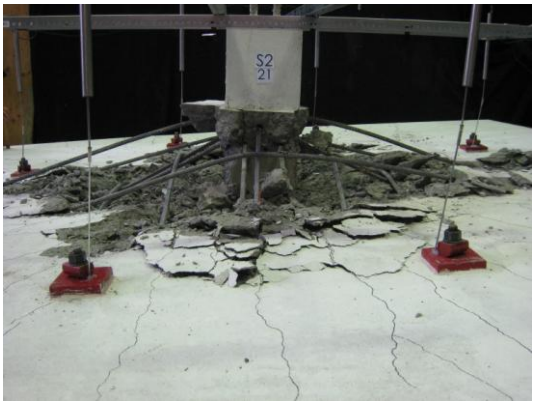

(a) S1 (Redl 2009) (L_i = 780 mm) (b) S2 (Redl 2009) (L_i = 1000 mm)

Fig. 6.6. Test specimens after testing completed: influence of length of integrity bars

6.2.3 Influence of Column Rectangularity and Distribution of Integrity Reinforcement

The post-punching responses of two pairs of specimens (SS and RS) and (S2 and R2) are compared to study the effect of column rectangularity and the arrangement of the structural integrity reinforcement on the post-punching behaviour of slab column connections. The details of the arrangement of structural integrity reinforcement are shown in Figs. 6.7 and 6.8. These slabs all contained the same total area of structural integrity reinforcement.

Figs. 6.9 and 6.10 show the load versus average deflection responses of these specimens. Comparing the post punching responses of slabs SS (225 mm square column) and S2 (250 square column) with the post punching responses of slabs RS (180×270 mm column) and R2 (200×300 mm column) shows that the column rectangularity and the distribution of the integrity reinforcement had no significant effect on the post punching strength of the slab column connections.

Slabs SS and S2 had the same amount of structural integrity reinforcement in the two principal directions whereas RS and R2 had three times the structural integrity reinforcement

perpendicular to the long column side than in the other direction. The use of 2 – 10M structural integrity bars in the direction perpendicular to the short column face in slabs RS and R2, with shorter embedment lengths have resulted in somewhat smaller ultimate displacements, Δ_u. Fig. 6.11 shows the four test specimens after testing was completed.

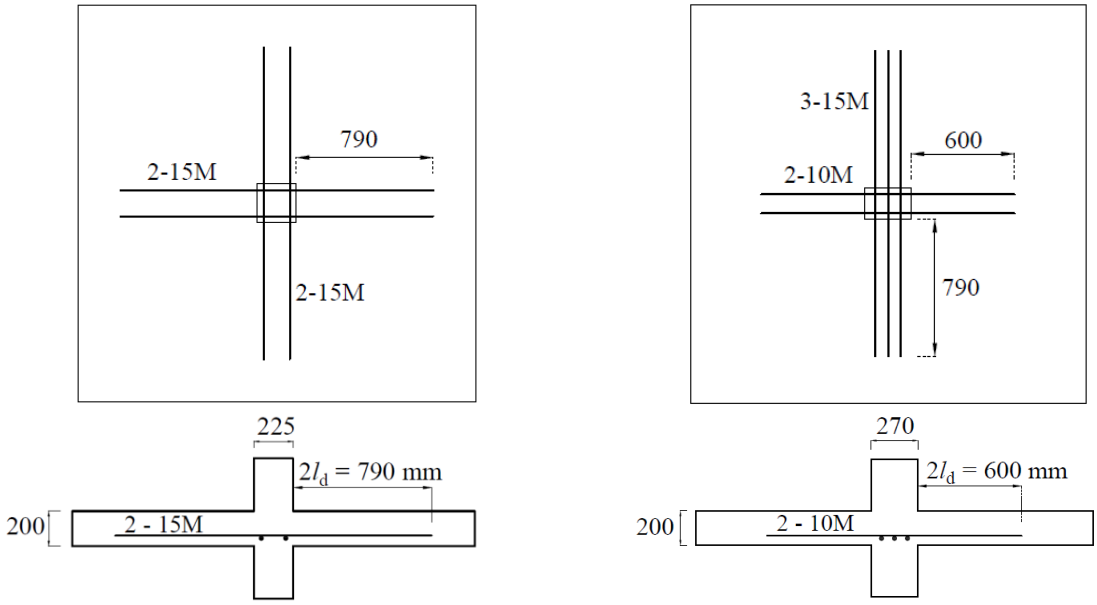

(a) Specimen SS (b) Specimen RS

Fig. 6.7. Details of arrangement of structural integrity reinforcement in specimens SS and RS (top and bottom flexural reinforcement not shown)

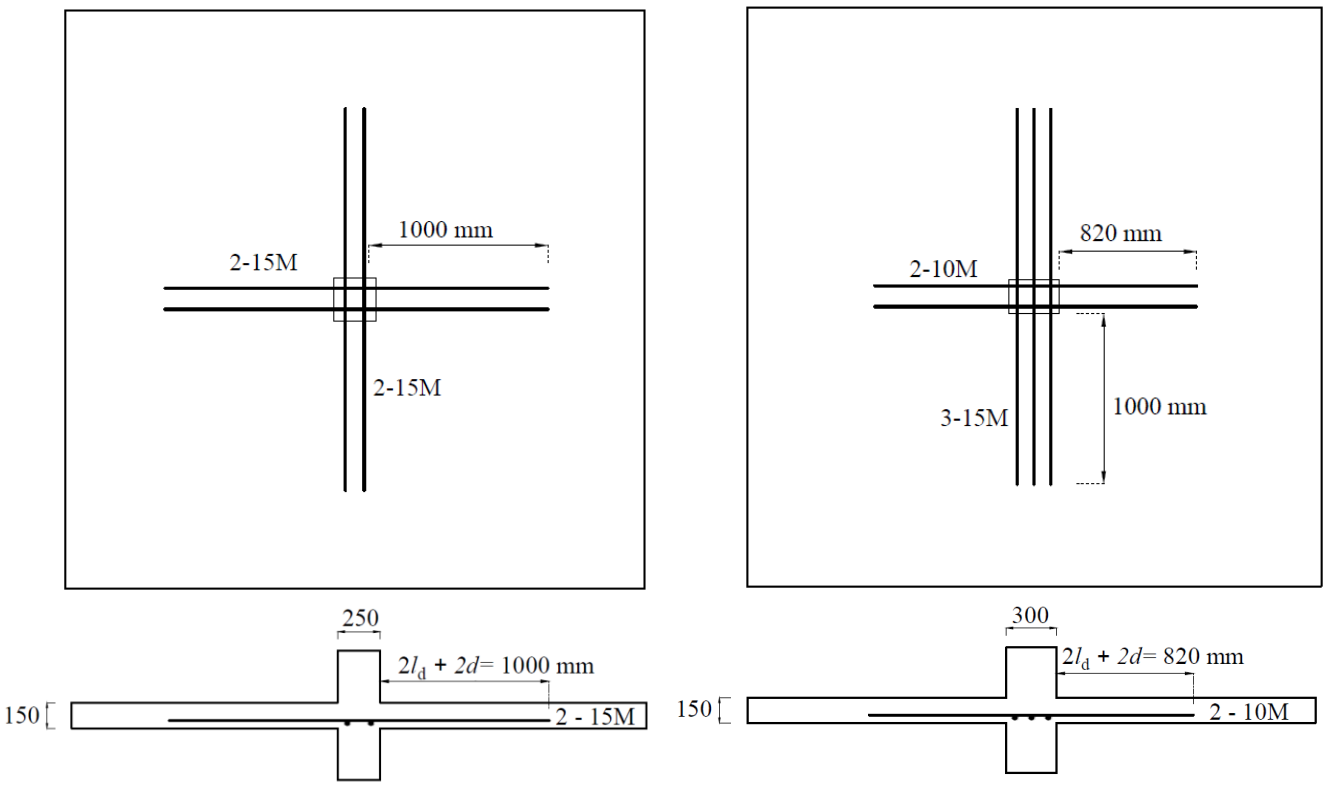

(a) Specimen S2 (b) Specimen R2

Fig. 6.8. Details of arrangement of structural integrity reinforcement in specimens S2 and R2 (top and bottom flexural reinforcement not shown)

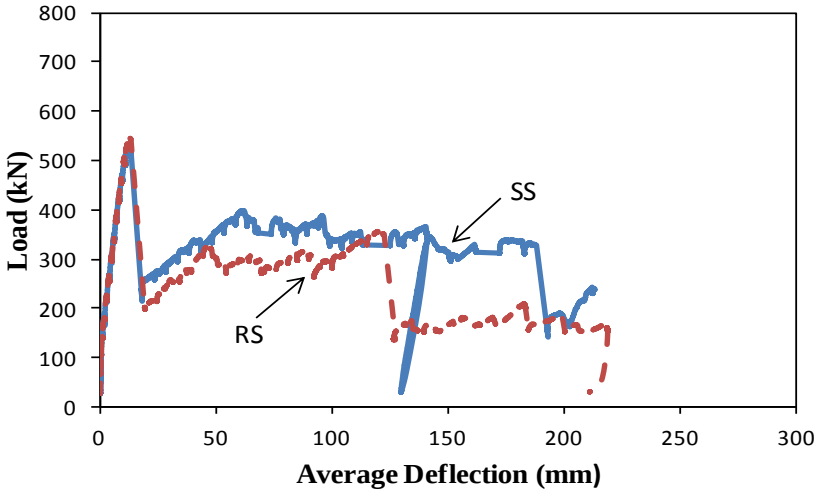

Fig. 6.9. Load versus average deflection responses: influence of column rectangularity and distribution of integrity reinforcement (Specimens SS and RS)

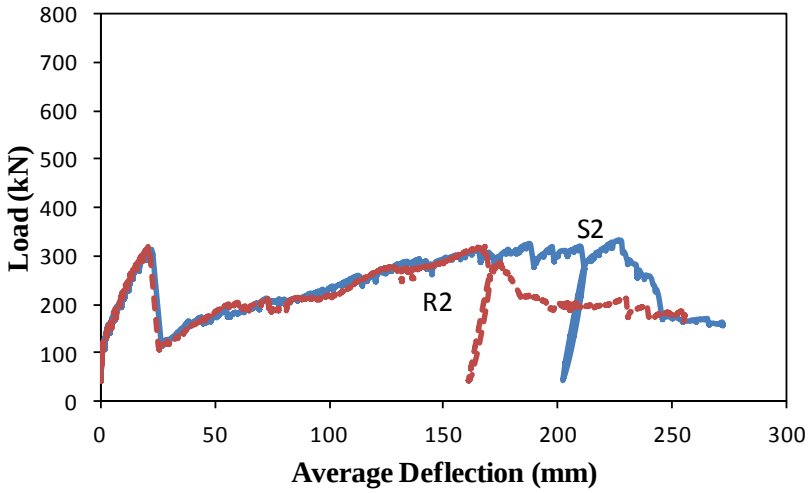

Fig. 6.10. Load versus average deflection responses: influence of column rectangularity and distribution of integrity reinforcement (Specimens S2 and R2)

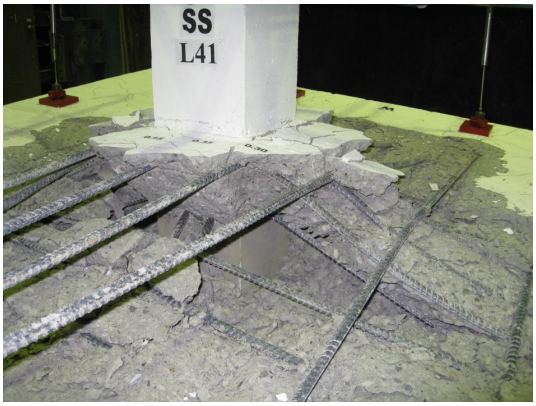

(a) SS

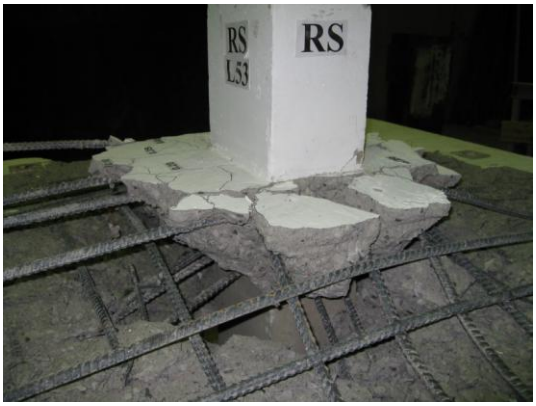

(b) RS

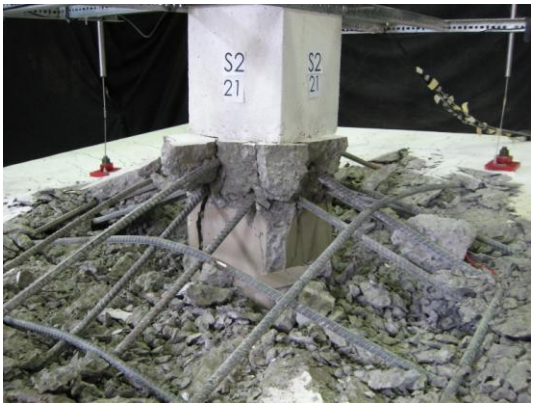

(d) S2 (Redl 2009)

(d) R2 (Egberts 2009)

Fig. 6.11. Test specimens after testing completed: influence of column rectangularity and distribution of integrity bars

6.2.4 Response of Slabs with Drop Panels

Fig. 6.12 compares the post-punching behaviour of specimens D1 and D2 with drop panels. Specimen D1 had two 15M bars passing through the column in each direction and placed near the bottom of the drop panel, while specimen D2 contained four 10M bars in each direction placed at the same level as bottom slab reinforcement (see Fig. 6.13). In specimen D2, two of the structural integrity bars in each direction passed through the column cage while the remainder was placed outside of the column in the punching shear cone region to demonstrate whether or not the bars outside of the column would be effective.

Specimen D1 reached a post-punching resistance of 519 kN, while specimen D2 reached a maximum post-punching resistance of 294 kN. Both of the slabs had the same top reinforcement, with both the top reinforcement and the structural integrity reinforcement contributing to the resistance at the early stages of the post-punching response. However, the structural integrity reinforcement in specimen D1 had a larger breakout resistance than the integrity steel in specimen D2 which enabled higher steel strains to develop, leading to a greater post-punching resistance in specimen D1. As the post-punching displacements increased, the 10M bars outside of the column in specimen D2 lost their effectiveness due to the fact that these bars suffered breakout failures from the inclined bottom surface of the punching cone. The results from testing specimen D2 illustrate the need to pass the structural integrity bars through the column core. The influence of the placement of structural integrity reinforcement in slabs with drop panels is shown in Fig. 6.14.

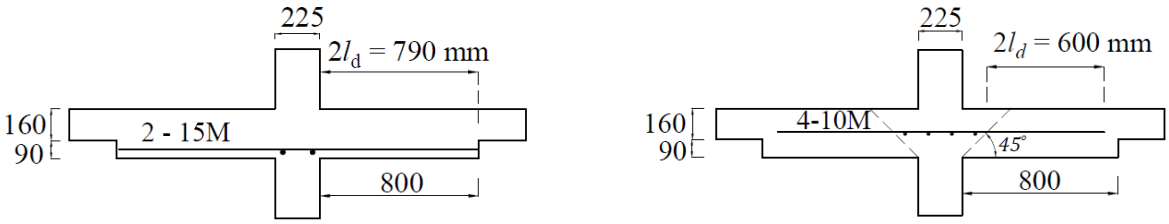

(a) Specimen D1 (b) Specimen D2

Fig. 6.12. Details of structural integrity reinforcement in slabs with drop panels (top and bottom flexural reinforcement not shown)

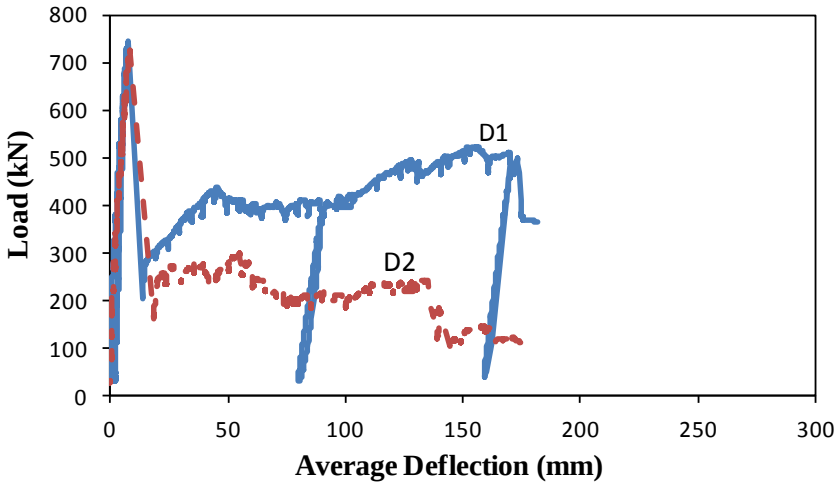

Fig. 6.13. Load versus average deflection responses: influence of arrangement and location of structural integrity reinforcement in slabs with drop panels

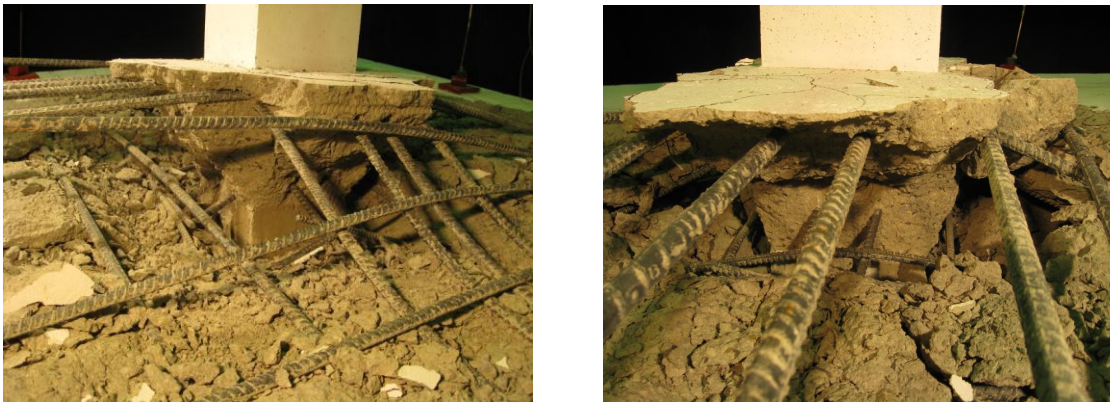

(a) D1 (b) D2

Fig. 6.14. Test specimens after testing completed: Influence of placement of structural integrity reinforcement in slabs with drop panels

6.3 Comparison of Punching and Post-Punching Loads with Code Predictions

The punching shear strengths and the peak post-punching loads for the slabs tested are compared with the equations in CSA A23.3-04. CSA A23.3-04 adopted the ACI 318M-11 equation for the punching shear resistance. The nominal punching shear resistance, V_c, for a square column can be expressed as:

$$V_c = 0.33\sqrt{f_c'}b_0 d \qquad (6.1)$$

where f_c' is the compressive strength of the concrete and $\sqrt{f_c'}$ is limited to 8 MPa in the CSA Standard. The term b_o is the perimeter of the critical section located at a distance *d/2* from the concentrated load or reaction area. The term *d* is taken as the average effective depth to the top reinforcement in the two directions. The expression for the factored shear resistance in the CSA Standard has a factor of 0.38 rather than 0.33 to adjust for the greater reduction in capacity provided by the lower value of ϕ_c of 0.65 in comparison to the ACI 318 ϕ factor for shear of

0.75. The CSA Standard is based on the same nominal resistance as the ACI Code. The CSA Standard also has a size effect factor of (1300/(1000+d)) for cases where d exceeds 300 mm. The predicted post-punching shear resistance in accordance with the CSA A23.3-04 standard is given by:

$$V_{se} = 0.50 \sum A_{sb} f_y \tag{6.2}$$

where $\sum A_{sb}$ is the total area of integrity reinforcement, and f_y is the yield strength of the structural integrity reinforcement.

Table 6.1 and Fig. 6.15 compare the predicted punching and post-punching shear strengths with the experimental results in this experimental program as well as the test results reported by Ghannoum (1998), Mirzaei (2010) and Melo and Regan (1998). It is noted that the code predictions of the nominal punching shear capacities are typically conservative, with an average test to predicted ratio of 1.17 and a standard deviation of 0.11. The tests by Melo and Regan (1998) were one-way slabs supported by a column with a preformed shear crack and hence there are no results for the punching shear failure load. The column did not contain longitudinal reinforcement or ties and tests where local crushing around the integrity bars occurred have been excluded.

The simple design expression for the post-punching shear resistance provided reasonable estimates of the peak load carrying capacity at extremely large displacements for the slabs tested. While the average test to predicted ratio is 1.08 there is significant variation in these ratios. It is noted that in making the predictions the measured yield stress of the structural integrity reinforcement was used. In design, the minimum specified yield strength is assumed and if these values are used then all of the predictions by this code expression are conservative. The

predictions for the post-punching resistance of the slabs with drop panels are quite conservative due to the greater concrete breakout resistance of the structural integrity reinforcement in these thicker slabs.

For the slabs investigated, the simple design equation in CSA A23.3-04 gives conservative design values for the post-punching shear resistance and furthermore the required details of the integrity steel provide the slabs an ability to undergo very large displacements after punching.

Table 6.1. Comparison of predicted and experimental shear resistances

Slab	c mm	h mm	d mm	f_c' MPa	$\sum A_{sb}$ mm^2	f_y MPa	Punching shear resistance			Post punching shear resistance		
							Predicted V_c kN	Test V_c kN	Test to predicted ratio	Predicted V_{se} kN	Test V_{se} kN	Test to predicted ratio
S1	250×250	150	110	28.0	1600	457	277	289	1.04	365.6	314	0.86
S2	250×250	150	110	30.0	1600	457	285	314	1.10	365.6	333	0.91
R2	200×300	150	110	33.0	1200 400	457 455	300	320	1.06	368.0	321	0.88
SS	225×225	200	160	26.0	1600	420	415	527	1.27	336.0	397	1.18
RS	180×270	200	160	30.0	1200 400	420 460	445	547	1.23	344.0	360	1.04
D1	225×225	250	210	22.0	1600	420	565	728	1.28	336.0	519	1.54
D2 [a]	225×225	250	210	22.0	800	460	565	704	1.24	184.0	294	1.60
S1-U [b]	225×225	150	110	37.2	1200	454	297	301	1.01	272.4	273	1.00
S1-B [b]	225×225	150	110	37.2	1200	454	297	317	1.06	272.4	245	0.90
S2-U [b]	225×225	150	110	57.1	1200	454	367.5	363	0.99	272.4	266	0.97
S2-B [b]	225×225	150	110	57.1	1200	454	367.5	447	1.21	272.4	298	1.09
S3-U [b]	225×225	150	110	67.1	1200	454	398	443	1.11	272.4	281	1.03
S3-B [b]	225×225	150	110	67.1	1200	454	398	485	1.21	272.4	340	1.25
PM-9 [c]	130×130	125	102	31.0	402	616	174	224	1.28	121.0	123	1.02
PM-10 [c]	130×130	125	102	31.1	628	560	174	228	1.31	176.0	159	0.90
6ST [d]	150×150	150	-	30.1	113	655	-	-	-	37.0	41	1.10
6LG [d]	150×150	150	-	41.4	113	655	-	-	-	37.0	41	1.10
8ST [d]	150×150	150	-	30.1	201	529	-	-	-	53.2	57	1.07
8LG [d]	150×150	150	-	41.4	201	529	-	-	-	53.2	57	1.07
10ST [d]	150×150	150	-	33.4	314	497	-	-	-	78.1	82	1.05
10LG [d]	150×150	150	-	38.3	314	497	-	-	-	78.1	90	1.15
12LG [d]	150×150	150	-	36.9	452	524	-	-	-	118.5	70	1.04
Average									1.17			1.08
Standard deviation									0.11			0.18
COV%									9.4			16.8

(a) Only the 2 integrity bars which passed through the column cage in each direction considered
(b) Specimens tested by Ghannoum (1998)
(c) Specimens tested by Mirzaei (2010)
(d) Slabs tested by Melo and Regan (1998) with integrity bars in one direction only

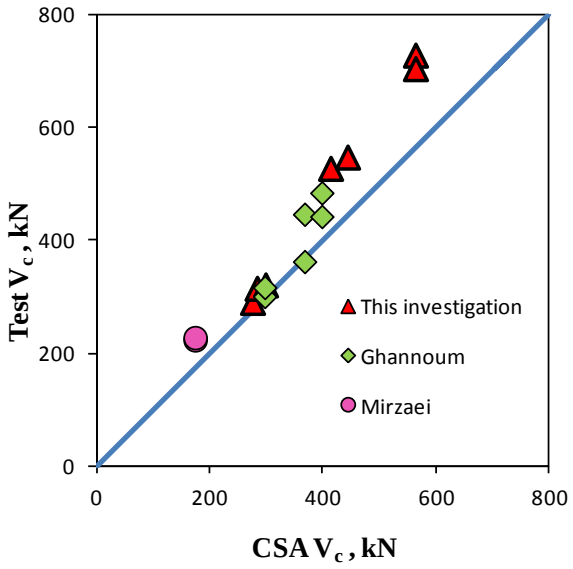

(a) punching shear

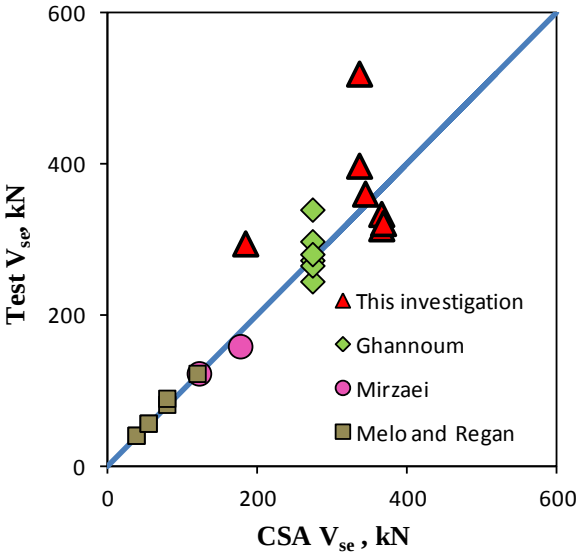

(b) post-punching resistance

Fig. 6.15. Comparisons of predicted and experimentally determined shear resistances

6.4 Verification of Analytical Model

The comparisons between the predictions obtained using the analytical model described in Chapter 5and the experimental results for slab-column specimens SS, RS, D1, S1, S2 and R2 are shown in Figs.6.16 through 6.21. Figs. 6.16(a) through 6.21(a) show the predicted contributions of the top bars to the post-punching shear resistance. The predicted contributions of the structural integrity bars to the post-punching response are shown in Figs. 6.16(b) through 6.21(b). In these figures the end of the contributions of the upper layer (point A) and lower layer (point B) of the top bars as well as the upper layer (point C) and lower layer (point D) of the structural integrity bars are shown. The combined responses, obtained by adding the individual responses together, are shown in Figs. 6.16(c) through 6.21(c).

It is noted that the top mat of bars becomes ineffective at a relatively early stage in the post-punching response and offers little resistance, whereas the structural integrity reinforcement is capable of providing significant post-punching resistance at very large displacements. The predictions of the post-punching load-deflection responses of these slabs are in good agreement with the experimentally determined responses, including the major behavioural aspects of the complex progressive damage to the concrete and the highly non-linear responses.

Table 6.2 shows the comparison between the results obtained by the CSA A23.3 Standard (CSA 2004) design method, the analytical model and the test data. It is noted that the simplified design equation used in the CSA A23.3 Standard (CSA 2004) provides reasonably accurate predictions of the post-punching shear resistance. There is a good agreement between the results predicted by the analytical model and the experimental results. The analytical model described in Chapter 5 is capable of predicting the maximum post-punching resistance, V_{pp}, and the ultimate average

displacement, $\Delta_{u,test}$ defined as the deflection reached when the load drops to 80% of the maximum post-punching shear resistance.

Fig. 6.22 compares the predicted post-punching shear strengths with the experimental results in this experimental program as well as the test results reported by Ghannoum (1998) and Mirzaei (2010).

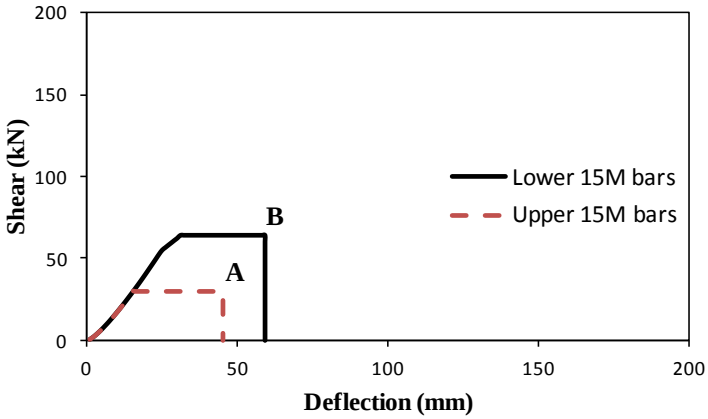

(a) Top Reinforcement

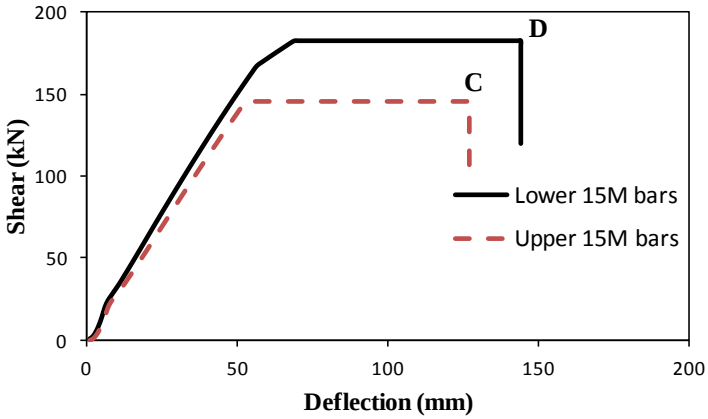

(b) Integrity Reinforcement

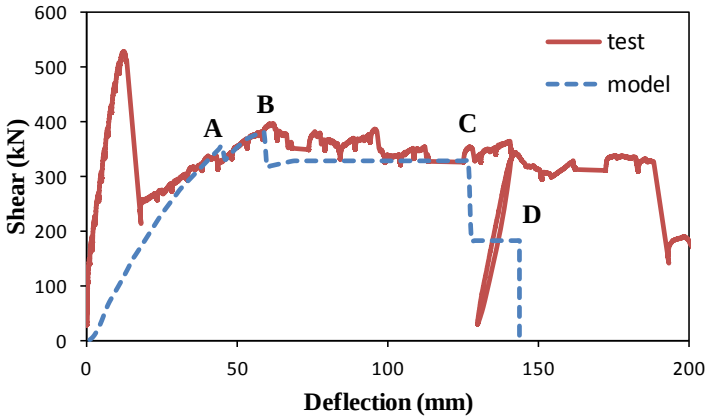

(c) Predicted vs. Experimental Results

Fig. 6.16. Contributions of top reinforcement and structural integrity reinforcement in predicting the shear vs. deflection response of specimen SS

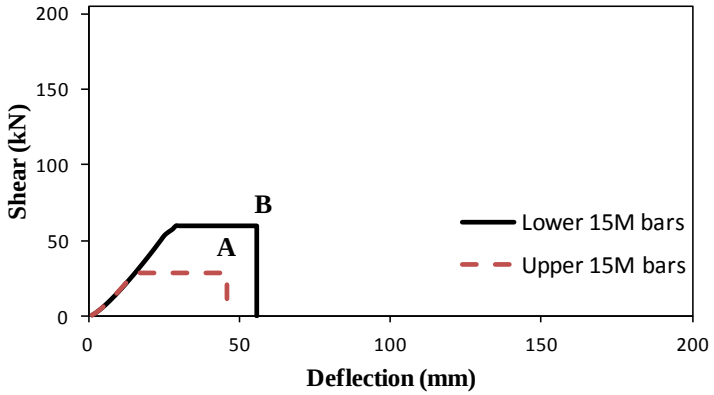

(a) Top Reinforcement

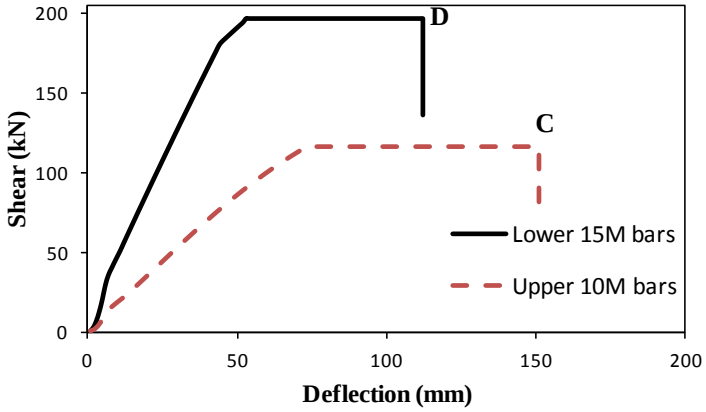

(b) Integrity Reinforcement

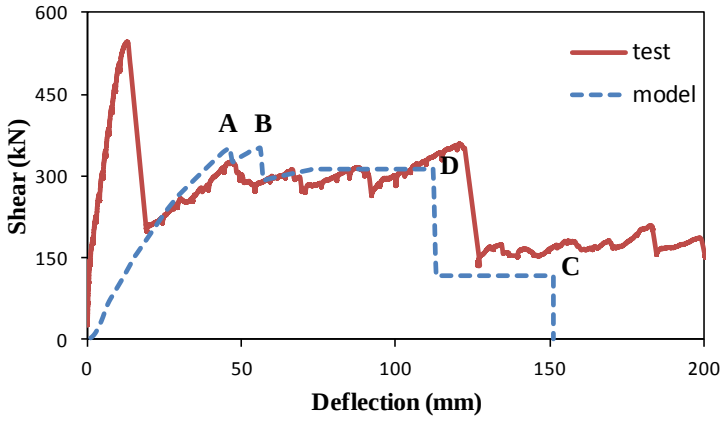

(c) Predicted vs. Experimental Results

Fig. 6.17. Contributions of top reinforcement and structural integrity reinforcement in predicting the shear vs. deflection response of specimen RS

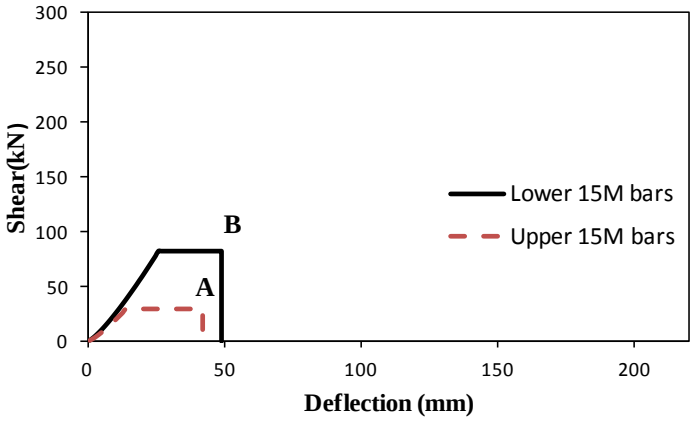

(a) Top Reinforcement

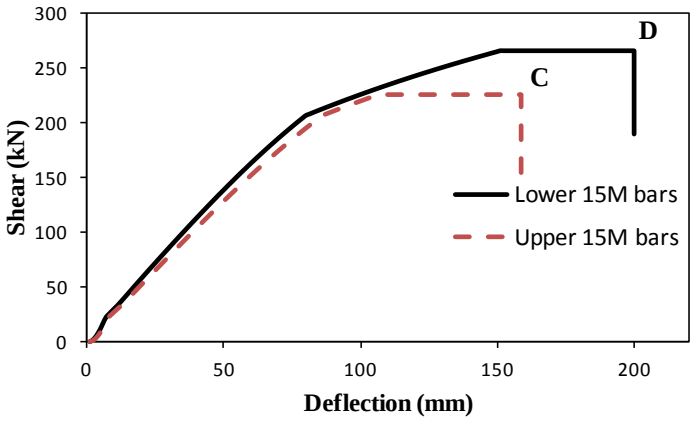

(b) Integrity Reinforcement

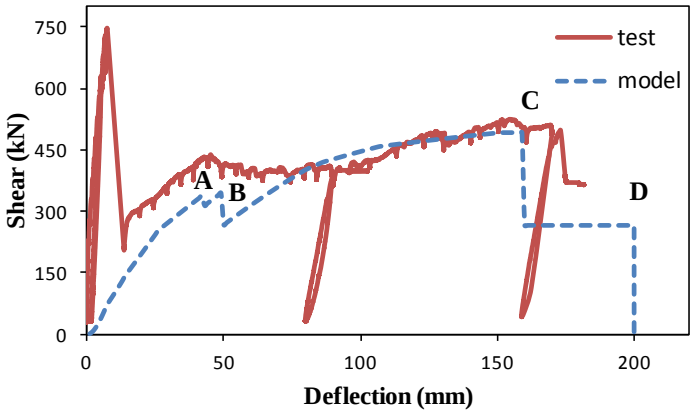

(c) Predicted vs. Experimental Results

Fig. 6.18. Contributions of top reinforcement and structural integrity reinforcement in predicting the shear vs. deflection response of specimen D1

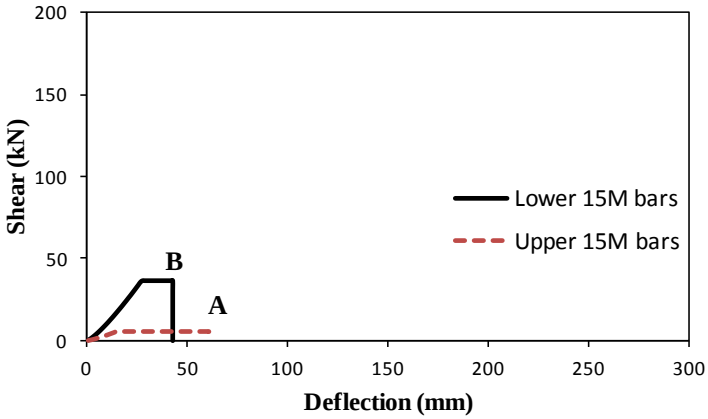

(a) Top Reinforcement

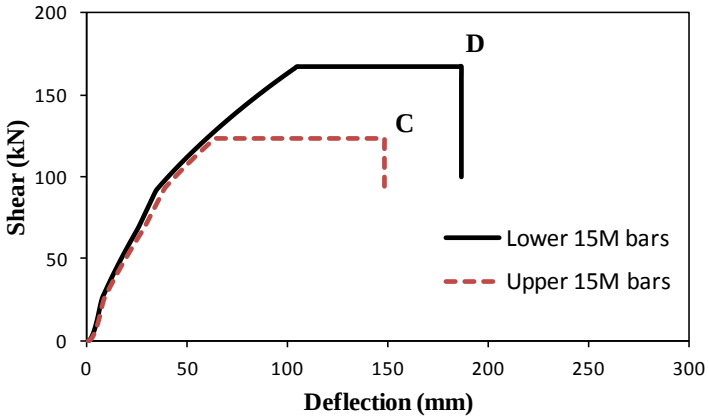

(b) Integrity Reinforcement

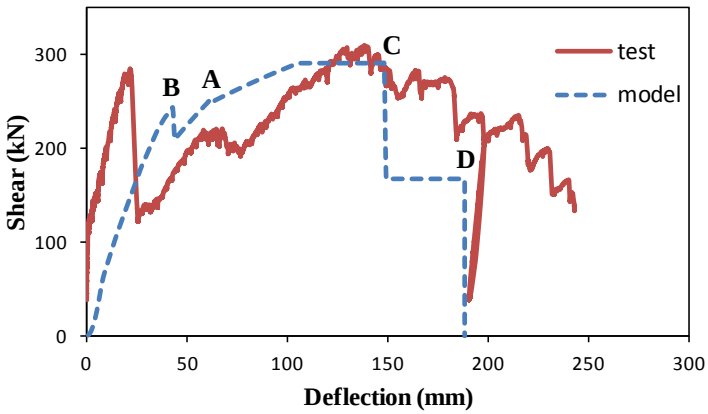

(c) Predicted vs. Experimental Results

Fig. 6.19. Contributions of top reinforcement and structural integrity reinforcement in predicting the shear vs. deflection response of specimen S1

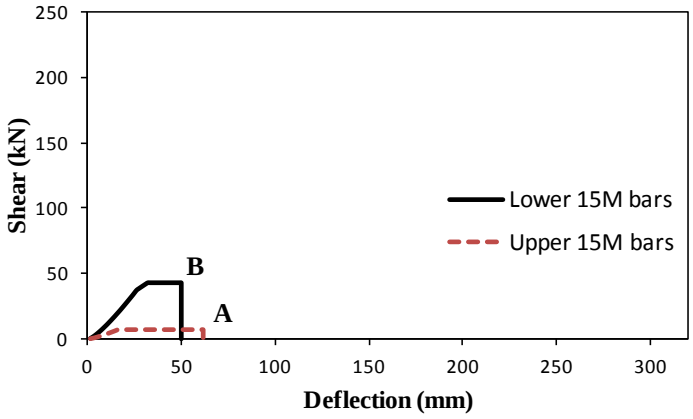

(a) Top Reinforcement

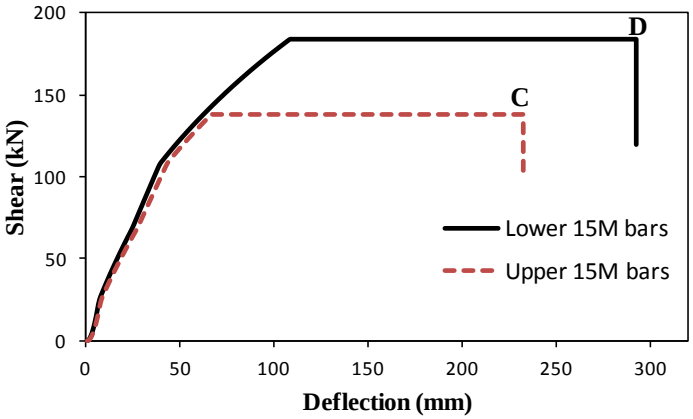

(b) Integrity Reinforcement

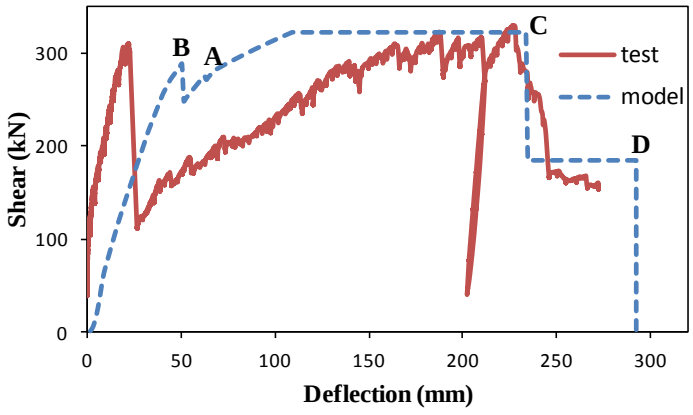

(c) Predicted vs. Experimental Results

Fig. 6.20. Contributions of top reinforcement and structural integrity reinforcement in predicting the shear vs. deflection response of specimen S2

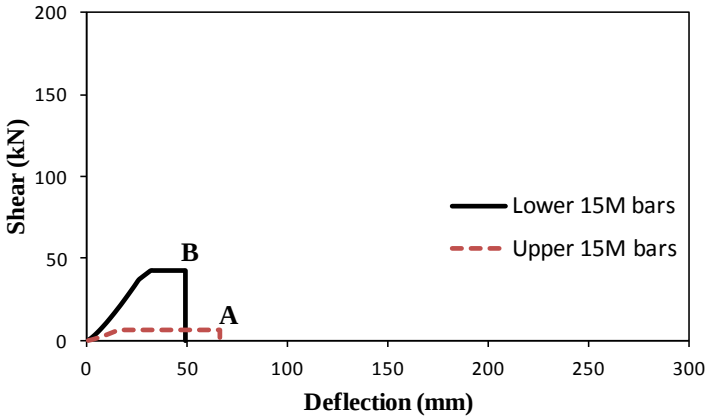

(a) Top Reinforcement

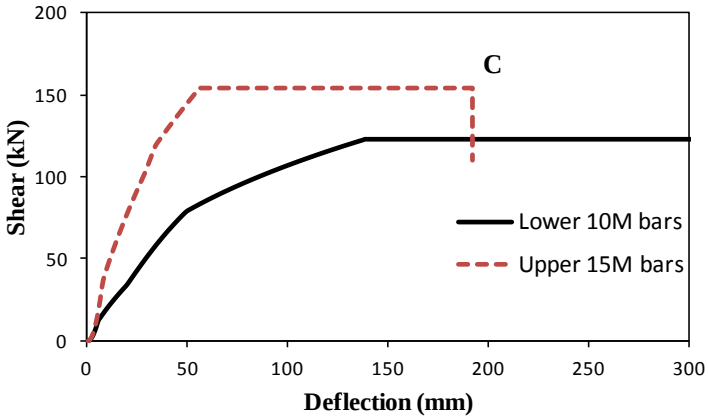

(b) Integrity Reinforcement

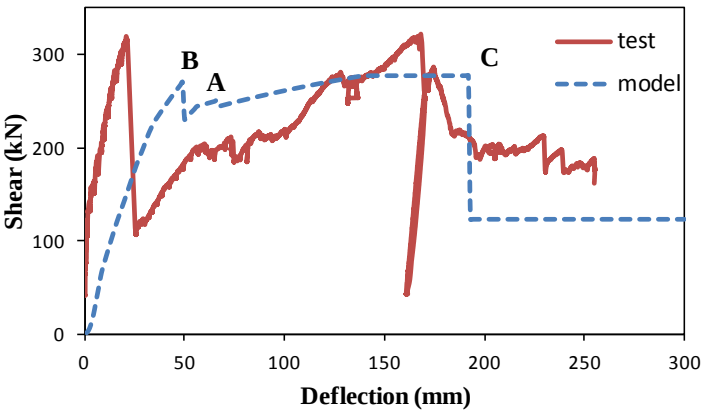

(c) Predicted vs. Experimental Results

Fig. 6.21. Contributions of top reinforcement and structural integrity reinforcement in predicting the shear vs. deflection response of specimen R2

Table 6.2. Comparison of theoretical and experimental results

Slab	h mm	f_c' MPa	Integrity bars	s mm	L_i mm	f_y MPa	Top bars	L_t mm	f_y MPa	V_{test} kN	V_{CSA} kN	$\frac{V_{test}}{V_{CSA}}$	V_{pp} kN	$\frac{V_{test}}{V_{pp}}$	$\Delta_{u,test}$ mm	$\Delta_{u,pred}$ mm	$\frac{\Delta_{u,test}}{\Delta_{u,pred}}$
S1	150	28	2-15M 2-15M	145 145	790 790	457 457	3-15M 1-15M	900 1350	457 457	314	365.6	0.86	290	1.08	183	149	1.22
S2	150	30	2-15M 2-15M	145 145	1000 1000	457 457	3-15M 1-15M	900 1350	457 457	333	365.6	0.91	321	1.04	234	234	1.00
R2	150	33	3-15M 2-10M	77 60	1000 820	457 455	3-15M 1-15M	875 1375	457 457	321	368	0.88	276	1.16	178	192	0.93
SS	200	26	2-15M 2-15M	120 120	790 790	420 420	5-15M 5-15M	1037 1037	420 420	397	336	1.18	381	1.04	188	128	1.46
RS	200	30	3-15M 2-10M	77 60	790 600	420 460	5-15M 5-15M	1010 1055	420 420	360	344	1.04	351	1.02	122	113	1.08
D1	250	22	2-15M 2-15M	120 120	790 790	420 420	8-15M 6-15M	1037 1037	420 420	519	336	1.54	492	1.05	174	160	1.08
S1-B [a]	150	37	3-10M 3-10M	55 55	1037 1037	454 454	6-15M 6-15M	1037 1037	445 445	245	272.4	0.90	270	0.9	75	48	1.56
S1-U [a]	150	37	3-10M 3-10M	55 55	1037 1037	454 454	4-15M 4-15M	1037 1037	445 445	273	272.4	1.00	227	1.20	50	48	1.04
S2-B [a]	150	57	3-10M 3-10M	55 55	1037 1037	454 454	6-15M 6-15M	1037 1037	445 445	298	272.4	1.09	335	0.89	38	51	0.74
S2-U [a]	150	57	3-10M 3-10M	55 55	1037 1037	454 454	4-15M 4-15M	1037 1037	445 445	266	272.4	0.97	282	0.94	54	51	1.05
S3-B [a]	150	61	3-10M 3-10M	55 55	1037 1037	454 454	6-15M 6-15M	1037 1037	445 445	340	272.4	1.25	357	0.95	57	53	1.07
S3-U [a]	150	61	3-10M 3-10M	55 55	1037 1037	454 454	4-15M 4-15M	1037 1037	445 445	281	272.4	1.03	302	0.93	43	53	0.81
PM-9 [b]	125	31	2-Ø8 2-Ø8	120 120	- -	616 616	7-Ø8 7-Ø8	- -	601 601	123	121	1.02	135	0.91	42	35	1.20
PM-10 [b]	125	31	2-Ø10 2-Ø10	120 120	- -	560 560	7-Ø8 7-Ø8	- -	601 601	159	176	0.9	172	0.92	50	41	1.21
AVG												**1.04**		**1.00**			**1.10**
STD												**0.18**		**0.09**			**0.22**
COV%												**17.3**		**9.0**			**20.0**

(a) Specimen tested by Ghannoum (1998)
(b) Specimen tested by Mirzaei (2010)

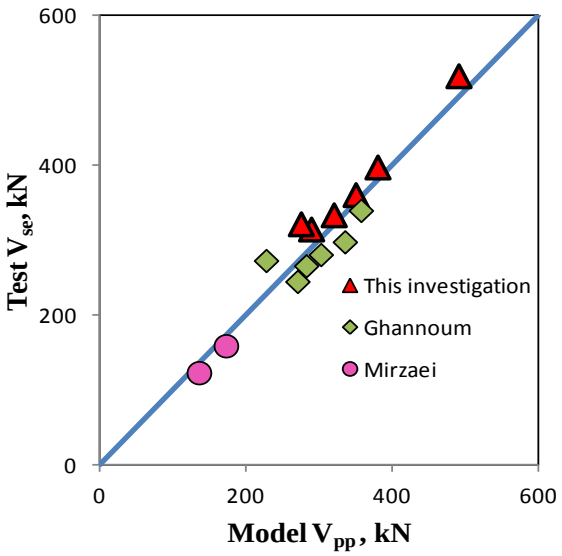

Fig. 6.22. Comparisons of model predictions with experimental results of post-punching shear resistance

Chapter 7: Conclusions

This thesis investigated the post-punching behaviour of interior slab-column connections. The effects of different parameters on the post-punching response were studied by comparing the results obtained from seven full-scale interior slab-column specimens tested at McGill University as well as experiments carried out by other researchers. All slabs had structural integrity reinforcement that fulfilled the requirements of the CSA A23.3-04 standard. In addition, an analytical model for predicting the complete post-punching shear response of slab-column connections was developed which accounts for the individual contributions of each layer of top reinforcement and each layer of the structural integrity reinforcement. The following conclusions are based on the observations from the test results of the slab-column connections and from the analytical model that was used to predict the complete post-punching responses:

(1) A slab without structural integrity reinforcement fails in a brittle manner immediately after a punching shear failure with the top bars ripping out of the top surface of the slab.

(2) The provision of structural integrity reinforcement in accordance with the requirements of CSA A23.3-04 gives a slab the ability to develop considerable post-punching resistance while permitting the slab to undergo very large displacements.

(3) Top slab reinforcing bars, in the vicinity of the column, provided a limited post-punching shear resistance and become ineffective at a deflection which is considerably less than that for the structural integrity reinforcement. The use of top reinforcement concentrated in a region close to the column increased the post-punching shear resistance.

(4) Increasing the thickness of a slab increases the post-punching resistance of slab-column connections due to the increase in the breakout resistance of the concrete above the structural integrity reinforcement. For very thick slabs the resistance is limited by either pullout or rupture of the structural integrity bars at very large displacements.

(5) Structural integrity reinforcement that protrudes a minimum distance of $2\ell_d$ from the column face is capable of developing the post-punching shear resistance as given in the design expression in the CSA A23.3-04 standard.

(6) The effect of increasing the protruding length of structural integrity reinforcing steel beyond a distance of $2\ell_d$ from the column face did not result in significant increases in the post-punching strength but provided the slab with an ability to undergo even larger displacements.

(7) Slab-column connections with rectangular columns and having three times the structural integrity reinforcement in one direction compared to the perpendicular direction exhibited similar post-punching strengths and ductility compared to specimens with square columns and having equal amounts of structural integrity reinforcement in the two directions.

(8) The placement of the structural integrity reinforcement is important with bars passing through the column core being the most effective, with bars passing through the column but outside of the core being less effective at very large displacements and with bars outside of the column region being ineffective.

(9) Structural integrity reinforcement, designed and detailed in accordance with the CSA A23.3-04 standard, and placed in the bottom of a drop panel was found to be effective, provided that 50% of the bottom bars in the column strip are extended a distance of 75 mm past the centreline of the column in both directions, as required for slabs without drop panels.

(10) The design expressions in the CSA standard A23.3-04 are based on nominal resistances that give typically conservative strength predictions for both punching shear and the post-punching resistance of slabs containing properly design and detailed structural integrity reinforcement.

(11) An analytical model was developed to predict the post-punching response of slab-column connections. This model satisfies compatibility of deformation and equilibrium, as well as including the non-linear response of the steel reinforcement. This model is capable of predicting the complete post-punching response of slab-column connections.

(12) The analytical model is capable of predicting the progressive breakout of each layer of the top reinforcing bars and the structural integrity bars, the pullout of the top bars and the structural integrity bars and the possible rupturing of the reinforcement.

(13) The predicted shear-deflection responses agree reasonably well with the post-punching shear responses of the slab-column specimens that were tested.

(14) The predicted maximum post-punching resistance and ultimate deflection agree well with the large variety of experiments reported by others.

Some recommendations for further studies on the post-punching behaviour of the slab-column connections are:

- Experiments on edge and corner slab-column connections would enable an assessment of the CSA A23.3-04 standard design philosophy.
- Experiments on multi-panel two-way slab structures would enable a study of the ability of load redistribution to adjacent supports after a local punching shear failure occurs.
- Develop a non-linear finite element analysis technique to simulate the initial punching shear failure and the possible propagation of the failure to adjacent supports. The initial failures at interior, exterior and corner column locations need to be studied to determine whether progressive collapse would occur.
- Experiments on the effects of misplaced reinforcement, corrosion of bars and delamination on the post-punching response of slab-column connections with and without structural integrity reinforcement. These effects can cause an initial failure and would affect the post-punching shear resistance.

References

ACI Committee 349. 1978. “Proposed Addition to: Code for Nuclear Safety Related Concrete Structures (ACI 349-76),” American Concrete Institute Journal, Vol. 75, No. 8, pp. 329-335.

ACI Committee 318. 1983. “Building Code Requirements for Reinforced Concrete,” American Concrete Institute, Detroit, MI, 111 pp.

ACI Committee 318. 2011. “Building Code Requirements for Structural Concrete (318-11) and Commentary,” American Concrete Institute, Farmington Hills, MI, 503 pp.

ASTM A370-08. 2008. “Standard Test Methods and Definitions for Mechanical Testing of Steel Products,” ASTM International, West Conshohocken, PA, 47 pp.

Black, M. S. 1975. “Ultimate Strength Study of Two-Way Concrete Slabs,” Journal of the Structural Division, American Society of Civil Engineers, Vol. 101, No ST1, pp. 311-324.

CEB-FIP MC 90. 1993. “Design of Concrete Structures, CEB-FIP Model Code 1990,” British Standard Institution, London, UK, 437 pp.

Cook, W.D. 1982. “Tensile Membrane Action in Reinforced Concrete Slabs,” M. Eng. Thesis, Department of Civil Engineering, McGill University, Montreal, QC, 144 pp.

CSA A23.3-M84. 1984. “Design of Concrete Structures,” Canadian Standards Association (CSA), Rexdale, ON, 281 pp.

CSA A23.3-94. 1994. “Design of Concrete Structures,” Canadian Standards Association (CSA), Mississauga, ON, Canada, 199 pp.

CSA A23.3-04. 2004. “Design of Concrete Structures,” Canadian Standards Association (CSA), Mississauga, ON, Canada, 214 pp.

Egberts, M. J. L. 2009. “Preventing Progressive Collapse of Flat Plate Structures with an Irregular Layout of Structural Integrity Reinforcement,” M. Eng. Thesis, Department of Civil Engineering, McGill University, Montreal, QC, 105 pp.

Eurocode 2. 2004. “Design of Concrete Structures - Part 1-1: General Rules and Rules for Buildings,” CEN, EN 1992-1-1, European Committee for Standardization, Brussels, Belgium, 225 pp.

Ghannoum, C.M. 1998. “Effect of High-Strength Concrete on the Performance of Slab-Column Specimens,” M. Eng. Thesis, Dept. of Civil Engineering, McGill University, Montreal, QC, 91 pp.

Hawkins, N.M., and Mitchell, D. 1979. “Progressive Collapse of Flat Plate Structures,” Journal of the American Concrete Institute, Vol. 76, No. 7, pp. 775-808.

King, S, and Delatte, N.J. 2004. “Collapse of 2000 Commonwealth Avenue: Punching Shear Case Study,” Journal of Performance of Constructed Facilities, American Society of Civil Engineers, Vol. 18, No. 1, pp. 54-61.

Kunnath, S. K., Heo, Y., and Mohle, J.F. 2009. “Nonlinear Uniaxial Material Model for Reinforcing Steel Bars,” Journal of Structural Engineering, American Society of Civil Engineers, Vol. 135, No. 4, pp. 335-343.

Lew, H.S., Carino, N. J., and Fattal, S. G. 1982. “Cause of the Condominium Collapse in Cocoa Beach, Florida,” Concrete International, American Concrete Institute, Vol. 4, No. 8, pp. 64-73.

Leyendecker, E.V., and Fattal, S.G. 1973. “Investigation of the Skyline Plaza Collapse in Fairfax County, Virginia,” Centre for Building Technology Report BSS 94 , Institute for Applied Technology, National Bureau of Standards, Washington, D.C., 57 pp.

McPeake, F. A. 1980. “Post-Punching Resistance of Internal Slab-Column Connection,” B.Sc. Honours Project, Department of Civil Engineering, Queen’s University of Belfast, U.K., 107 pp.

Melo, G. S. S. A., and Regan, P. E. 1998. “Post-Punching Resistance of Connections between Flat Slabs and Interior Columns,” Magazine of Concrete Research, Vol. 50, No. 4, pp. 319-327.

Mirzaei, Y. 2010. “Post-Punching Behaviour of Reinforced Concrete Slabs,” Ph.D. Thesis, École Polytechnique Fédérale de Lausanne (EPFL), Switzerland, 140 pp.

Mitchell, D. 1993. “Controversial Issues in the Seismic Design of Reinforced Concrete Frames,” Recent Developments in Lateral Force Transfer in Buildings, Thomas Paulay Symposium, American Concrete Institute, La Jolla, CA, pp.73- 93.

Mitchell, D., and Cook, W. D. 1984. “Preventing Progressive Collapse of Slab Structures,” Journal of Structural Engineering, American Society of Civil Engineers, Vol. 110, No.7, pp.1513-1532.

Mitchell, D., Adams, J., DeVall, R.H., Lo, R.C., and Weichert, D. 1986. “Lessons from the 1985 Mexican Earthquake,” Canadian Journal of Civil Engineering, Vol. 13, No. 5, pp. 535-557.

Orangun, C.O., Jirsa, J. O., and Breen, J. E. 1977. “A Reevaluation of Test Data on Development Length and Splices,” Journal, American Concrete Institute, Vol. 74, No. 3, pp. 114-122.

Park, R. 1964. “Tensile Membrane Behaviour of Uniformly Loaded Rectangular Reinforced Concrete Slabs with Fully Restrained Edges,” Magazine of Concrete Research, Vol. 16, No. 36, pp. 39-44.

Powell, D. S.1956. “The Ultimate Strength of Concrete Panels Subjected to Uniformly Distributed Loads,” M.Sc Thesis, Cambridge University, U.K., 169 pp.

Redl, E. 2009. “Post-Punching Response of Flat Plate Slab-Column Connections,” M. Eng. Thesis, Department of Civil Engineering, McGill University, Montreal, QC, 81 pp.

Regan, P. E., Walker, P. R., and Zakaria, K. A. A. 1979. “Tests of Reinforced Concrete Flat Slabs,” School of the Environment, CIRIA Project RP 220, Polytechnic of Central, London, U.K., 217 pp.

Appendix A: Design of Test Specimens

This appendix describes the design of the prototype structures and the test specimens. The detailed drawings are presented in Chapter 3.

A.1 Flat Plate Structure (Specimens SS and RS)

The prototype structure was designed with 6.0 m by 6.0 m bays. The applied loads on this structure were a superimposed dead load of 1.0 kPa and a live load of 2.4 kPa. A specified 28-day concrete compressive strength of 30 MPa was used for the design. The minimum specified steel yield stress was 400 MPa and the top and bottom clear covers were 25 mm. Specimen SS had 225 mm square central column stubs and specimen RS had 180×270 mm rectangular column stubs. The structure was designed according to the CSA A23.3-04 Standard. The same amount of top and bottom reinforcement was used for both specimens. The key steps of the design for specimen SS with square columns are given below:

1. Minimum Slab Thickness (Clause 13.2.3)

$$h_s \geq \frac{\ell_n}{30}\left(0.6+\frac{f_y}{1000}\right)$$

$$\geq \frac{(6000-225)}{30}\left(0.6+\frac{400}{1000}\right)$$

$$\geq 192.5\,mm$$

Use $h_s = 200\,mm$

2. Critical Shear Section (Clause 13.3.3)

It is noted that a small column was chosen such that the test specimens would be critical for punching shear.

$$d_{avg} = h_s - cover - d_b$$

$$= 200 - 25 - 15 = 160\,mm$$

$$b_0 = 4 \times \left(d_{avg} + c\right)$$

$$= 4 \times (160 + 225) = 1540\,mm$$

3. Maximum Shear Resistance (Clause 13.3.4)

Nominal shear resistance, V_n,

$$V_n = 0.33\sqrt{f_c'}b_0 d$$

$$= 0.33\sqrt{30}(1540)(160)$$

$$= 445.4\,kN$$

Factored shear resistance, V_r,

$$V_r = 0.38\lambda\phi_c\sqrt{f_c'}b_0 d$$

$$= 0.38(1.0)(0.65)\sqrt{30}(1540)(160)$$

$$= 333.3\,kN$$

4. Applied Shear Force (Clause 13.3.5)

Tributary area: $T.A = (6.0)^2 - (0.225 + 0.160)^2 = 35.85\,m^2$

Self weight: $s.w = (0.2\,m) \times \left(23.5\,kN/m^3\right) = 4.7\,kPa$

Factored loads: $w_f = 1.25w_D + 1.5w_L$

$$= 1.25(4.7 + 1.0) + 1.5(2.4) = 10.725\,kPa$$

Factored applied shear: $V_f = T.A \times w_f$

$$= 35.85 \times 10.725 = 384.5\, kN$$

5. Design for Moment (Clause 13.9)

Using the direct design method

$w_f = 10.725\, kPa$

$$M_o = \frac{w_f \ell_2 \ell_n{}^2}{8}$$

$$= \frac{10.725 \times 6.0 \times 5.775^2}{8} = 268.3\, kN.m$$

Negative factored moment: $M_f{}^- = 0.65 M_o = 174.4\, kN.m$

Positive factored moment: $M_f{}^+ = 0.35 M_o = 93.9\, kN.m$

5.1 Positive Moment (Bottom) Reinforcement

Use 10M bars

$d_{\min} = 200 - 25 - 10 - 5 = 160\, mm$

$M_f{}^+ = 93.9\, kN.m$

$$M_r = \phi_s (A_s f_y)\left[d - \frac{a}{2} \right]$$

$$= \phi_s (A_s f_y)\left[d - \frac{\phi_s (A_s f_y)}{2\alpha_1 \phi_c f_c' b} \right]$$

where $\alpha_1 = 0.85 - 0.0015 f_c' \geq 0.67$ (Clause 10.1.7)

$$= 0.805$$

$$M_r = 0.85A_s(400)\left[160 - \frac{0.85A_s(400)}{2(0.805)(0.65)(30)(6000)}\right]$$

Minimum reinforcement requirement: $0.002A_g = 0.002(200)(6000) = 2400mm^2$

Try $A_s = 2400mm^2 \rightarrow M_r = 127\,kN.m > 93.9 \quad OK$

Use 24-10M bars @ 240mm

5.2 Negative Moment (Top) Reinforcement

Use 15M bars

$d_{\min} = 200 - 25 - 15 - 7.5 = 152.5\,mm$

$M_f^- = 174.4\,kN.m$

$$M_r = \phi_s(A_s f_y)\left[d - \frac{a}{2}\right]$$

$$= \phi_s(A_s f_y)\left[d - \frac{\phi_s(A_s f_y)}{2\alpha_1\phi_c f_c' b}\right]$$

where $\alpha_1 = 0.85 - 0.0015 f_c' \geq 0.67$ (Clause 10.1.7)

$= 0.805$

$$M_r = 0.85A_s(400)\left[152.5 - \frac{0.85A_s(400)}{2(0.805)(0.65)(30)(6000)}\right]$$

To ensure that the slabs would not fail in flexure:

Try 28 bars, $A_s = 5600mm^2 > A_{s,\min} \rightarrow M_r = 271.1\,kN.m > 174.4 \quad OK$

Band width: $b_b = c + 3h = 825mm$

One-third of total steel must be in band width:

Use 9-15M bars @ 115 *mm* in band width and remaining 19-15M bars @ 200 *mm* for lower layer of top bars.

To ensure that almost equal negative moment resistance is provided each way, the upper layer of top reinforcement was determined to be: 7-15M bars @ 160 *mm* in band width and remaining 19-15M bars @ 200 *mm* for lower layer of top bars

6. Curtailment of Reinforcement (Clause 13.10.8)

Only column strip considered

Top Reinforcement:

50% extends $0.3\ell_n$ = 1800*mm*

50% extends $0.2\ell_n$ = 1200*mm*

Maximum length available in test specimen is 0.5(2300-225) =1037.5mm

Bottom reinforcement:

50% extends 75 *mm* over the column centreline

50% terminates $0.125\ell_1$ = 750 *mm* from column centreline.

7. Structural Integrity Reinforcement (Clause 13.10.6)

$$\sum A_{sb} \geq \frac{2V_{se}}{f_y}$$

Specified loads: (4.7+1.0+2.4)× (6×6-0.225^2) =291 *kN*

Twice the self-weight: 2×4.7× (6×6-0.225^2) = 338 *kN* (**governs**)

$$\sum A_{sb} = \frac{2\times 338\times 1000}{400} = 1690mm^2$$

Required for each side: $\frac{1690}{4} = 422.5mm^2$

It was decided to use 2 - 15M bars in each direction (i.e., 400 mm^2 in each direction) and extend the bars $2\ell_d = 790mm$ from column face

8. Checking the Failure Mode

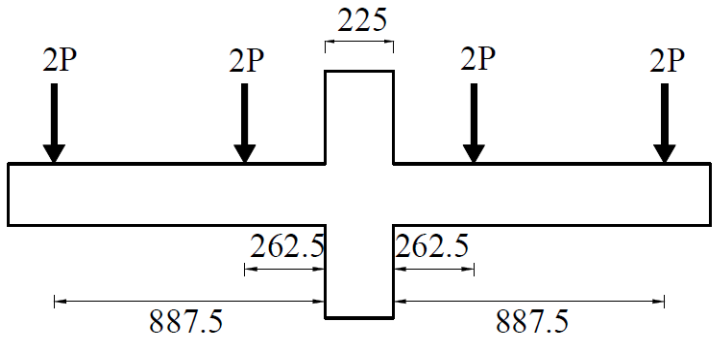

$V_f = 8P$

$M_f = (0.8875 + 0.2625) \times 2P$

$= 2.3P = 2.3 \cdot \frac{V_f}{8} = 0.2875 \cdot V_f$

If, $V_f = V_n = 445.4\,kN$ then

$M_f = 0.2875 \times 445.4 = 128\,kN.m$

$M_{n,15\text{–}15M} = 169.4\,kN.m$

$\rightarrow \frac{M_n}{M_f} = 1.32 > 1.0$

It is noted that punching shear failure is predicted to occur prior to flexural yielding.

A.2 Slabs with Drop Panels (Specimens D1 and D2)

A prototype structure was designed according to the CSA A23.3-04 Standard with 5.6 m by 5.6 m bays for loads including a superimposed dead load of 1.0 kPa and a live load of 4.8 kPa. Design assumptions included a clear cover of 25 mm, a concrete compressive strength of 30 MPa and minimum specified reinforcing steel yield strength of 400 MPa. The key steps of the design are described below:

1. Minimum Slab Thickness (Clause 13.2.4)

$$h_s \geq \frac{\ell_n}{30}\left(0.6+\frac{f_y}{1000}\right)-\frac{2x_d}{\ell_n}\Delta_h$$

$$\geq \frac{(5600-225)}{30}\left(0.6+\frac{400}{1000}\right)-\frac{2(800)}{(5600-225)}(0.9)$$

$$\geq 153\,mm$$

Use $h_s = 160\,mm$

2. Critical Shear Section (Clause 13.3.3)

$$d_{avg} = h_s - cover - d_b$$

$$b_o = 4\times\left(d_{avg}+c\right)$$

At column face:

$$d_{avg} = 250-25-15 = 210mm$$

$$b_o = 4\times(210+225) = 1740\,mm$$

At the edge of the drop panel:

$$d_{avg} = 160-25-15 = 120mm$$

$$b_o = 4 \times (120 + 1825) = 7780\ mm$$

3. Maximum Shear Resistance (Clause 13.3.4)

Nominal shear resistance, V_n, is the smaller of:

$$V_n = 0.33\sqrt{f_c'}b_0 d$$

$$V_n = 0.083(\frac{\alpha_s d}{b_o} + 2)\sqrt{f_c'}b_o d$$

At column face: $V_n = 0.33\sqrt{f_c'}b_0 d$

$$= 0.33\sqrt{30}(1740)(210) = 660.4\ kN$$

At face of drop: $V_n = 0.083(\frac{\alpha_s d}{b_o} + 2)\sqrt{f_c'}b_o d$

$$= 0.083(\frac{40(120)}{7780} + 2)\sqrt{30}(7780)(120) = 1110.7\ kN$$

Factored shear resistance, V_r

At column face: $V_r = 0.38\lambda\phi_c\sqrt{f_c'}b_o d = 495\ kN$

At face of drop: $V_r = \left(\frac{\alpha_s d}{b_o} + 0.19\right)\lambda\phi_c\sqrt{f_c'}b_o d = 836\ kN$

4. Applied Shear Force (Clause 13.3.5)

Self weight: $s.w = (0.16m) \times (23.5\ kN/m^3) + \frac{(1.825m \times 1.825m)}{(5.6m \times 5.6m)}(0.09m) \times (23.5\ kN/m^3) = 4.0\ kPa$

Factored loads: $w_f = 1.25w_D + 1.5w_L$

$$= 1.25(4.0 + 1.0) + 1.5(4.8) = 13.4\ kPa$$

Factored applied shear: $V_f = T.A \times w_f$

At column face:

$$T.A = (5.6)^2 - (0.225 + 0.21)^2 = 31.17\, m^2$$

$$V_f = (31.17)(13.4) = 417.6\, kN$$

At face of drop:

$$T.A = (5.6)^2 - (1.825 + 0.120)^2 = 27.6\, m^2$$

$$V_f = (27.6)(13.4) = 370\, kN$$

5. Design for Moment (Clause 13.9)

Using direct design method

$w_f = 13.4\, kPa$

$$M_o = \frac{w_f \ell_2 \ell_n{}^2}{8}$$

$$= \frac{13.4 \times 5.6 \times 5.375^2}{8} = 271\, kN.m$$

Negative factored moment: $M_f{}^- = 0.65 M_o = 176\, kN.m$

Positive factored moment: $M_f{}^+ = 0.35 M_o = 94\, kN.m$

5.1 Positive Moment (Bottom) Reinforcement

Use 10M bars

$d_{\min} = 160 - 25 - 10 - 5 = 120\, mm$

$M_f{}^+ = 94\, kN.m$

$$M_r = \phi_s (A_s f_y)\left[d - \frac{a}{2} \right]$$

$$= \phi_s (A_s f_y)\left[d - \frac{\phi_s (A_s f_y)}{2\alpha_1 \phi_c f_c' b} \right]$$

where $\alpha_1 = 0.85 - 0.0015 f_c' \geq 0.67$ (Clause 10.1.7)

$$= 0.805$$

$$M_r = 0.85 A_s (400)\left[120 - \frac{0.85 A_s (400)}{2(0.805)(0.65)(30)(5600)} \right]$$

Minimum reinforcement requirement: $0.002 A_g = 0.002(200)(5600) = 2240 mm^2$

Try $A_s = 2400 mm^2 \rightarrow M_r = 94\, kN.m$ OK

Use 24-10M bars @ $240 mm$

5.2 Negative Moment (Top) Reinforcement

Use 15M bars

$M_f^- = 176\, kN.m$

In drop: $d_{\max} = 250 - 25 - 7.5 = 217.5\, mm$

Outside drop: $d_{\max} = 160 - 25 - 7.5 = 127.5\, mm$

Approximate moment resistance per bar in drop:

$$M_{r\,bar} = \phi_s A_{bar} f_y \times 0.9 d_{\max}$$

$$= 0.85 \times 200 \times 400 \times 0.9 \times 217.5 = 13.3\, kN.m$$

Approximate moment resistance per bar outside drop:

$$M_{r\,bar} = \phi_s A_{bar} f_y \times 0.9 d_{\max}$$

$$= 0.85 \times 200 \times 400 \times 0.9 \times 127.5 = 7.8\, kN.m$$

Band width: $b_b = c + 3h = 975 mm$

Required moment resistance within width b_b is 176/3 = 58.66 *kN.m*

Try extending same spacing throughout column strip.

Column strip: 5600/2 = 2800 *mm*

Number of bars in column strip: $= \frac{58.66}{13.3} \times \frac{2800}{975} = 12.6$

To ensure that the slabs would not fail in flexure:

Use 24 – 15M bars @ 120 mm for lower layer of top bars in column strip

Number bars in drop = 14

Number bars outside of drop = 10

Moment resistant provided in column strip:

$M_r = 14 \times 13.3 + 10 \times 7.8 = 264.2 \ kN.m$

To ensure that almost equal negative moment resistance is provided in each direction, a total of 22 bars spaced at 150 mm will be used in the upper layer of top reinforcing steel, with 12 bars located within the drop panel region.

6. Curtailment of Reinforcement (Clause 13.10.8)

Only column strip considered

Top Reinforcement:

50% extends $0.33\ell_n$ = 1850*mm*

50% extends $0.2\ell_n$ = 1100*mm*

Maximum length available in test specimen is 0.5(2300-225) =1037.5*mm*

Bottom reinforcement:

It was decided that 50% of the bottom bars would extend 75mm over the column centreline as required for slabs without drop panels.

50% terminates $0.125\ell_1 = 700mm$ from column centreline.

7. Structural Integrity Reinforcement (Clause 13.10.6)

$$\sum A_{sb} \geq \frac{2V_{se}}{f_y}$$

Specified loads: (4.0+1.0+4.8) × (5.6×5.6-0.225^2) =306 *kN* (**governs**)

Twice the self-weight: 2×4.0× (5.6×5.6-0.225^2) = 250 *kN*

$$\sum A_{sb} = \frac{2 \times 306 \times 1000}{400} = 1532mm^2$$

Required for each side: $\frac{1532}{4} = 384mm^2$

Use 2 – 15M bars in each direction (i.e., 400 mm^2 in each direction) and extend

$2\ell_d = 790mm$ from column face for specimen D1 and 4 – 10M (i.e., 400 mm^2 in each direction)

and extend 725 mm from column face for specimen D2.

8. Checking the Failure Mode

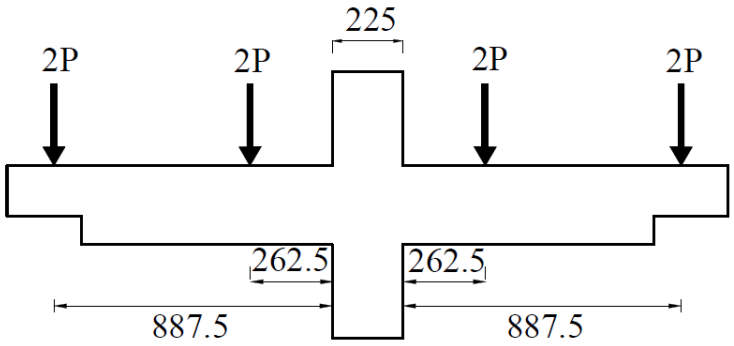

$V_f = 8P$

$M_f = (0.8875 + 0.2625) \times 2P$

$$= 2.3P = 2.3 \cdot \frac{V_f}{8} = 0.2875 \cdot V_f$$

If, $V_f = V_n = 660.4\,kN$ then

$$M_f = 0.2875 \times 660.4 = 190\,kN.m$$

$$M_{n,18\text{–}15M} = M_{n,14\text{–}15M}\,(inside\ drop) + M_{n,4\text{–}15M}(outide\ drop)$$

$$= 215 + 35 = 240\ kN.m$$

$$\rightarrow \frac{M_n}{M_f} = 1.27 > 1.0$$

Therefore it is predicted that punching shear failure would occur prior to flexural yielding.

Appendix B: Example of Calculation of the Predicted Post-Punching Response

B.1 Introduction

This appendix presents typical predictions using the computer program that was developed and also provides sample hand calculations of the post-punching shear response of specimen SS to illustrate the application of the analytical model that was developed. Details of the model are given in Chapter 5.

B.2 Detailed Predictions Using Computer Program

A computer program was developed to solve the nonlinear equilibrium and compatibility equations and calculate the post-punching shear response corresponding to increments of deflection. The program is capable of predicting the different possible failure modes and the contribution of each layer of the top mat of reinforcement and each layer of the integrity reinforcement to the post-punching response.

The input data for the each layer of top reinforcement and integrity reinforcement for specimen SS are shown in Figs B1, B2, B3 and B4.

Figs B5, B6, B7 and B8 present the detailed calculation results for the contribution of each layer of the top and integrity bars to the post-punching response.

The total predicted post-punching response for specimen SS is shown in Fig. B9.

Fig B1. Input data for upper layer of the top bars

Fig B2. Input data for lower layer of the top bars

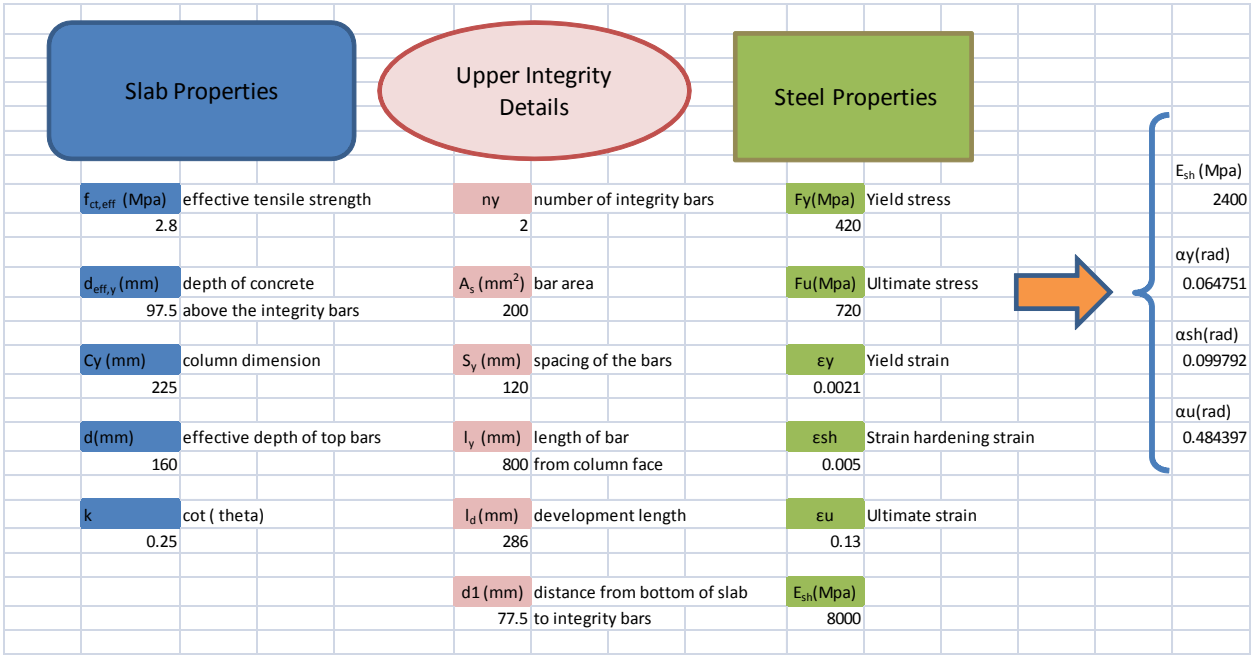

Fig B3. Input data for upper layer of the integrity bars

Fig B4. Input data for lower layer of the integrity bars

x(mm)	s/2x	ϕ(Rad)	sinϕ	A1(mm^2)	Ach(mm^2)	V_{br}(N)	α(rad)	δ(mm)	Strain	Stress
1	250	#NUM!	0	0	0.98125	1.76625	0.002095	0.067054	2.2E-06	0.439086
2	125	#NUM!	0	0	3.925	7.065	0.003236	0.110014	5.23E-06	0.000369
3	83.33333	#NUM!	0	0	8.83125	15.89625	0.004262	0.15343	9.08E-06	1.816401
4	62.5	#NUM!	0	0	15.7	28.26	0.005174	0.196618	1.34E-05	2.677171
5	50	#NUM!	0	0	24.53125	44.15625	0.006086	0.243455	1.85E-05	3.704373
6	41.66667	#NUM!	0	0	35.325	63.585	0.00677	0.284364	2.29E-05	4.583998
7	35.71429	#NUM!	0	0	48.08125	86.54625	0.007569	0.333026	2.86E-05	5.728557
8	31.25	#NUM!	0	0	62.8	113.04	0.008253	0.379637	3.41E-05	6.811035
9	27.77778	#NUM!	0	0	79.48125	143.0663	0.008937	0.428984	3.99E-05	7.987141
10	25	#NUM!	0	0	98.125	176.625	0.009621	0.481069	4.63E-05	9.256878
11	22.72727	#NUM!	0	0	118.7313	213.7163	0.010191	0.529961	5.19E-05	10.38652
12	20.83333	#NUM!	0	0	141.3	254.34	0.010875	0.587292	5.91E-05	11.82792
13	19.23077	#NUM!	0	0	165.8313	298.4963	0.011445	0.640975	6.55E-05	13.10062
14	17.85714	#NUM!	0	0	192.325	346.185	0.012016	0.696939	7.22E-05	14.43835
15	16.66667	#NUM!	0	0	220.7813	397.4063	0.012586	0.755184	7.92E-05	15.8411
16	15.625	#NUM!	0	0	251.2	452.16	0.013156	0.81571	8.65E-05	17.3089
17	14.70588	#NUM!	0	0	283.5813	510.4463	0.013612	0.871219	9.26E-05	18.52996
18	13.88889	#NUM!	0	0	317.925	572.265	0.014182	0.93608	0.000101	20.11482
19	13.15789	#NUM!	0	0	354.2313	637.6163	0.014752	1.003223	0.000109	21.76472
20	12.5	#NUM!	0	0	392.5	706.5	0.015208	1.064663	0.000116	23.13148
21	11.90476	#NUM!	0	0	432.7313	778.9163	0.015778	1.136141	0.000124	24.89846
22	11.36364	#NUM!	0	0	474.925	854.865	0.016235	1.201461	0.000132	26.35888
23	10.86957	#NUM!	0	0	519.0813	934.3463	0.016691	1.268605	0.000139	27.86094
24	10.41667	#NUM!	0	0	565.2	1017.36	0.017147	1.337576	0.000147	29.40463
25	10	#NUM!	0	0	613.2813	1103.906	0.017717	1.417496	0.000157	31.39279

Arrange

$V_{br,max}$ (kN)

29.84963

Failure Mode: pull out of the bar

$V_{rupture}$ (kN)

648.4896

δ_{max} (mm)

44.85334

Fig B5. Detailed calculation results for upper layer of the top bars

x(mm)	s/2x	ϕ(Rad)	sinϕ	A1(mm^2)	Ach(mm^2)	V_{br}(N)	α(rad)	δ(mm)	Strain	Stress
1	200	#NUM!	0	0	0.98125	1.76625	0.002095	0.067054	2.2E-06	0.439086
2	100	#NUM!	0	0	3.925	7.065	0.003236	0.110014	5.23E-06	0.000392
3	66.66667	#NUM!	0	0	8.83125	15.89625	0.004262	0.15343	9.08E-06	1.816401
4	50	#NUM!	0	0	15.7	28.26	0.005174	0.196618	1.34E-05	2.677171
5	40	#NUM!	0	0	24.53125	44.15625	0.006086	0.243455	1.85E-05	3.704373
6	33.33333	#NUM!	0	0	35.325	63.585	0.00677	0.284364	2.29E-05	4.583998
7	28.57143	#NUM!	0	0	48.08125	86.54625	0.007569	0.333026	2.86E-05	5.728557
8	25	#NUM!	0	0	62.8	113.04	0.008253	0.379637	3.41E-05	6.811035
9	22.22222	#NUM!	0	0	79.48125	143.0663	0.008937	0.428984	3.99E-05	7.987141
10	20	#NUM!	0	0	98.125	176.625	0.009621	0.481069	4.63E-05	9.256878
11	18.18182	#NUM!	0	0	118.7313	213.7163	0.010191	0.529961	5.19E-05	10.38652
12	16.66667	#NUM!	0	0	141.3	254.34	0.010875	0.587292	5.91E-05	11.82792
13	15.38462	#NUM!	0	0	165.8313	298.4963	0.011445	0.640975	6.55E-05	13.10062
14	14.28571	#NUM!	0	0	192.325	346.185	0.012016	0.696939	7.22E-05	14.43835
15	13.33333	#NUM!	0	0	220.7813	397.4063	0.012586	0.755184	7.92E-05	15.8411
16	12.5	#NUM!	0	0	251.2	452.16	0.013156	0.81571	8.65E-05	17.3089
17	11.76471	#NUM!	0	0	283.5813	510.4463	0.013612	0.871219	9.26E-05	18.52996
18	11.11111	#NUM!	0	0	317.925	572.265	0.014182	0.93608	0.000101	20.11482
19	10.52632	#NUM!	0	0	354.2313	637.6163	0.014752	1.003223	0.000109	21.76472
20	10	#NUM!	0	0	392.5	706.5	0.015208	1.064663	0.000116	23.13148
21	9.52381	#NUM!	0	0	432.7313	778.9163	0.015778	1.136141	0.000124	24.89846
22	9.090909	#NUM!	0	0	474.925	854.865	0.016235	1.201461	0.000132	26.35888
23	8.695652	#NUM!	0	0	519.0813	934.3463	0.016691	1.268605	0.000139	27.86094
24	8.333333	#NUM!	0	0	565.2	1017.36	0.017147	1.337576	0.000147	29.40463
25	8	#NUM!	0	0	613.2813	1103.906	0.017717	1.417496	0.000157	31.39279
26	7.692308	#NUM!	0	0	663.325	1193.985	0.018173	1.490346	0.000165	33.03016
27	7.407407	#NUM!	0	0	715.3313	1287.596	0.018629	1.565021	0.000174	34.70917
28	7.142857	#NUM!	0	0	769.3	1384.74	0.019085	1.641522	0.000182	36.42983
29	6.896552	#NUM!	0	0	825.2313	1485.416	0.019541	1.719849	0.000191	38.19212

Arrange

$V_{br,max}$ (kN)

63.76163

Failure Mode: pull out of the bar

$V_{rupture}$ (kN)

648.4896

δ_{max} (mm)

59.44457

Fig B6. Detailed calculation results for lower layer of the top bars

x(mm)	s/2x	ϕ(Rad)	sinϕ	A1(mm^2)	Ach(mm^2)	V_{br}(N)	α(rad)	δ(mm)	Strain	Stress
1	60	#NUM!	0	0	6.28	17.584	0.006071	0.476576	1.84E-05	3.685701
2	30	#NUM!	0	0	25.12	70.336	0.009618	0.764659	4.63E-05	9.251047
3	20	#NUM!	0	0	56.52	158.256	0.012574	1.012258	7.91E-05	15.81151
4	15	#NUM!	0	0	100.48	281.344	0.015175	1.236872	0.000115	23.0308
5	12	#NUM!	0	0	157	439.6	0.017658	1.456948	0.000156	31.18505
6	10	#NUM!	0	0	226.08	633.024	0.019905	1.662257	0.000198	39.62601
7	8.571429	#NUM!	0	0	307.72	861.616	0.022033	1.862081	0.000243	48.55469
8	7.5	#NUM!	0	0	401.92	1125.376	0.024161	2.066181	0.000292	58.39037
9	6.666667	#NUM!	0	0	508.68	1424.304	0.026053	2.25409	0.000339	67.8948
10	6	#NUM!	0	0	628	1758.4	0.028063	2.456155	0.000394	78.77887
11	5.454545	#NUM!	0	0	759.88	2127.664	0.029837	2.641316	0.000445	89.05482
12	5	#NUM!	0	0	904.32	2532.096	0.03161	2.830044	0.0005	99.96126
13	4.615385	#NUM!	0	0	1061.32	2971.696	0.033384	3.02234	0.000557	111.4984
14	4.285714	#NUM!	0	0	1230.88	3446.464	0.035039	3.207375	0.000614	122.8355
15	4	#NUM!	0	0	1413	3956.4	0.036694	3.395742	0.000674	134.7223
16	3.75	#NUM!	0	0	1607.68	4501.504	0.03835	3.587443	0.000736	147.159
17	3.529412	#NUM!	0	0	1814.92	5081.776	0.039887	3.771287	0.000796	159.1999
18	3.333333	#NUM!	0	0	2034.72	5697.216	0.041424	3.958229	0.000859	171.7152
19	3.157895	#NUM!	0	0	2267.08	6347.824	0.042961	4.148268	0.000924	184.705
20	3	#NUM!	0	0	2512	7033.6	0.044498	4.341408	0.000991	198.1695
21	2.857143	#NUM!	0	0	2769.48	7754.544	0.045917	4.525977	0.001055	211.0197
22	2.727273	#NUM!	0	0	3039.52	8510.656	0.047336	4.713408	0.001121	224.2748
23	2.608696	#NUM!	0	0	3322.12	9301.936	0.048754	4.903702	0.00119	237.9346
24	2.5	#NUM!	0	0	3617.28	10128.38	0.050173	5.09686	0.00126	251.9996
25	2.4	#NUM!	0	0	3925	10990	0.051592	5.292883	0.001332	266.4696
26	2.307692	#NUM!	0	0	4245.28	11886.78	0.053011	5.491774	0.001407	281.345
27	2.222222	#NUM!	0	0	4578.12	12818.74	0.054312	5.68114	0.001477	295.337
28	2.142857	#NUM!	0	0	4923.52	13785.86	0.055612	5.873133	0.001548	309.6697
29	2.068966	#NUM!	0	0	5281.48	14788.14	0.056913	6.067757	0.001622	324.3434

Arrange

$V_{br,max}$ (kN) 145.8677

Failure Mode: pull out of the bar

$V_{rupture}$ (kN) 268.2289

δ_{max} (mm) 125.0521

Fig B7. Detailed calculation results for upper layer of the integrity bars

x(mm)	s/2x	ϕ(Rad)	sinϕ	A1(mm^2)	Ach(mm^2)	V_{br}(N)	α(rad)	δ(mm)	Strain	Stress
1	60	#NUM!	0	0	6.28	17.584	0.006071	0.38551	1.84E-05	3.685701
2	30	#NUM!	0	0	25.12	70.336	0.009618	0.620383	4.63E-05	0.005638
3	20	#NUM!	0	0	56.52	158.256	0.012574	0.823638	7.91E-05	15.81151
4	15	#NUM!	0	0	100.48	281.344	0.015175	1.009227	0.000115	23.0308
5	12	#NUM!	0	0	157	439.6	0.017658	1.192049	0.000156	31.18505
6	10	#NUM!	0	0	226.08	633.024	0.019905	1.363648	0.000198	39.62601
7	8.571429	#NUM!	0	0	307.72	861.616	0.022033	1.531534	0.000243	48.55469
8	7.5	#NUM!	0	0	401.92	1125.376	0.024161	1.703693	0.000292	58.39037
9	6.666667	#NUM!	0	0	508.68	1424.304	0.026053	1.863207	0.000339	67.8948
10	6	#NUM!	0	0	628	1758.4	0.028063	2.0351	0.000394	78.77887
11	5.454545	#NUM!	0	0	759.88	2127.664	0.029837	2.193635	0.000445	89.05482
12	5	#NUM!	0	0	904.32	2532.096	0.03161	2.355735	0.0005	99.96126
13	4.615385	#NUM!	0	0	1061.32	2971.696	0.033384	2.5214	0.000557	111.4984
14	4.285714	#NUM!	0	0	1230.88	3446.464	0.035039	2.681576	0.000614	122.8355
15	4	#NUM!	0	0	1413	3956.4	0.036694	2.845081	0.000674	134.7223
16	3.75	#NUM!	0	0	1607.68	4501.504	0.03835	3.011917	0.000736	147.159
17	3.529412	#NUM!	0	0	1814.92	5081.776	0.039887	3.17267	0.000796	159.1999
18	3.333333	#NUM!	0	0	2034.72	5697.216	0.041424	3.336517	0.000859	171.7152
19	3.157895	#NUM!	0	0	2267.08	6347.824	0.042961	3.50346	0.000924	184.705
20	3	#NUM!	0	0	2512	7033.6	0.044498	3.673499	0.000991	198.1695
21	2.857143	#NUM!	0	0	2769.48	7754.544	0.045917	3.836742	0.001055	211.0197
22	2.727273	#NUM!	0	0	3039.52	8510.656	0.047336	4.002844	0.001121	224.2748
23	2.608696	#NUM!	0	0	3322.12	9301.936	0.048754	4.171806	0.00119	237.9346
24	2.5	#NUM!	0	0	3617.28	10128.38	0.050173	4.343629	0.00126	251.9996
25	2.4	#NUM!	0	0	3925	10990	0.051592	4.518315	0.001332	266.4696
26	2.307692	#NUM!	0	0	4245.28	11886.78	0.053011	4.695864	0.001407	281.345
27	2.222222	#NUM!	0	0	4578.12	12818.74	0.054312	4.865665	0.001477	295.337

Arrange

$V_{br,max}$ (kN) 183.0623

Failure Mode: pull out of the bar

$V_{rupture}$ (kN) 268.2289

δ_{max} (mm) 140.6257

Fig B8. Detailed calculation results for lower layer of the integrity bars

δ(mm)	$V_{br,total}$
1	1.698087
2	6.468132
3	14.08527
4	24.38121
5	36.8824
6	51.45147
7	64.94207
8	75.49466
9	84.9905
10	94.50179
11	104.154
12	114.188
13	124.5395
14	135.109
15	146.7168
16	155.0402
17	163.4286
18	171.9106
19	180.4547
20	189.0928
21	197.7718
22	206.4165
23	215.1518
24	223.8304
25	232.1478
26	239.5483
27	246.9281
28	254.2801
29	261.6213

Calculate total response

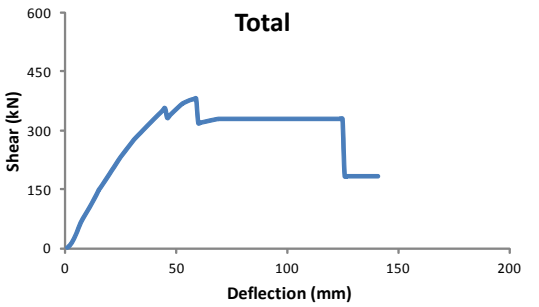

Fig B.9. Total predicted post-punching response for specimen SS

B.3 Hand calculation for bars in top mat

The following calculations present the contribution of each layer of top bars in specimen SS, to the post-punching shear response:

B.3.1 Upper 15M top bars

The number of effective top bars that pass through the punching shear failure cone and participate in the post-punching response is determined based on the geometry of failure surface that was presented in chapter 5 (see Fig.5.2).

Number of effective upper top bars: 5-15M

The depth of concrete over the reinforcing bars measured to the center of the bar:

$d_1 = 32.5\,mm$

The effective tensile strength of the concrete above the top reinforcement is taken as:

$f'_{ct,eff} = 0.55 f_{sp} = 1.8\,Mpa$

It is noted that the effective tensile strength of the concrete for the top bars is less than that for the integrity bars.

1. Reaching maximum post-punching resistance

The deflection corresponding to the maximum post-punching resistance of upper layer of top bars is:

$\delta = 15mm$

Based on the equilibrium conditions, the vertical component of the force developed in a reinforcing bar is equal to concrete breakout strength of the concrete above the bar:

$$A_s f_s \sin\theta_t = V_t(x')$$

Applying compatibility of deformations:

$$\delta = \ell_t \tan\theta_t = \ell_t \tan\left[\cos^{-1}\left(\frac{1}{1+\varepsilon_s}\right)\right]$$

Where

$$\varepsilon_s = \frac{1}{\cos\theta_t} - 1$$

The maximum breakout resistance for upper 15M bars can be calculated by:

$$V_t(x') = A_{ch}(x') f'_{ct,eff} = \left(\frac{\pi}{2} \times d_1^{\,2}\right) f'_{ct,eff}$$

$$V_t(x')_{total} = V_{t,\max} = (\frac{\pi}{2} \times 32.5)^2 \times 1.8 \times 2 \times 5 = 29.84\,kN$$

Check for rupture:

The computed strain in the reinforcing steel for the upper 15M bars is equal to:

$$\varepsilon_s = 0.0014 < \varepsilon_u \quad Ok$$

Check for pullout:

To ensure that the pullout does not occur, the remaining embedded length of the upper 15M bars is compared with the development length of the bar.

Protruding length of top reinforcement from column face:

$$L_t = 1037mm$$

The remaining embedded length of the upper 15M bars:

$$\ell_{rem} = 1037 - \ell_t$$

where

$$\ell_t = 2x' + 2d_b$$

The computed x' for upper 15M bars is equal to:

$$x' = 130mm$$

$$\ell_t = 2 \times 130 + 2 \times 15 = 290mm$$

$$\ell_{rem} = 1037 - 290 = 747 > \ell_d \quad Ok$$

2. Limiting displacement

Limiting displacement for the upper layer of the top bars is defined as the deflection corresponding to the stage that the remaining embedded length of upper layer of top bars is reduced to the development length of the bar, ℓ_d (see Fig. 5.8).

The maximum breakout resistance for upper 15M top bars:

$$V_{t,\max} = 29.84\,kN$$

The computed angle of inclination of the upper 15M bars corresponding to the maximum breakout resistance is:

$$\theta_{t,\max} = 3.04^{\circ}$$

The computed stress of reinforcement is:

$$f_s = 282\,Mpa$$

The computed stress of the reinforcement is used to calculate the nominal development length of the bar:

$$\ell_d = 0.8 \times \left(\frac{f_s \cos\theta_{t,\max}}{1.1\lambda\sqrt{f_c'}} \frac{\psi_t \psi_e \psi_s}{\left(\frac{c_b + K_{tr}}{d_b} \right)} \right) d_b$$

$$\ell_d = 223mm$$

The limiting displacement is calculated by:

$$\delta_{\max} = \left(L_t - \ell_d + 2d_b\right)\tan\theta_{t,\max}$$

The exposed length of the bars includes a concrete damage zone at the locations where the bar enters the concrete of a length equal to the bar diameter, d_b.

$$\delta_{\max} = (1037 - 223 + 30)\tan(3.04) = 45mm$$

B.3.2 Lower 15M top bars

Number of effective lower 15M bars: 5-15M

The depth of concrete over reinforcing bar measured to the center of the bar:

$$d_1 = 47.5\,mm$$

The effective tensile strength of the concrete above the top reinforcement is taken as: $f'_{ct,eff} = 1.8\,Mpa$

1. Reaching maximum post-punching resistance

The deflection corresponding to the maximum post-punching resistance of lower layer of top bars is:

$\delta = 31mm$

Applying the equilibrium condition and compatibility of deformation:

$$\left\{\begin{array}{l} A_s f_s \sin\theta_t = V_t(x') \\ \delta = \ell_t \tan\theta_t = \ell_t \tan\left[\cos^{-1}\left(\dfrac{1}{1+\varepsilon_s}\right)\right] \end{array}\right\}$$

where

$$\varepsilon_s = \frac{1}{\cos\theta_t} - 1$$

$$V_t(x') = A_{ch}(x') f'_{ct,eff} = \left(\frac{\pi}{2} \times d_1^{\,2}\right) f'_{ct,eff}$$

$$V_t(x')_{total} = V_{t,\max} = (\frac{\pi}{2} \times 47.5^2 \times 1.8) \times 2 \times 5 = 63.76\,kN$$

Check for rupture:

The computed strain in the reinforcing steel for the lower 15M bars is equal to:

$\varepsilon_s = 0.0029 < \varepsilon_u \quad Ok$

Check for pullout:

$L_t = 1037mm$

The remaining embedded length of the lower 15M bars:

$$\ell_{rem} = 1037 - \ell_t$$

where

$$\ell_t = 2x' + 2d_b$$

The computed x' for upper 15M bars is equal to:

$$x' = 190mm$$

$$\ell_t = 2 \times 190 + 2 \times 15 = 410mm$$

$$\ell_{rem} = 1037 - 410 = 627 > \ell_d \quad Ok$$

2. Limiting displacement

Limiting displacement for the lower layer of top bars is defined as the deflection corresponding to the stage that the remaining embedded length of the lower layer of top bar is reduced to the development length of the bar.

The maximum breakout resistance for lower 15M bars:

$$V_{t,\max} = 63.76\,kN$$

The computed angle of inclination of the lower 15M top bars corresponding to the maximum breakout resistance is:

$$\theta_{t,\max} = 4.36^{\circ}$$

The computed stress of reinforcement is:

$$f_s = 420\,Mpa$$

The nominal development length of the bar corresponding to the computed stress of the bar is:

$\ell_d = 285mm$

The limiting displacement is calculated by:

$\delta_{\max} = (L_t - \ell_d + 2d_b)\tan\theta_{t,\max}$

$\delta_{\max} = (1037 - 285 + 30)\tan(4.36) = 60mm$

B.4 Hand calculation for structural integrity bars

The following calculations present the contribution of each layer of integrity bars in specimen SS, to the post-punching shear response:

B.4.1 Upper 15M integrity bars

Number of integrity bars: 2-15M

The depth of concrete over reinforcing bar measured to the center of the bar:

$d_2 = 97.5\,mm$

The effective tensile strength of the concrete above the integrity reinforcement is taken as:

$f_{ct,eff} = 0.85 f_{sp} = 2.8\,Mpa$

1. Reaching maximum post-punching resistance

The deflection corresponding to the maximum post-punching resistance of upper layer of integrity bars is:

$\delta = 53mm$

Applying the equilibrium condition and compatibility of deformation:

$$\left\{\begin{array}{l} A_s f_s \sin\theta_t = V_i(x) \\ \delta = \ell_i \tan\theta_i = \ell_i \tan\left[\cos^{-1}\left(\dfrac{1}{1+\varepsilon_s}\right)\right] \end{array}\right\}$$

where

$$\varepsilon_s = \frac{1}{\cos\theta_i} - 1$$

$$V_i(x) = A_{ch}(x) f_{ct,eff} = \left(2 \times \frac{\pi}{2} \times d_1{}^2 - A_1(d_2)\right) f_{ct,eff}$$

To calculate the horizontal projection of the conical failure surface, $A_{ch}(x)$, for more than one structural integrity bar, the interaction between the failure surfaces of the breakout cones must be considered:

$$V_i(x)_{total} = V_{i,\max} = (2 \times \frac{\pi}{2} \times 97.5^2 - 4108.76) \times 2.8 \times 2 = 145\,kN$$

Check for rupture:

The computed strain in the reinforcing steel for the upper layer of 15M bars is equal to:

$$\varepsilon_s = 0.044 < \varepsilon_u \quad Ok$$

Check for pullout:

$$L_i = 790mm$$

The remaining embedded length of the upper 15M integrity bars:

$$\ell_{rem} = 790 - \ell_i$$

where

$\ell_i = d_3 + x + 2d_b$

The computed x for upper layer of integrity bars is equal to:

$x = 98mm$

The distance measured from bottom face of the slab to center of a bar:

$d_3 = 25 + 15 + 7.5 = 47.5mm$

$\ell_i = 47.5 + 98 + 2 \times 15 = 175.5mm$

$\ell_{rem} = 790 - 175.5 = 614.5 > \ell_d \quad Ok$

2. Limiting displacement

Limiting displacement for the upper layer of integrity bars is defined as the deflection corresponding to the stage that the remaining embedded length of the upper layer of integrity bar is reduced to the development length of the bar, ℓ_d (see Fig. 5.8).

The maximum breakout resistance for upper 15M integrity bars:

$V_{i,\max} = 145\,kN$

The computed angle of inclination of the upper 15M integrity bars corresponding to the maximum breakout resistance is:

$\theta_{i,\max} = 16.72^\circ$

The computed stress of reinforcement is:

$f_s = 635\,Mpa$

The nominal development length of the bar corresponding to the computed stress of the bar is:

$\ell_d = 414mm$

The limiting displacement is calculated by:

$\delta_{\max} = (L_i - \ell_d + 2d_b)\tan\theta_{i,\max}$

$\delta_{\max} = (790 - 414 + 30)\tan(16.72) = 125mm$

B.4.2 Lower 15M integrity bars

Number of integrity bars: 2-15M

The depth of concrete over reinforcing bar measured to the center of the bar:

$d_2 = 112.5\,mm$

The effective tensile strength of the concrete above the integrity reinforcement is taken as:

$f_{ct,eff} = 2.8\,Mpa$

1. Reaching maximum post-punching resistance

The deflection corresponding to the maximum post-punching resistance of lower layer of integrity bars is:

$\delta = 69mm$

Applying the equilibrium condition and compatibility of deformation:

$$\begin{Bmatrix} A_s f_s \sin\theta_t = V_i(x) \\ \delta = \ell_i \tan\theta_i = \ell_i \tan\left[\cos^{-1}\left(\frac{1}{1+\varepsilon_s}\right)\right] \end{Bmatrix}$$

where

$$\varepsilon_s = \frac{1}{\cos\theta_i} - 1$$

$$V_i(x) = A_{ch}(x) f_{ct,eff} = \left(2 \times \frac{\pi}{2} \times d_1^{\,2} - A_1(d_2) \right) f_{ct,eff}$$

$$V_i(x)_{total} = V_{i,\max} = (2 \times \frac{\pi}{2} \times 112.5^2 - 7050.94) \times 2.8 \times 2 = 184\,kN$$

Check for rupture:

The computed strain in the reinforcing steel for the lower layer of 15M integrity bars is equal to:

$$\varepsilon_s = 0.061 < \varepsilon_u \quad Ok$$

Check for pullout:

$$L_i = 790mm$$

The remaining embedded length of the lower 15M integrity bars:

$$\ell_{rem} = 790 - \ell_i$$

where

$$\ell_i = d_3 + x + 2d_b$$

The computed x for upper layer of integrity bars is equal to:

$$x = 130mm$$

The distance measured from bottom face of the slab to center of a bar:

$$d_3 = 25 + 7.5 = 32.5.5mm$$

$\ell_i = 32.5 + 130 + 2 \times 15 = 192.5mm$

$\ell_{rem} = 790 - 192.5 = 597.5 > \ell_d \quad Ok$

2. Limiting displacement

Limiting displacement for the lower layer of integrity bars is defined as the deflection corresponding to the stage that the remaining embedded length of the lower layer of integrity bar is reduced to the development length of the bar.

The maximum breakout resistance for lower 15M integrity bars:

$V_{i,\max} = 184\,kN$

The computed angle of inclination of the lower 15M integrity bars corresponding to the maximum breakout resistance is:

$\theta_{i,\max} = 20^\circ$

The computed stress of reinforcement is:

$f_s = 680\,Mpa$

The nominal development length of the bar corresponding to the computed stress of the bar is:

$\ell_d = 435mm$

The limiting displacement is calculated by:

$\delta_{\max} = \left(L_i - \ell_d + 2d_b\right)\tan\theta_{i,\max}$

$\delta_{\max} = (790 - 435 + 30)\tan(20) = 141mm$